The Photochemistry of Liquid Aerosols

A thesis submitted in partial fulfilment of

the requirements for the degree of

Doctor of Philosophy in Chemistry

at the

University of Canterbury

Christopher James Henry Knox

University of Canterbury

Christchurch

New Zealand

2002

The observer and the observed – Karen Derges

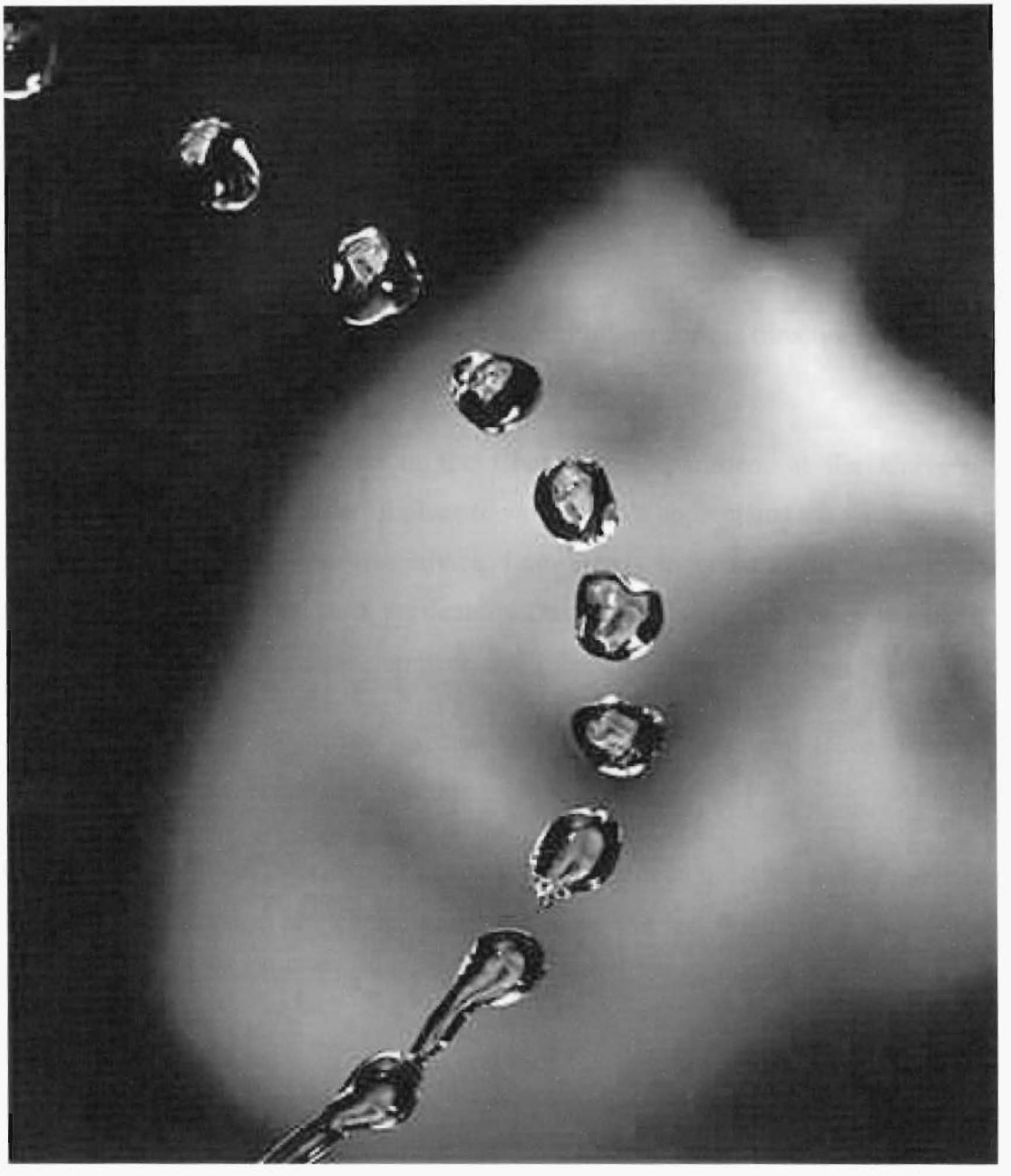

The true scientist never loses the faculty of amazement. It is the essence of his being.

Hans Selye – 1958

Acknowledgements

Countless people have assisted me in the completion of my thesis, and I am very grateful to them all.

I would particularly like to thank Professor Leon Phillips for his direction, understanding, and patience, and for his role as my supervisor.

I would like to thank everyone in the Chemistry Department at the University of Canterbury; it has been a wonderful place to work. I have appreciated the willingness of all the academic staff to help and give advice. I am hugely indebted to the fantastic support provided by all the technical staff, particularly Dave, Rob, Nick, and Danny who all had to endure the process of system development, and John who kept my computer running.

I have enjoyed working with my research group, Clint, Glenn, and Dave. Thanks very much for all your advice, support, and fun.

All the other students in the chemistry department have been great to have around. Thanks especially to the Sponge Munchers, who have made the last few months more bearable, and a huge thanks to Chris Fitchett for his support, advice, and encouragement while I have been writing up.

Thank-you Mum and Dad, Jo, Abi, and Johnny for all you support over the last few years and to my new family John, Lynda, Tim, and Ben for all yours.

Thank-you Professor Robert Gilbert for your generosity and for the lessons that you taught me.

Lastly, thank-you Anna, you have been and are amazing.

Contents

Abstract

The photochemistry of liquid aerosols has been investigated with the aim of using the physical properties of liquid aerosols to enhance the reactivity of photochemical and photocatalytic systems.

The properties of aerosols that enhance reactivity are summarised under four headings: the optics of microdroplets, diffusion into small particles, surface and interfacial reactivity, and capillarity effects.

A range of systems have been developed for the photochemistry of liquid aerosols. A number of photocatalytic systems have been studied and a significant enhancement in the photolysis of molybdenum hexacarbonyl has been observed, relative to the liquid phase.

A computational study of the light intensity distribution inside liquid aerosols droplets in photochemical and photocatalytic systems has been carried out. Large enhancements of the internal field intensity relative to the incident field have been observed. It is proposed that the internal intensity distributions are the source of the increased rate of molybdenum hexacarbonyl photolysis.

A model has been proposed for gas-liquid transfer, based on the capillary wave motion of the liquid surface.

1 Introduction

1.1 Synopsis of Present Work

This thesis is an investigation of the photochemistry of liquid aerosols. The thesis begins with a description of the context of the present work relative to the rest of aerosol chemistry. In order to do this the concept of process aerosol chemistry is introduced. In Chapter 2, the areas that motivate liquid aerosol photochemistry are summarised. A significant part of this thesis was the development of systems for the study of liquid aerosol photochemistry; these are described in Chapter 3. Liquid aerosol photocatalysis is a promising application of liquid aerosol photochemistry, the investigation of liquid aerosol photocatalytic systems is discussed in Chapter 4. One very interesting aspect of the photochemistry of liquid aerosols is the non-trivial interaction of light with aerosol droplets; this is investigated in Chapter 5. Processes at the gas-liquid interface are very important in aerosol chemistry; a model of exchange at the gas-liquid interface is presented in Chapter 6.

1.2 A Survey of Related Work

Aerosol chemistry is an area of increasing importance and interest. Due to the importance of aerosols in the atmosphere, atmospheric chemists virtually dominate the field. However, there is significant amount of research done on non-atmospheric aerosol chemistry. I provide here, a brief summary, grouped as atmospheric and non-atmospheric, of some of the aerosol chemistry that is of relevance to the present work.

1.2.1 Atmospheric chemistry

The present thesis is not a work on atmospheric chemistry. However, the motivation for the work comes largely from atmospheric chemistry so it would be remiss not to mention related work in atmospheric chemistry, albeit briefly.

Atmospheric chemists have done a lot of research on the chemical reactions involving aerosols that are of important to atmospheric chemistry and there are a large number of reviews and books on the topic. A recently edited congress, *Aerosol Chemical Processes in the Environment* provides an overview of current research (Spurný 2000). It also contains work on non-atmospheric processes, some of these are discussed below. Finlayson-Pitts and Pitts's (2000) text contains a lot of information on and references to atmospheric aerosol chemical processes. Mészáros (1999) has written a more specific text solely called *Atmospheric Aerosol Chemistry*.

Processes at the air-water interface are very important in atmospheric chemistry, because of this interfacial reactivity and transfer rates have been the subject of a number of investigations. The uptake rate of SO_2 has been observed to be considerably faster into droplets than was expected based on the uptake rate into bulk liquid (Jayne, Davidovits, Worsnop, Zahniser and Kolb 1990). Jayne et al. proposed that a chemisorbed surface state was involved. In 1995, the existence of this surface state was demonstrated (Donaldson, Guest and Goh 1995) using second harmonic generation (SHG) spectroscopy (Eisenthal 1996a, 1996b). The magnitude of the surface tension decrease observed in the Donaldson et al.'s paper is very large (37 dynes cm^{-1}). This makes the work in this paper a little suspect. However, there is little doubt about the existence of a sulfur dioxide surface state (Yang, Wright, Gagnon, Gerber and Finlayson-Pitts 2002). Subsequently, Donaldson has developed a thermodynamic and kinetic framework for studying the surface states of volatile soluble species (Donaldson 1999, Donaldson and Anderson 1999). Donaldson has studied ammonia and a range of short chain alcohols, acids, and ketones. This raises the possibility of molecules not simply passing through the interface by physical processes, but rather forming unique chemical species at the interface. Solid surfaces are very important in many chemical processes, because they can influence chemical reactivity and these results have raised the possibility of a similar, though obviously more complicated, significance for liquid surfaces. Clearly, this is very important for understanding atmospheric processes. Finlayson-Pitts and Pitts (2000 p. 308) describe these results as, "...intriguing hints that there may also be some chemistry that is unique to the interface which may be thought of as a 'fourth phase,' in addition to gases, liquids and solids."

1.2.2 Non-Atmospheric Chemistry

The chemistry and photochemistry of aerosols has a long history. Tyndall (1869) reported the formation of particles from the photochemical 'decomposition' of gases and vapours. He observed that no matter what the original reactants the cloud formed is blue. As the reaction progressed and bigger particles formed, the blue colour went away. He concluded that the blue colour of the sky was the result of the presence of very small particles. He also observed the polarisation of light by the particles that formed photochemically, and that this polarisation also disappeared as the particle size increased. Tyndall published his results four years before Lord Rayleigh demonstrated theoretically that the cause of the blue colour of the sky was scattering from molecules and small particles. This is probably the first report of the formation of an aerosol by the photochemical reaction of vapours and the vapour's subsequent reaction with, or condensation onto, the particles formed.

Despite these early beginnings, it was not until the 1970s that the study of reactions between aerosols and gases, hereafter called aerosol chemical reactions, began. Davis (1998) attributes the pioneering work[i] on chemical reactions of highly monodisperse aerosols to Matijevic (McRae, Matijevic and Davis 1975, 1978). The first of these two papers begins, "Whereas numerous studies have been reported on the physics and chemistry of aerosols, chemical reactions in such systems have been much less frequently investigated." Since 1975, many more people have studied these chemical reactions; however, Matijevic's statement is probably still true. There remains a significant bias in the study of aerosols towards more physical rather than chemical phenomena. A corollary of Matijevic's statement forms the basis of my work: while there has been considerable investigation into the chemical reactions of aerosols pertinent to atmospheric chemistry, very few investigations have examined aerosols as a reaction medium in and of themselves.

In these first two papers, Matijevic and co-workers investigate the bromination of octadecene droplets with molecular bromine. The first paper reports their experiments and

---

[i] Matijevic emphasises the scarcity of studies on the chemical reactions of formed aerosols, and cites only three publications which mention the chemisorption of gases on solid aerosols as a special case of the interaction of airborne particles with gases.

gives a theoretical discussion of the reaction mechanism, looking in particular at the possibility of various forms of diffusion control or liquid phase reaction control (McRae et al. 1975). The second paper is a study of the effects of carrier gas flow rate, temperature, and bromine vapour concentration on the same reaction, concluding that the reaction rate is controlled by liquid-phase processes (McRae et al. 1978).

Following these two publications Matijevic and co-workers used aerosol chemical reactions to prepare monodisperse suspensions of metal and metal oxide colloids (Ocana and Matijevic 1990, Ingebrethsen and Matijevic 1980, Visca and Matijevic 1979, Ingebrethsen, Matijevic and Partch 1983, Balboa, Partch and Matijevic 1987, Matijevic, Zhong and Partch 1995). In these reactions, they used the evaporation condensation process. They also produced monodisperse organic microspheres by reacting monodisperse monomer aerosol with a gas phase initiator (Partch, Matijevic, Hodgson and Aiken 1983, Nakamura, Partch and Matijevic 1984, Partch, Nakamura, Wolfe and Matijevic 1985)

In 1984, a substantial advance in the study of aerosol chemical reactions occurred when Thurn and Kiefer demonstrated that an optically levitated microdroplet could be analysed by Raman spectroscopy. (Thurn and Kiefer 1984) A surprising result in this experiment was that the Raman spectra of microdroplets were more complicated than the spectrum of the bulk material. This is a consequence of the optical effects associated with small particles, specifically, morphology dependent-resonances, which are one of the motivating factors behind this work. Prior to 1984, samples were collected using an impactor or filter and they were then analysed by conventional techniques. The ability to observe a single droplet while it reacted opened up a huge range of possibilities for more detailed studies. Since then, aerosol chemical reactions have been increasingly dominated by the elaborate experiments that are made possible by high resolution optical effects (Barber and Chang 1988, Chang and Campillo 1996). Davis (1998) has published recent review of Raman studies of aerosol chemical reactions.

Aerosol processes enhance a large number of industrial processes, including the fabrication of materials for high technology applications such as optical waveguides, thin films for microelectronics and powders for the manufacture of advanced ceramics, as well as commodity products such as pigments and carbon blacks. Kodas and Hampden-Smith (1999) have written a monograph entitled *Aerosol Processing of Materials*. In this

monograph, they define aerosol processing as, "systems in which the presence of particles in the gas phase is an integral part of the materials synthesis or processing scheme". In this definition, the bias towards materials science is evident, and the majority of the discussion is on the use of aerosol processes to form powders and films and occasionally macroscopic objects. In their introduction, they also note the lack of emphasis on the study of beneficial aerosols in the aerosol science community. The main concern of the book is to introduce the range of chemical and physical processes that are important in the industrial application of aerosol processes.

A typical example of aerosol processing in materials science is in the synthesis of titania particles that have been coated with a catalytically active material such as zirconium dioxide (Fotou, Kodas and Anderson 2000). Zirconium dioxide is much more expensive than titania, and it is only catalytically useful on the surface of a particle. Titania particles form by the reaction of titanium tetrachloride with oxygen in a 1300°C tube reactor. One the titania particles have formed the zirconium dioxide is introduced into the reactor. This reacts with the particles and forms coated particles.

In a recent congress entitled *Aerosol Chemical Processes in the Environment* there are three chapters in a section called 'Aerosol Synthetic Chemistry' (Spurný 2000). Two of these chapters address the use of advanced structural techniques to optimise the production of ceramics by aerosol processes (Landron 2000a, 2000b). The other chapter looks at Modified Chemical Vapour Deposition (Matejec, Kašík and Chomát 2000). Ceramic processing and chemical vapour deposition account for almost all of the 'synthetic', as opposed to diagnostic applications of aerosol technology.

Two research groups, one from the Institut für Mechanische Verfahrenstechnik und Mechanik at the Universität Karlsruhe in Germany, (Seipenbusch, Binnig, Heim, Weber and Kasper 2001, Weber, Seipenbusch and Kasper 2001); the other from the State Design and Research Institute for Chemical Engineering in Ukraine, (Glikin, Kutakova and Prin 1999, Glikin, Kutakova, Glikina and Volga 2001, Glikin 1996) have used a process which they call 'aerosol catalysis' with differing emphases.

The Ukrainian group, headed by Glikin, has developed and patented a process that uses aerosol technology to generate sub-0.1 μm solid particles of catalytically active material. Using catalytically active solid aerosols for gas-solid heterogeneous catalysis has a number

of advantages, most of which stem from no longer requiring a carrier and the absence of any physical contact between the catalyst and other materials like supports. The process that they have applied aerosol catalysis to is the oxidation of organic waste by iron oxide. They use acetic acid to model organic waste and they report acetic acid oxidation rates five orders of magnitude higher than the acetic acid oxidation rates in conventional heterogeneous catalysis systems (Glikin et al. 1999).

The German group, headed by Weber, are sceptical about Glikin's results (Weber et al. 2001). However, they do acknowledge that Glikin's work sparked their interest in the area. Weber's approach uses aerosol catalysis in a slightly different way to Glikin's. Weber is interested in the aerosol techniques introduced by Glikin, not because they provide enhanced rates but because they provide a way of studying catalytic nanoparticles in the absence of inert supporting material. They also note that, despite its potential, the aerosol route to nanoparticles has not found much use in heterogeneous catalysis. They believe aerosol catalysis has the potential to help close the so-called pressure gap between ultra-high vacuum methods for studying catalysts and the real catalytic process.

1.3 Scope of the present work

It is useful to make a distinction between 'fundamental' and 'applied' aerosol chemistry. This distinction is analogous to, but not the same as, the commonly used distinction between applied and fundamental science. It also has many of the same weaknesses. The definition of fundamental aerosol chemistry that I use is the study of chemical and physical aerosol processes for understanding the observed behaviour of aerosols. Into this category falls most of the work done by atmospheric chemists on aerosol processes. Applied aerosol chemistry is the use of some property of the aerosol phase to enhance or influence the outcome of a reaction. Aerosol processing of materials falls into this category, as does aerosol catalysis. The aerosol chemical reactions discussed above are both process and structural aerosol catalysis. The early work of Matijevic and co-workers on the reaction of bromine with octa-decene would be fundamental while the later work, on the preparation of uniform colloidal dispersions, is applied.

It is useful to make a further distinction within applied aerosol chemistry, between structure-oriented reactions and process-oriented reactions. Structure-oriented reactions are

those that utilise the morphology of aerosols as a way of controlling the structure of the final product. Some processes that take advantage of morphological control of aerosol chemistry are the production of a high surface area catalytic particle, a fine powder, a monodisperse colloid, or a thin film. Almost all the applied aerosol chemical processes that are mentioned above are structurally oriented. Matijevic's work on bromine and octa-decene is the only exception, and it appears from his subsequent publications that the investigation of the reaction of bromine and octa-decene was a step on the way to structural aerosol chemistry rather than an investigation of process aerosol chemistry. Given that process aerosol chemistry has not been the subject of any previous investigation, it may seem unusual to introduce it as a category of aerosol chemistry. I have introduced this new terminology because process aerosol chemistry is the subject of my work.

The aim of this thesis is to demonstrate that the aerosol phase is a useful phase for carrying out chemical reactions, even when there is no particular morphological requirement for the product. Using the classification outlined above, this is process aerosol chemistry, where the morphological characteristics of aerosols enhance the actual process of the reaction or provide access to reactivity that is not available in the bulk reactions of the same system.

The first part of this work is devoted to the justification of the reasonableness of this claim, drawing on areas of electrochemistry, surface and interfacial science, photochemistry, light scattering and, of course, aerosol science. Following that, I describe some experimental investigations into process aerosol chemistry. In addition, I present a theoretical investigation into the nature of the gas-liquid interface, which is of fundamental importance in liquid aerosol processes.

As an investigation into the use of aerosols to enhance reactivity, this work represents a deliberate step away from the very elegant investigations that are possible in aerosol chemistry, for example the Raman studies of single droplet reactions that are reviewed by Davis (1998). The aim of the present work is to explore, using polydisperse aerosol and polychromic (broadband) radiation, the aerosol phase is a useful phase for scientific and industrial reactions. In this sense, it runs in somewhat the opposite direction to the general trend in physical chemistry, exemplified by the laser, towards greater specificity and more control.

I am very conscious that this represents, I hope, the beginning of a potentially long investigation into process aerosol chemistry and photochemistry. I have therefore written this not just as a report on the work that I have done, but also as an introduction to the area for others interested in continuing the investigation. For a number of reasons this line of research is likely to continue in the Department of Chemistry of the University of Canterbury. I have tried to be aware of this, particularly in the descriptions of my experimental work. My aim is to provide my successors with a detailed picture of the work done, so they can avoid some of the mistakes I made and dead ends that I pursued.

2 The Basis of Liquid Aerosol Photochemistry

2.1 General Overview of Chapter

There are four areas that provided the motivation to investigate aerosol photochemistry as a way of enhancing reactivity. They are 'the optics of microdroplets', 'diffusion into small particles', 'capillarity', and 'the importance of interfacial reactivity'.

2.2 Optics of Microdroplets

Bohren and Huffman (1983) begin their classic monograph 'Absorption and Scattering of Light by Small Particles' with this paragraph:

> Cumulus clouds in the summer afternoon sky present a striking contrast of white against a bright blue sky. During a sudden thundershower the primary and secondary rainbows display their multicoloured arches. Other colours in nature are dark green of forest foliage and the red and orange hues of the Grand Canyon in the early morning. High in the mountains or on the desert when the air is clean one can clearly see dark patches in the broad band of the Milky Way. Chimney smut turns all it touches to dirty blackness, and iridescent opal shimmers with a variety of colours. All these visual phenomena and many more are manifestations of scattering and absorption of light by small particles.

The optics of microdroplets has a very long history (Descartes 1639, Nussenzveig 1977, Biggus 2002) and is broad in range (Zuev 1980, Kerker 1969, Barber and Chang 1988, Barber and Hill 1990, Chang and Campillo 1996, Bohren and Huffman 1983, Hulst 1957). The beauty, and somewhat striking nature, of its phenomena have attracted the investigations of many great minds and inspired the words of many poets. It will be demonstrated that the interaction of light with small particles is not solely of optical interest, but that these optical effects could have a significant effect on the photochemistry of systems made up of microdroplets.

2.2.1 Early Theories - Rainbows

A large range of phenomena are observed in the study of the optics of microdroplets. However, the field has its roots in the study of highly visible atmospheric events such as rainbows, the glory, and solar halos.

Figure 2.1 A rainbow, a solar halo and a glory

In 1304 the German Monk, Theodoric of Freiberg, developed a sophisticated theory of refraction in droplets, which he used to explain the rainbow (Biggus 2002, Nussenzveig 1977). He also tested his theory using large spherical flasks filled with water and was able to trace the path followed by the light. This was the first explanation of the rainbow based on the interaction of light with a single droplet. Theodoric's theory was very similar to the modern formulation, but it did not become widely known. It was not until 300 years later that Descartes independently rediscovered the same theory.

Both Descartes and Theodoric showed that a rainbow consists of rays entering a droplet and reflecting once from the inner surface, and that a secondary rainbow results from two internal reflections. They were the first people to use the interaction of light with individual droplets in the explanation of large scale phenomena such as rainbows. However, water droplets in the atmosphere are illuminated at all impact parameters simultaneously, and, while it is not difficult to find paths that contribute to the rainbow, there are an infinite number of paths that direct light elsewhere. Thus, Theodoric was unable to explain why the scattered light intensity is enhanced in the vicinity of the rainbow angle[ii]. Descartes calculated the paths of rays with many different impact

[ii] The rainbow angle is the angle between the observer, the sun, and the rainbow. Alternatively it is the angle through which a ray of sunlight is bent when it passes through a raindrop.

parameters. He found that when the impact parameter is 0° the scattering angle is 180° and the rays are backscattered to the sun. The scattering angle does not decrease monotonically with increases in impact parameter, but passes through a minimum at 130°. Because a droplet is illuminated at all possible impact parameters, the scattered light is brightest where the scattering angle varies most slowly with changes in impact parameter, which is, of course, the scattering angle minimum at 130°. Similarly, a minimum scattering angle of 138° can be derived for double reflected rays, which demonstrates why the secondary rainbow is observed at 138°. This also explains the dark band between the primary and secondary rainbows. Neither the singly reflected rays, nor any of the doubly reflected rays, are scattered into angles between 130° and 138°.

When Descartes published his treatise on rainbows, he was already considering possible applications of the phenomena which he described in the rainbow. At the end of his eighth discourse on meteorology, in which he discusses the rainbow, he outlines a scheme for using fountains of droplets of different liquids, with different refractive indices, to make signs such as crosses or columns appear in the sky. He concludes: "But I admit that skill and much work would be necessary in order to proportion these fountains, and to cause the liquids there to leap so high that these figures could be seen from afar by a whole nation, without the trick being discovered" (Descartes 1639).

2.2.2 Mathematical Treatment

The exact mathematical treatment of the interaction of a monochromatic plane wave with a spherical particle is known as Mie theory[iii]. Bohren and Hoffman (1983 pp. 82-129) provide an excellent description of Mie Theory. This discussion is complemented by Barber and Hills' (1990 pp. 188-252), which is more practically oriented. Because there are already excellent discussions available, only the salient features of Mie theory will be summarised here.

[iii] Mie was not the first to derive the solution and there is some debate about who was first Kerker, M. 1969, *The scattering of light, and other electromagnetic radiation*, Academic Press, New York.. However I shall use the most common term, Mie theory.

The Mie solution of Maxwell's equations considers the boundary conditions that result from the incidence of a plane wave on a sphere. The solution is obtained by expressing the incident field in terms of vector spherical harmonics, $\mathbf{M}$, $\mathbf{N}$ (see appendix).

The incident, internal, and scattered fields, expressed in terms of vector spherical harmonics for parallel incident polarisation, are (Barber and Hill 1990 p. 189)

$$\mathbf{E}^i(k\mathbf{r}) = E_0 \sum_{n=1}^{\infty} i^n \frac{2n+1}{n(n+1)} \left(\mathbf{M}^1_{o1n} - i\mathbf{N}^1_{e1n} \right) \tag{1}$$

$$\mathbf{E}^{\text{int}}(mk\mathbf{r}) = E_0 \sum_{n=1}^{\infty} \left(c_{o1n}\mathbf{M}^1_{o1n} + d_{e1n}\mathbf{N}^1_{e1n} \right) \tag{2}$$

$$\mathbf{E}^s(k\mathbf{r}) = E_0 \sum_{n=1}^{\infty} \frac{2n+1}{2\left[n(n+1)\right]^2} \left(f_{o1n}\mathbf{M}^3_{o1n} + g_{e1n}\mathbf{N}^3_{e1n} \right) \tag{3}$$

In the equivalent expressions for perpendicular incident polarisation, all the odd functions become even, and vice versa. E_0 is the amplitude of the incident electric field, c_{o1n} and d_{e1n} are the internal field expansion coefficients, and f_{o1n} and g_{e1n} are the scattered field expansion coefficients. These coefficients differ by a factor of n from the more common c_n, d_n, a_n, and b_n coefficients used by Bohren and Hoffman. I have used Barber and Hills' derivation and notation because I found it was better suited to calculations of the internal field intensity distribution.

The expansion coefficients for a particular droplet are a function of the size parameter x, and the complex refractive index m. The size parameter is a fundamental feature of the optics of microdroplets. The nature of the interaction of radiation with a particle is determined by the relative size of the incident wavelength and the particle radius. The size parameter expresses this as

$$x = \frac{2\pi a}{\lambda} \tag{4}$$

In equation (4), a is the droplet radius and λ is the incident wavelength. The internal field expansion coefficients are functions of spherical Bessel functions j_n, and spherical Hankel functions $h_n^{(1)}$ (see appendix).

$$c_{oln} = i^n \frac{2n+1}{n(n+1)} \left\{ \frac{i/x}{j_n(mx)\left[xh_n^{(1)}(x)\right]' - h_n^{(1)}(x)\left[mxj_n(mx)\right]'} \right\} \tag{5}$$

$$d_{eln} = -i^{n+1} \frac{2n+1}{n(n+1)} \left\{ \frac{mi/x}{m^2 j_n(mx)\left[xh_n^{(1)}(x)\right]' - h_n^{(1)}(x)\left[mxj_n(mx)\right]'} \right\} \tag{6}$$

In equations (5) and (6) the prime indicates a derivative with respect to the argument. The scattered field coefficients are also functions of Bessel and Hankel functions; they are not defined here because I have not made use of them in the course of my studies.

From the point of view of photochemistry in liquid aerosols, the most important result of Mie theory is that the internal electric field inside an aerosol droplet will not be uniform. There will be regions of significant intensity enhancement, and the area with the greatest field intensity will not necessarily be the part of the droplet that is directly illuminated. In chapter five there is a detailed study of the internal intensity distributions inside photochemically relevant droplets.

2.2.3 Modification of Physiochemical Properties

Related to the effect of microdroplets on the electric field intensity distribution is the effect of a microdroplet on the physiochemical properties of molecules located inside the droplet. While the interaction of a microdroplet droplet with an electromagnetic field can be understood classically, the interaction of droplets, electromagnetic fields, and molecules requires a quantum mechanical treatment.

One way in which the modification of physiochemical parameters can be observed experimentally is as fluorescence enhancement or inhibition of a species inside a microdroplet (Campillo, Eversole and Lin 1996). Clearly, fluorescence enhancement would decrease the lifetime of an excited state species, which would also decrease the

probability of that species undergoing photochemical reaction. Fluorescence inhibition would promote photochemical reaction. Arnold, Holler and Druger (1996b) report amazing enhancements in intermolecular energy transfer facilitated by the interaction of molecules with Morphology Dependent Resonance (MDR) modes.

One of the most interesting effects associated with microdroplets is the modification, inside the microdroplet, of the Einstein A and B coefficients of an atom. Both the enhancement and inhibition of the fluorescence of species inside microdroplets have been experimentally observed. The insight that the nature of cavities could effect the physicochemical properties of molecules embedded in them was first made by Purcell (1946). The topic is treated thoroughly by Ching, Lai and Young (1987b, 1987a) and is discussed in three chapters (Ching, Leung and Young 1996, Bronson and Skovgaard 1996, Campillo et al. 1996) of the book *Optical Processes in Microcavities* (Chang and Campillo 1996).

The experimentally observed fluorescence enhancement, or inhibition, inside droplets, indicates that the Einstein A and B coefficients of the species inside the droplet are being modified. Spontaneous emission is the emission of a photon into the vacuum state. A molecule in free space interacts with a continuous vacuum, and a photon can be emitted into any vacuum state. When a molecule is placed in a cavity such as a microdroplet, boundary conditions apply to the molecule's interaction with the vacuum state. The molecule is no longer interacting with a continuous vacuum state, but with a quantised vacuum state. If the spontaneous emission frequency of the molecule is resonant with the quantised vacuum state, fluorescence will be enhanced. Conversely, if the spontaneous emission frequency of the molecule is not also a frequency of the quantised vacuum state, then fluorescence will be inhibited and the excited state lifetime will be increased.

The effect of the vacuum state boundary conditions on the rate of fluorescence can also influence the rate of photochemical reactions inside a droplet. When fluorescence is enhanced, the excited state lifetime will decrease and so will the rate of photochemical reaction. Conversely, vacuum state boundary conditions that correspond to inhibited fluorescence imply enhanced photochemical reaction rates.

The majority of theoretical treatments of photochemistry use the so-called semi-classical theory (Craig and Thirunamachandran 1984, 1982). The semi-classical theory treats atoms and molecules quantum-mechanically, but radiation classically. Implicit in this is the assumption that the interaction of the radiation with the molecule does not affect the radiation. A number of people have advocated a greater emphasis on quantum electrodynamic treatments of photochemistry rather than semi-classical methods, including E. Bright Wilson and Richard Feynman (Andrews, Craig and Thirunamachandran 1989). The quantum electrodynamic approach has a number of advantages; most notably, it provides a unified approach to molecule-molecule and molecule-radiation interactions (Craig and Thirunamachandran 1986). The semi-classical method is likely to be insufficient for a theoretical treatment of the photochemistry in aerosols, which requires a quantum electrodynamic perspective.

The electromagnetic modes associated with microdroplets have a startling effect on the energy transfer between donor and acceptor molecules. This effect offers yet another characteristic of microdroplets that promises to make the photochemical processes in aerosols unique, useful and interesting. This effect is reviewed by Arnold, Holler and Druger (1996b), and is investigated experimentally by a number of authors (Armstrong, Xie, Ruekgauer and Pinnick 1992, Campillo, Eversole and Lin 1992, Folan, Arnold and Druger 1985, Druger, Arnold and Folan 1987, Arnold and Folan 1989, Folan and Arnold 1992, Arnold, Holler, Li, Serpenguzel and Auffermann 1995, Arnold, Holler and Druger 1996a, Arnold, Holler and Goddard 1997).

Experimentally, an enhancement of more than 100 fold is found in energy transfer between molecules in microdroplets relative to the usual energy transfer mechanisms. Furthermore, the energy transfer is most efficient between molecules at the light's entry and exit points in the droplet, a distance of 180,000 Å. This is in agreement with the predictions of Mie theory. The acceptor fluorescence image shows that the majority of the fluorescence comes from around the edges of the droplet. This is consistent with theoretical predictions (Druger et al. 1987), and is what would be expected intuitively, given that the greatest density of electromagnetic modes, which the acceptor can couple to, is around the outside of the sphere. This enhancement is most effective when the solutions are dilute; this is where the losses from electromagnetic modes due to absorption are least. The proposed

mechanism for microdroplet enhanced energy transfer involves the emission of a photon into a droplet mode, and its subsequent absorption elsewhere in the droplet. Energy transfer to the poles is favoured because the density of electromagnetic modes is greatest at the poles of the droplet.

In the laser photochemistry of droplets, radiation accumulates inside transparent droplets to the extent that dielectric breakdown occurs and the droplet becomes a plasma (Eickmans, Hsieh and Chang 1987, Hsieh, Zheng, Wood, Chu and Chang 1987). This is an experimental confirmation of the importance of the internal intensity enhancements discussed earlier. Although droplet vaporisation would not be advantageous in liquid aerosol photochemistry, the large light intensity enhancements implied by these results offer the possibility of enhanced photochemistry.

When light is incident on a droplet that is part of a large cloud of aerosol droplets, any light that is not absorbed by the droplet is scattered. This scattered light is then either absorbed or scattered by another aerosol droplet. The ratio of scattering to absorption for an individual droplet depends on its size parameter.

In a liquid aerosol system it would be possible to select the size parameter so that the absorption cross section of the droplets was such that only the required amount of light for the reaction was absorbed. The rest of the light incident on a droplet would be scattered onto another droplet, which in turn would scatter excess incident light. This would effectively increase the spatial penetration of the light into the system. In comparison with a liquid phase system, where excess light incident on the system would be consumed by relaxation processes.

2.3 Diffusion into Small Particles

The mass transfer of gases into the liquid phase is of considerable importance in a large number of industrial processes. It is particularly important in homogeneous catalysis where one or more of the reactants is a gas such as hydrogen, carbon monoxide or carbon dioxide. In these reactions the absorption of the reactant gas into the liquid phase is commonly a critical step in controlling the overall rate of the reaction. In order to achieve a fast transfer rate, industrial homogeneous catalytic reactions are frequently carried out at extremely

high pressures, sometimes as high as 500 bar. In some catalytic reactions, high pressures are required to generate the actual catalytic species from the pre-catalyst. In these cases, reducing the operating pressure would not necessarily be beneficial but, in general, increasing the rate of gas-liquid mass transfer without increasing the pressure would be beneficial. Another factor that needs to be taken into account is the importance of the actual concentration of the dissolved reactant in the liquid phase to the rate of the reaction. It would not be beneficial to increase the rate of gas-liquid transfer if the limiting factor was the Henry's Law constant rather than the transfer rate.

It is well known that an increase in the surface to volume ratio of a material increases the rate of mass transfer into and out of that material. However, it is less well known that such a change can be caused not only by the increase in surface area for transfer, but also by changes in the morphology of the particles: a more curved surface has a higher rate of diffusion to that surface than a flat surface.

This effect, known as spherical diffusion, is very important in electrochemistry with small electrodes and this is where most discussions and derivations of the effect can be found. I have relied extensively on Rieger's (1994 pp. 162-5)) treatment. A similar derivation is used to determine the diffusion limited rate in a homogeneous medium.

Spherical diffusion can be demonstrated by solving the diffusion equation (7) in three dimensions (Strauss 1992 p. 235) with appropriate boundary conditions:

$$\frac{\partial \psi}{\partial t} = \kappa \nabla^2 \psi \tag{7}$$

The boundary conditions used in the electrochemical treatment of the problem are based on a spherical surface in a solution of known initial concentration. It is assumed that a reaction occurs instantaneously when a molecule is at $r = a$, the surface of the sphere. By transforming the diffusion equation into spherical coordinates and applying it to the concentration $C(r,t)$ of a species with the diffusion coefficient D, which depends on time and the radial coordinate only we get (8).

$$\frac{\partial C(r,t)}{\partial t} = D\left(\frac{\partial^2 C(r,t)}{\partial r^2} + \frac{2}{r}\frac{\partial C(r,t)}{\partial r}\right) \tag{8}$$

The initial condition is $C(r,0)=C_0,\ r>r_0$, where the initial concentration is C_0 and the sphere radius is r_0. The boundary condition is $C(r_0,t)=0,\ t>0$. Using a Laplace transform, the solution is found to be (Rieger 1994 pp. 163,454-5):

$$C(r,t)=C_0\left[1-\frac{r_0}{r}\left(1-\operatorname{erf}\frac{r-r_0}{2\sqrt{Dt}}\right)\right] \tag{9}$$

By differentiating (9) with respect to r, and setting $r=r_0$, the flux at the surface can be obtained:

$$J(r_0,t)=-D\left(\frac{\partial C(r,t)}{\partial r}\right)_{r=r_0}=-C_0\left(\sqrt{\frac{D}{\pi t}}+\frac{D}{r_0}\right) \tag{10}$$

In comparison, the flux at a planar surface is (Rieger 1994 p. 155):

$$J(0,t)=-C_0\sqrt{\frac{D}{\pi t}} \tag{11}$$

The flux at a spherical surface (10) contains a steady state term that the flux at a planar surface (11) does not. The steady state term is inversely proportional to the radius of the sphere, thus very important for small spheres, for which it becomes the dominant term after a short time has elapsed.

The assumption that every molecule will be accommodated on contact with the surface of the sphere might not be valid when considering the diffusion of gases to the surface of aerosols; however, I think that it is clear from this simple treatment of spherical diffusion that aerosols have the potential for extremely fast gas-liquid transfer rates.

The enhancement of the rate of diffusion to a spherical reactive surface relative to a planar reactive surface can be thought of as being due to changes in the nature of the reaction coordinate for diffusion to a point on the surface. The reaction coordinate for molecules diffusing to a planar surface is just a plane perpendicular to the surface, whereas for molecules diffusing to spherical surface the reaction coordinate is a cone. The greater the curvature of the surface, the greater the angle of the cone.

In aerosol chemistry the sticking coefficient defines the probability that a molecule that collides with a surface is adsorbed on the surface. The mass accommodation coefficient defines the probability that a molecule, which collides with the surface is absorbed into the liquid. Note that this use of the term 'sticking coefficient' is different to that used by the surface science community. Due the fact that mass accommodation is not common in solids, within the context of surface science 'sticking coefficient' also refers to species that react at the surface. If we consider the 'reaction' of a molecule that strikes the surface of an aerosol as entering the liquid phase, or being accommodated, then the assumption used in the derivation of (10) is invalid. However, if we consider the 'reaction' as sticking to the surface, then the assumption is valid. Saecker and Nathanson (1993) have shown that the probability of a molecule sticking to a surface is close to unity for most molecules striking a liquid surface. Although all molecules stick, the fact that they do not all accommodate means that molecules are being 'produced' at the surface of the sphere and then diffusing outwards from the sphere. This is something that the boundary conditions used in the derivation of (10) do not take into account.

There are treatments of diffusion to reacting droplets which explicitly consider gaseous diffusion to droplets, as opposed to electrochemical treatments (Zarzycki and Chacuk 1993, Danckwerts 1951, 1970). Although more rigorous, they lack the simplicity for explanation that the electrochemical treatment provides. Despite their greater complexity they remain unsuitable when considering reaction at the interface; however, work is being done on deriving expressions that account for reaction at the interface (Hanson 1997). Of course, the more rigorous treatments would be necessary to try and model what was happening in any real system.

A further factor that can influence the rate of diffusion of molecules to small particles is the surface charge of the particles. Previous work in this laboratory has shown that the effective cross section of charged aerosols is much larger than the geometric cross section (Phillips 1993), by a factor that depends on the nature of the electrical force between the aerosol and the colliding molecule.

2.4 Surface and Interfacial Reactivity

As was discussed in the introduction, atmospheric chemists are starting to realise the possible importance of a 'fourth phase' in the understanding of air-droplet heterogeneous chemistry. One of the consequences of this 'fourth phase' is the enhanced reactivity of certain species at the interface. By carrying out photochemistry in the aerosol phase we may be able to use this surface reactivity to gain access to, or enhance, reactions that are either not possible or only a minor reaction pathway in the liquid phase.

In order to understand any effects in liquid aerosol photochemistry that are due to interfacial reactivity, it is necessary to first understand the nature of the gas-liquid interface. This is discussed in more detail in Chapter 6.

The nature of the liquid surface and its effect on the reactivity of molecules adsorbed at the surface is an area of increasing research (Knipping, Lakin, Foster, Jungwirth, Tobias, Gerber, Dabdub and Finlayson-Pitts 2000, Yang et al. 2002). At present, the nature of liquid surface is insufficiently characterised to design liquid aerosol systems that take advantage of surface reactivity. However, this aspect of aerosol chemistry has considerable promise.

2.5 Capillarity Effects

Albert Sanfeld has published a number of investigations into the importance of capillarity effects for chemical reactions in droplets and bubbles (Sanfeld and Steinchen 1999, Sanfeld, Sefiane, Benielli and Steinchen 2000, Sanfeld, Carlier and Mouvier 1995, Sanfeld 1998). Sanfeld is motivated by the development of chemical processing in dispersed systems. Dispersed systems include emulsions, microemulsions, aerosols, clouds, foams, micronic suspensions of bubbles, and droplets included in molten metals. Sanfeld gives two reasons for his interest in chemistry in dispersed systems (2000):

1) a considerable increase in the area of contact between the phases through which reactants and products of reactions may be exchanged; and

2) the influence of the capillary pressure on the standard chemical potentials of the species present in the dispersed small bubbles or droplets that may significantly change equilibrium constants.

The work I have done could be described as chemistry in a dispersed system. Given the well-known synthetic importance of some dispersed mediums, it is even more surprising that the interest in aerosol chemistry has remained largely fundamental and that very little applied aerosol chemistry has been investigated.

The second reason for interest in chemical reactions in dispersed systems has been the focus of Sanfeld's work. He has shown that curvature associated with small droplets can affect the equilibrium constant of reactions taking place inside droplets. Changes are only observed for reactions whose equilibrium constants are affected by pressure. In general, the effects are only significant for droplets smaller than one micron.

2.5.1 The Vapour Pressure of Volatile Species Produced Inside an Involatile Droplet

The Kelvin equation describes the effect of curvature in a single component system (Defay, Prigogine and Bellemans 1966 p. 218).

$$\ln\left(\frac{p'}{(p')_0}\right) = \frac{2\gamma}{r}\cdot\frac{v''}{RT} \qquad (12)$$

In equation (12), p is the pressure, v is the standard molar volume, γ is the surface tension, and r is the droplet radius. I have adopted the usual notation convention for capillary systems; the second phase, denoted by$('')$, being the phase on the concave side of the surface. Therefore, in this discussion it is the liquid phase. Conversely the phase on the convex side of the surface is denoted with a single prime. Throughout this discussion, the use of 0 as a subscript signifies the limit as $1/r$ tends to zero. The Kelvin equation has important implications for the stability of droplets.

The Kelvin equation can be extended to multicomponent systems (Defay et al. 1966 p. 261).

$$\ln\left(\frac{p_i'}{(p_i')_0}\right)=\frac{2\gamma}{r}\cdot\frac{v_i''}{RT} \tag{13}$$

In equation (13) the subscript i indicates a property of the ith component. When equation (12) is applied to a two-component drop where one component is volatile and the other involatile, then (13) becomes (ibid p. 264)

$$\ln\left(\frac{p_1'}{(p_1')_0}\right)=\frac{2\gamma}{r}\cdot\frac{v_1'}{RT}+\ln(\gamma_1'')_0-\ln\left[1+\frac{n_2''v_1''}{\frac{4}{3}\pi r^3-n_2''v_2''}\right] \tag{14}$$

In equation (14), the subscript 1 indicates a property of the volatile component and the superscript 2 indicates a property of the involatile component. $(\gamma_1'')_0$ is defined by

$$p_1' = p_{1,pure}(\gamma_1'')_0\, x_1'' \tag{15}$$

In equation (15), $p_{1,pure}$ is the vapour pressure of the pure liquid and $(\gamma_1'')_0$ is the activity coefficient of component 1 of mole fraction x_1'' at the pressure that exists when the surface is a plane.

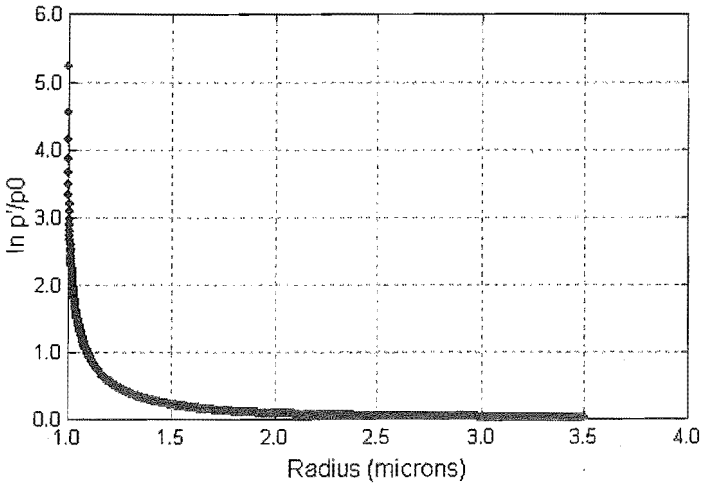

Figure 2.2 Logarithmic ratio of the pressure enhancement versus radius

Assuming that the two components form an ideal solution that obeys Henry's law, $(\gamma_1'')_0 = 0$, the only variable in equation (14) is the radius of the droplet. Figure 2.2 is a

plot of the enhancement of the vapour pressure of a volatile component produced in an involatile one-micron droplet. From Figure 2.2 it can be seen that any volatile species produced inside a small involatile drop will immediately have a very high vapour pressure. If the rate of production of the volatile species exceeds the rate of transfer of the species out of the droplet, the droplet will grow and the vapour pressure will quickly reach its normal value for the species. However, if the rate of transfer of the volatile species out of the droplet exceeds its rate of production inside the droplet, the droplet will always be in the high vapour pressure regime. This is equivalent to the instability of water droplets predicted by Kelvin's equation, but because it consists of an involatile liquid, the droplet cannot be unstable. Rather, under these conditions, it is impossible for the droplet to grow because all the species produced inside it will evaporate.

This effect makes involatile liquid aerosols a useful phase for reactions that produce volatile species that are normally difficult to separate from their reactant mixture. Consider the production of methanol. At twenty degrees over a flat surface, methanol has a vapour pressure of 13 kPa. Even if methanol that is being produced inside a one-micron involatile droplet increases the droplet radius to 1.025 μm, in other words at 2.5% methanol solution by volume, the vapour pressure of methanol will still be greater than atmospheric pressure. The application of this principle to catalysis is discussed in detail in Chapter Four.

The use of equation (14) in this situation is an approximate treatment of the problem of the production of volatile species inside an involatile droplet, although I believe that the trends derived here are qualitatively correct.

3 Experimental Systems for the Study of Liquid Aerosol Photochemistry

The study of liquid aerosol photochemistry required the development of suitable systems. This chapter describes these systems and the route by which effective systems were developed. Through the evolution of the systems used for photochemistry in liquid aerosols it is possible to see the changes in my understanding of liquid aerosol systems.

3.1 A Summary of the Equipment Available

Our laboratory has a range of equipment for generation and characterisation of aerosols and for control and monitoring of photochemical reactions. Some of these instruments are commercially available and others were built in-house.

3.2 Commercially Available Equipment

As part of my work on liquid aerosol photochemistry, I have used a number of commercially available instruments. These include both specifically designed aerosol instruments and a range of instruments that are among the standard tools of photochemistry and physical chemistry.

3.2.1 Aerosol Instruments

Vibrating Orifice Aerosol Generators are the most commonly used instruments for the generation of monodisperse aerosols. They not only allow control of the particle size, they also enable a user to control the flow rate of the aerosol and the amounts of dispersion and dilution airflow. This provides control over both the concentration and the residence time of the aerosol in an irradiation cell. However, they only generate a small amount of aerosol.

The fundamental part of a VOAG is a piezoelectric crystal mounted around a small orifice. The orifice is so small that only pressurised liquid can pass through it. As the liquid passes

through the orifice a liquid jet forms. A liquid jet that forms by passing through a stationary orifice becomes unstable at a certain distance from the orifice and breaks up into droplets of a range of sizes. Capillary waves on the surface cause the instability and the eventual break-up of the liquid jet. The wavelength of the capillary waves determines the size of the droplets. Under normal conditions, there is a thermal distribution of capillary wave wavelengths on the surface of a liquid jet. Hence, a range of droplet sizes form from the jet break-up.

Figure 3.1 The VOAG in operation

In the VOAG, the piezoelectric crystal vibrates at a user-controlled, well-defined frequency that generates capillary waves of a well-defined frequency along the long axis of the liquid jet. The ultrasonically generated capillary waves have greater amplitudes than thermal capillary waves, so in the presence of ultrasonically generated capillary waves the thermal capillary waves are no longer significant. In fact, one oscillation of the piezoelectric crystal produces one droplet. The break-up of a liquid jet that forms on passage through a vibrating orifice occurs much closer to the orifice than the similar break-up of a normal jet. If the orifice frequency is resonant with the jet, the jet breaks up in a defined and consistent manner into droplets of a known and uniform size. The particle size is related to the frequency by the empirical expression (Hinds 1982 p. 382)

$$\Xi_{CM} = \sqrt[3]{\frac{\gamma}{\rho_L f^2}} \tag{16}$$

In equation (16), Ξ_{CM} is the count median diameter, γ and ρ_L are the surface tension and density of the liquid, and f is the excitation frequency. This expression is valid for frequencies from 13 kHz to 3 MHz. Equation (17) is an alternative empirical formula which also relates droplet size to the orifice vibration frequency. This equation is of greater utility because is expresses droplet diameter in terms of the frequency and the liquid flow rate, and both of these are experimental parameters.

$$d_d = \sqrt[3]{\frac{6Q_L}{\pi f}} \tag{17}$$

In equation (17), Q_L is the flow rate of the liquid. In equation (16) the droplet size depends on the -⅔ power of the frequency and in equation (17) it depends on the -⅓ power of the frequency which suggests that these empirical expressions have a limited application. Of course, the count median diameter and the droplet diameter are not necessarily the same quantity, but for a monodisperse or nearly monodisperse aerosol, they ought to be the same. Both expressions work reasonably well by ignoring the actual complexities of a real system, including the parameters that the other formula takes into account. Among these complexities is the requirement for some sort of resonant frequency to generate monodisperse aerosol.

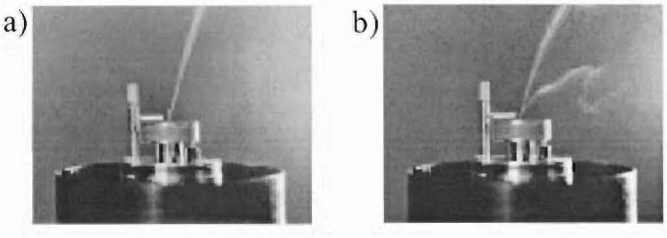

Figure 3.2 The VOAG producing aerosols with different size distributions

Many excitation frequencies produce polydisperse or bi-disperse aerosol. Figure 3.2 demonstrates this nicely. 3.2a is a photograph of a monodisperse aerosol; when a small gas flow deflects the jet of droplets all deflect at the same angle. Figure 3.2b is a photograph of a droplet jet that contains droplets of two different sizes. Both Figure 3.1 and Figure 3.2 have been reproduced from the TSI manual for the VOAG. The majority of excitation frequencies produce non-monodisperse droplet distributions. Late in my work I discovered that even when the deflected jet looks like Figure 3.2a, the VOAG is not necessarily producing monodisperse aerosol.

The TSI VOAG that we used can be fitted with a 10 μm or a 20 μm orifice. Equation (17) incorporates the effect of changing the orifice size of the droplet size as a change in the liquid flow rate. If droplets smaller than the size range possible by varying the flow rate and frequency in (17) are required then the liquid used in the VOAG can be made up as a mixture of volatile and involatile solvents. When small droplets are generated using this method the droplet diameter is calculated from a modified version of equation (17) that includes the volumetric concentration of the involatile component, C.

$$d_d = \sqrt[3]{\frac{6QC}{\pi f}} \tag{18}$$

The liquid jet breaks up into droplets of a size described by (3.3) and then evaporation of the volatile solvent gives a smaller droplet size. To ensure consistency it is necessary that there is sufficient time for the volatile component to evaporate before the aerosol enters a reaction or sampling chamber.

Aerodynamic Particle Sizers provide the size distribution and total concentration of an aerosol flow in real time. They can operate in all the usual modes for aerosol measurement: mass, number, and surface distribution. They also enable the correlation of aerodynamic diameter and light scattering information.

Particles are drawn into the aerodynamic particle sizer in a 5 $L \cdot min^{-1}$ flow, but only 1 $L \cdot min^{-1}$ of the aerosol containing flow is actually sampled. The rest of the flow splits off and passes through a filter and it becomes the sheath flow. The aerosol flow accelerates through a nozzle and the sheath flow flows around the nozzle so that as the aerosol flow exits the nozzle the sheath flow confines the aerosol flow into a narrow beam. The narrow beam then passes through two broadly focused 675 nm laser beams. The aerosol beam scatters light that an elliptical mirror collects and focuses onto a solid-state avalanche photodiode. The timing between the diode pulses is used to calculate the speed of the particles.

The manufacturers used polystyrene latex spheres of known sizes to calibrate the instrument. The instrument can detect particles in the size range between 0.5 μm and 20 μm and the particle size information is stored in 52 channels spread logarithmically over this range. The instrument also measures light-scattering intensity in the equivalent optical size range of 0.37 μm to 20 μm. It is possible to use this data to obtain more information about the make-up of

the droplet, but I did not use this feature because I already knew the basic composition of the aerosols. Figure 3.3 is a schematic of the aerosol flow in the aerodynamic particle sizer, adapted from the TSI manual for the APS 3321.

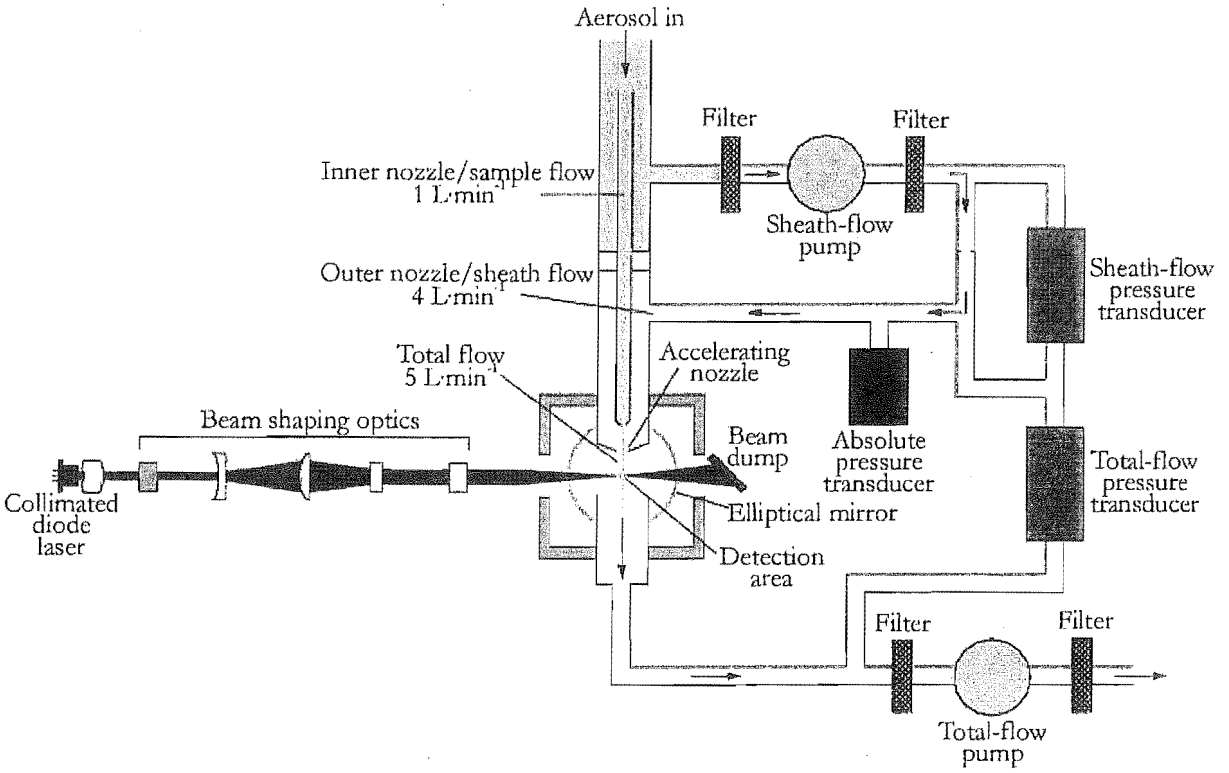

Figure 3.3 A schematic of the aerosol flow in the aerodynamic particle sizer

3.2.2 'Standard' Instruments

In addition to specially designed aerosol instruments I used a number of 'standard' instruments. The instrument I used most was a quadrupole mass spectrometer. I also used ultraviolet-visible and infrared spectrometers and I made use of nuclear magnetic resonance spectrometry.

The mass spectrometer that I used was a MKS PPT Quadrupole Residual Gas Analyser. This instrument is a complete system; the pumps (a turbopump backed up by a corrosion resistant diaphragm pump), the sampling system, and the quadrupole mass filter are combined in a single unit making the instrument very easy to use. The instrument uses electron ionisation to generate ions. MKS also provides software to drive the instrument and collect data in a number of different ways.

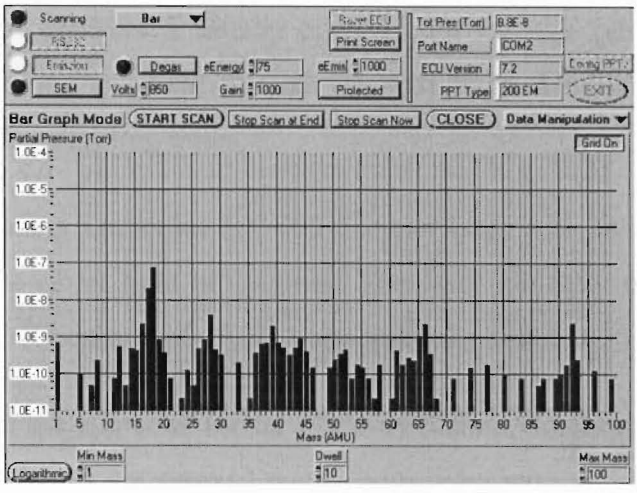

Figure 3.4 Screenshot of the mass spectrometer software operating in bar mode

Generally I used the bar mode (Figure 3.4) or the pressure versus time mode (Figure 3.5). The instrument has a mass resolution of one mass unit and a range from 0 to 200 mass units.

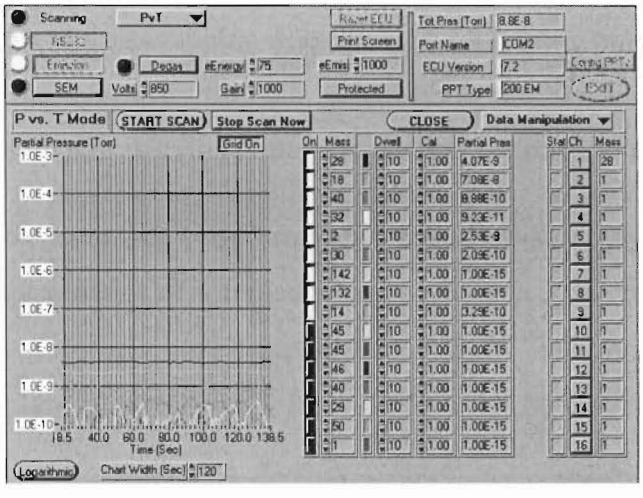

Figure 3.5 Screenshot of the mass spectrometer software operating in PvT mode

The system uses two pumps: a Pfeiffer turbo-molecular pump and a Vacuubrand BMBH and Co. diaphragm pump. This pumping system was not ideal for sampling my reaction cell as it was usually at atmospheric pressure. However, it worked reasonably well in practice. The mass spectrometer itself had two sampling stages, one of which I kept at a pressure between and 1 torr and 10 torr. The ideal operating pressure was 1 torr. A very fine needle valve regulated the flow into the quadrupole chamber. I ran the quadrupole at a pressure between 1 $\times 10^{-5}$ torr and 5 $\times 10^{-5}$ torr; the maximum pressure the quadrupole could tolerate was 1 $\times 10^{-4}$ torr. Two valves controlled the pressure and flow into the first stage. Because I was sampling

a system at atmospheric pressure, I usually opened both valves so that the turbo-molecular pump was actually drawing gas right through the first stage. This was the only way that I could achieve reasonable sampling times.

The laser that I used was a Lumonics EX-700 excimer laser with an argon-fluoride gas fill. This fill produces ultra-violet light at 193 nm. The laser typically operated with a power output of 3 W and a repetition rate of 45 Hz, corresponding to about 70 mJ per pulse.

The flash lamps I used are a special model made by Xenon Corporation and given the part number 890-1980. The lamps are suprasil quartz with filled with xenon gas. A Xenon model 457A high intensity micropulse system fires the lamps. The maximum energy pulse the flash lamps can withstand is 400 J. However, I used the lamps with pulses well below this limit. In fact, it was necessary to modify the triggering system because the voltages of the triggering pulses that I wanted to use, between 4 kV and 6 kV, were too low to trigger the lamps. To get around this problem I used a sensitising pulse just before the triggering pulse. I wrapped the lamps in nichrome wire and this wrapping delivered the sensitising pulse. This pulse partially ionised the gas inside the lamps, so that the resistance to discharge was decreased and the lamp could be triggered by pulses in the voltage range that I wanted to use.

The high-pressure xenon lamp that I used was an Osram-Sylvania XBO W lamp. Figure 3.6 shows the spectral characteristics of a typical Osram-Sylvania XBO lamp. Figure 3.7 shows in more detail the ultra-violet spectral characteristics. The 'W' in a lamp's specification code means that it is a standard quartz lamp. I have reproduced both of these figures from the product specifications.

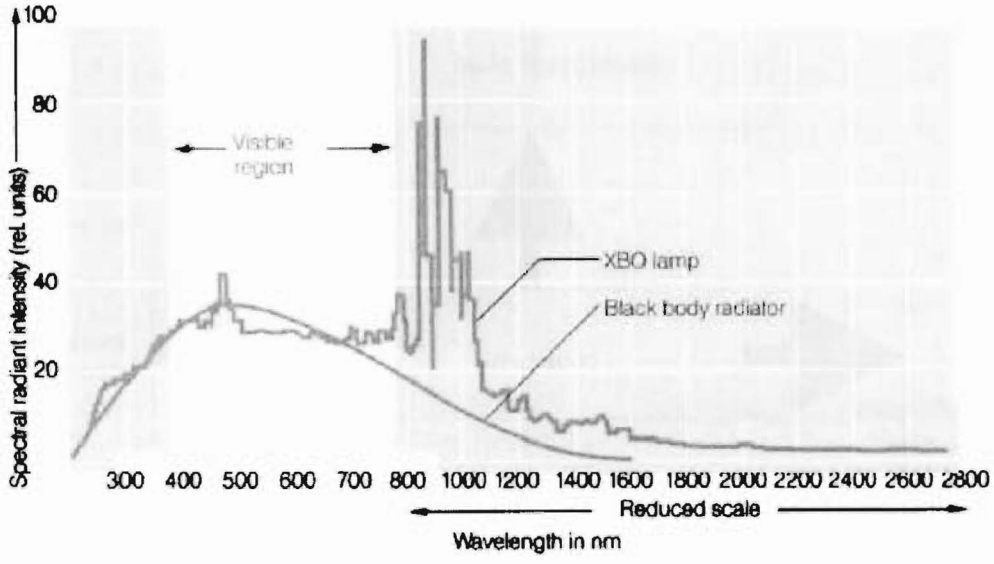

Figure 3.6 Typical spectral characteristics of an XBO lamp compared with a 6200K blackbody radiator

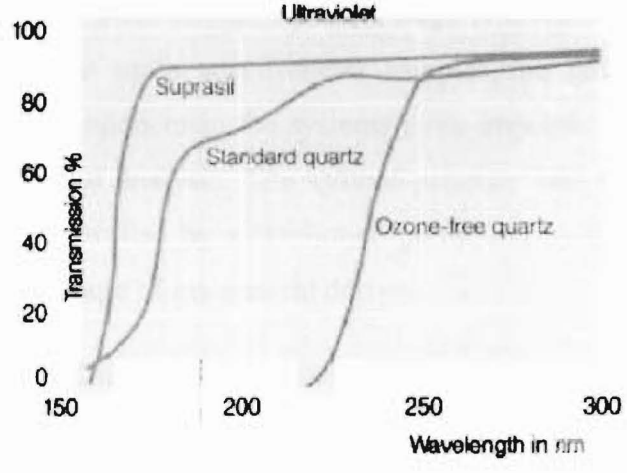

Figure 3.7 UV spectral characteristics of an XBO lamp

A system constructed in-house, ignites, and runs the lamp. I used this lamp for the majority of my experiments.

3.3 Systems Designed and Built In-house

The systems that I designed and that I had built in-house were all systems for the study of liquid aerosol photochemistry. In this section, I discuss the evolution of these systems. Almost all of the experimental systems that I used had the same basic design.

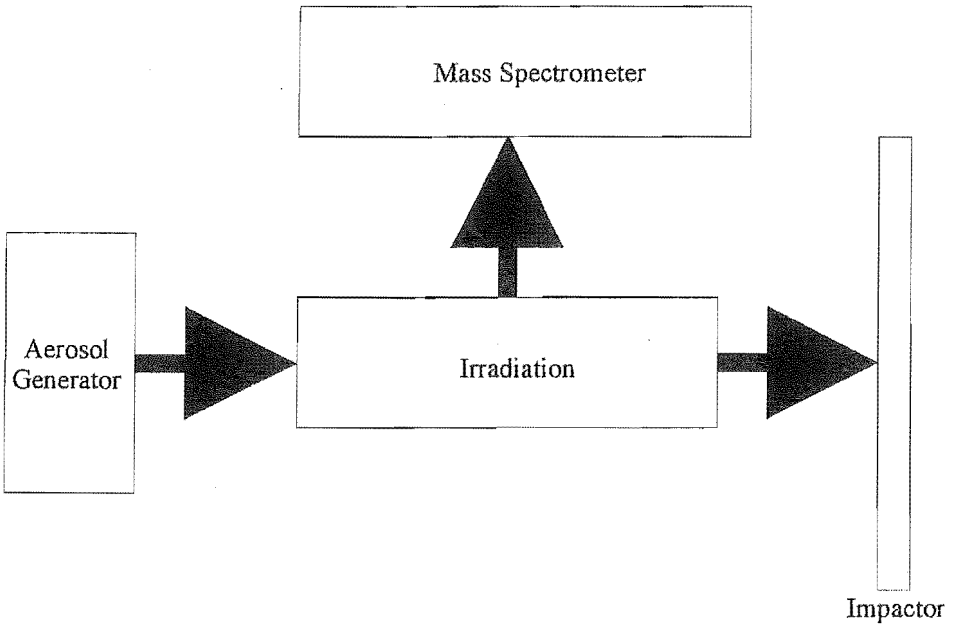

Figure 3.8 A schematic of the basic design of all the photochemistry of aerosols systems

Essentially, the systems have three stages. The first stage is aerosol generation, followed by irradiation; if necessary, the mass spectrometer samples the gas phase species in the irradiation cell. The final component in the systems is an impactor for the collection of the droplets for later liquid-phase analysis. The system pressure and the rate of aerosol flow through the system were controlled by a diaphragm pump and by the gas flow rate into the system. Figure 3.8 is a schematic of my general design.

In general, the strengths and limitations of the various system components are what drove the changes in the system. In order to demonstrate how these factors affected the system design I discuss the systems and their components in chronological order.

3.3.1 Summary of designs

The first systems I designed and used were glass systems, the final and the most effective system was a stainless steel system. The systems themselves reflect the changes in my approach to liquid aerosol photochemistry. I designed the first system to irradiate monodisperse aerosol with a laser. In the final system, a thermal light source irradiates polydisperse aerosol.

When designing and constructing my aerosol system I paid particular attention to the mitigation of aerosol losses that were due to collisions with walls in bends or constrictions. A spreadsheet called the 'Aerosol Calculator' written by Paul Baron (2001) was especially useful for this. The principles of aerosol science are discussed in both Hinds'(1982) and Willeke and Baron's (1993) texts. The 'Aerosol Calculator' spreadsheet contains many of the equations from these books. The calculation of quantities such as the percentage transmission of certain sized particles, at a given flow rate, around a 180° bend of a given diameter is simply a matter of entering all the values in the right units.

Supported by calculations made with this spreadsheet, I checked that the bends and constriction that were necessary in the aerosol system kept aerosol losses to a minimum. In general, I designed bends so that the radius of the bend was always larger than the radius of the tubing, and I designed any constrictions as slow tapers rather than abrupt steps. When I was designing impactors, I applied the opposite principles and made sure the impaction surface was as directly in the aerosol flow as possible.

3.3.2 Liquid Aerosol Photochemistry Systems Made of Glass

Due to historical inertia[iv] in our laboratory's approach to gas phase and aerosol chemistry, and to the high quality of the departmental glass blowers, the first systems for aerosol photochemistry were glass systems. I designed and used four different glass systems, but eventually found that stainless steel was a superior material for the construction of liquid aerosol photochemistry systems. However, glass was a much better material to use for the development of the systems, and I would not have been able to try the range of systems and components that I did try if I had used stainless steel from the outset.

The first system accurately and unsurprisingly reflects the assumptions that I had before I started about what would be a good photochemical system for liquid aerosols.

[iv] The two students who worked in the laboratory prior to and with me had both carried out research on concentrated sulfuric acid aerosol. They did not have a lot choice about what materials they could make their systems out of.

The first system that I designed used the VOAG as the aerosol generator. Initially I was going to work with monodisperse aerosol because I knew that droplet size was going to be an important variable in these systems, and it made sense to start by trying to control it.

I modified the VOAG by removing the aerosol generation assembly from its case and mounting it so that the aerosol flowed downwards rather than upwards. This idea came from the experimental setup of Davidovits and co-workers (for example Jayne et al. 1990). I did this to try to increase the amount of aerosol that was getting to the irradiation cell.

Perhaps ironically, the irradiation cell, the part of the experimental set-up that was most fundamental, was the simplest part of the experiment, although I was able to make substantial improvements on my original design. The irradiation cell was a horizontal glass cylinder thirty centimetres long, with an internal diameter 35 mm, and the ends of the tube were suprasil quartz windows. The aerosol entered from above at one end of the tube and exited downwards at the other end. Along the bottom of the cell were three gas inlets. These ports introduced a small gas flow to stir up the aerosol and ensure that it did not sink below the path of the light.

Out of all of my initial assumptions about liquid aerosol chemistry, the one that proved to be the worst was the assumption that it would be possible to follow the course of a reaction by monitoring the gas phase of the reaction system. Because of this assumption, the first system that I designed did not even have an impactor. I used a filter to remove the aerosol from the gas. The mass spectrometer sampled the gas flow after the filter to prevent the inadvertent entry of aerosol particles into the mass spectrometer.

I designed the first version of the glass system for the study of liquid aerosol photochemistry for use with the VOAG and the Eximer laser. The part of the VOAG that actually generated the aerosol was removed from the casing of the instrument and fitted with longer hoses and tubing. A custom-built Perspex case housed the aerosol generation unit and allowed downwards generation of aerosol. I decided that it was not necessary to include the aerosol neutraliser that comes with the VOAG in the system because I was not planning to use the electrostatic classifier or any other instrument that requires a uniform charge on each droplet. Nor was I planning to generate droplets that were so small that their charge would dramatically affect their motion. However, I did recognise that droplet charge may affect

reactivity and that at some point in the future it might be important to include a neutraliser in the system to be able to control the droplet charge. However, I suspected that my work would not reach that stage. The VOAG housing and the aerosol delivery tube was actually a separate piece of glassware to the irradiation cell; they were joined by a B45 quick-fit joint which was sealed with halocarbon wax.

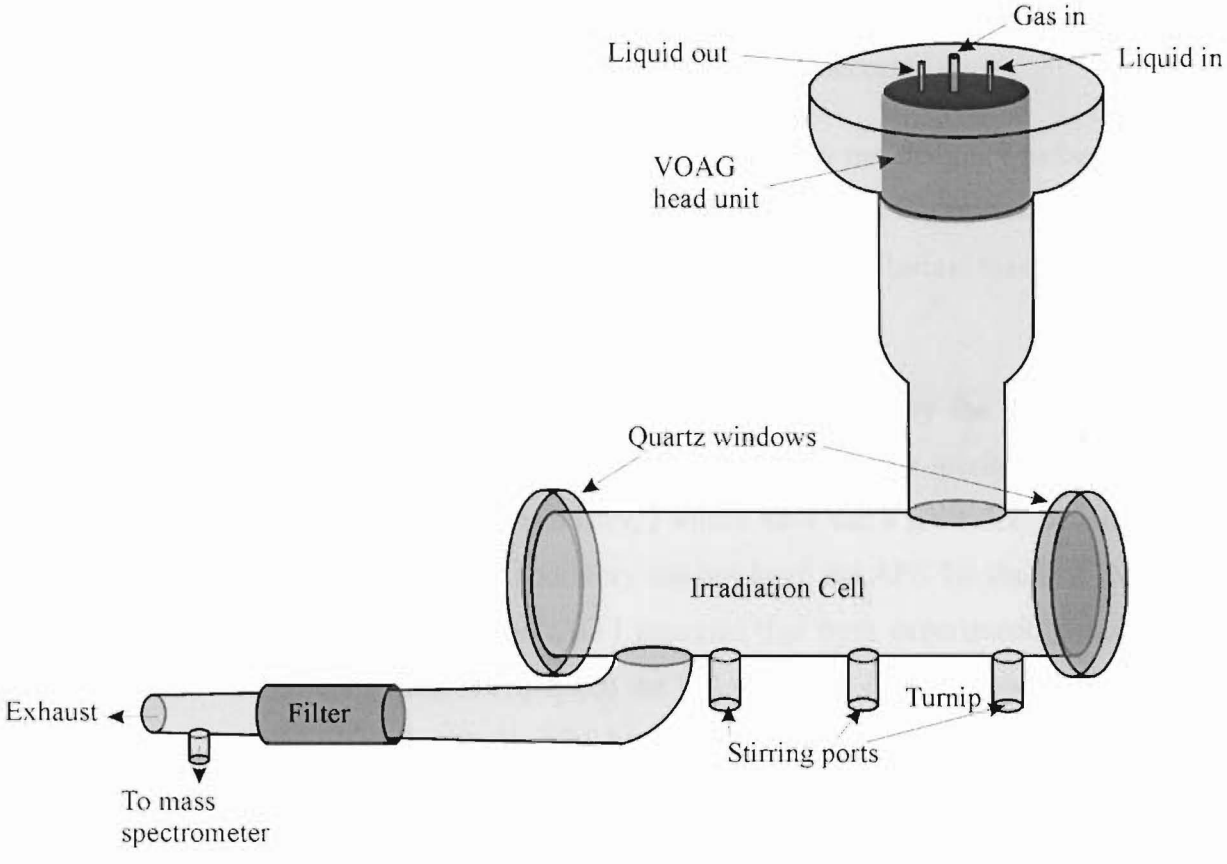

Figure 3.9 Schematic of the first aerosol photochemistry cell

Figure 3.9 and all the other pictures of experimental systems are not scale drawings. For example, the irradiation cell shown in Figure 3.9 is a glass tube with an internal diameter of 35 mm, whereas the distance between the irradiation cell and the VOAG head unit is a little over one metre.

Unfortunately, I was unable to observe any reactions with the VOAG-generated aerosols. I decided that a number of factors could be responsible for this. Firstly, the VOAG may not have been producing enough aerosols to enable the observation of a reaction. Secondly, if the droplet size was an important parameter then it was conceivable that I could be trying to carry

be trying to carry out reactions with droplets of a size that was inhibiting the reaction. Alternatively, the system that I was studying may have just been the wrong one for aerosol photochemistry and photocatalysis. Therefore, rather than trying a reaction at a range of droplet sizes when I was unsure even if it would work at any droplet size I decided to use a polydisperse aerosol. I hoped this would solve a number of problems. For example, it is much easier to produce a high volume of polydisperse aerosol, making any reaction that occurs easier to observe. In addition, if the reaction has a strong dependence on droplet size then the range of droplet sizes present should ensure that some reaction occurred.

This decision shaped the rest of my work and even now I am not certain whether it was a good or a bad decision. In hindsight, I can see that in this decision my mistaken assumption about the usefulness of the mass spectrometer as a tool for monitoring reactions in liquid aerosols influenced me.

Subsequent work on the characterisation of the aerosol produced by the VOAG with the Aerodynamic Particle Sizer has shown that, regardless of the relative merits of polydisperse and monodisperse liquid aerosol photochemistry, I would have had a great deal of difficulty if I had continued with the VOAG. Our laboratory did not have the APS for the first two years of my work, so while I was using the VOAG I assumed that from experiment to experiment the droplet size would be the same if I operated the VOAG under exactly the same conditions. However, the use of the VOAG with the APS has shown that this was not a valid assumption. The VOAG is evidently very sensitive to the operating conditions and it is not actually possible to keep the operating conditions the same from run to run. Stopping the VOAG and refilling the syringe with the same solution, while keeping everything else the same, and then restarting it, generally results in aerosols of a different size or a polydisperse aerosol. Restoring the original droplet size requires adjustments of the gas flow rates and the piezoelectric crystal oscillation frequency. Additionally, the VOAG instructions state that the jet of droplets deflects consistently, as in Figure 3.2a and the aerosol being produced is monodisperse. However, this is not the case. Even though I was not aware of it at the time, this was another reason for switching to polydisperse aerosol.

In building this system, I attempted to incorporate existing nebulisation system equipment into a photochemical system for liquid aerosols. Although it was unsuccessful it did enable me to become familiar with different types of nebulisers.

The nebulisation of liquids is crucial to the function of most engines, it is obviously important in spraying and in the application of thin films like paint, and it is becoming increasingly important in drug delivery. Consequently, there are a large number of systems available for the nebulisation of liquids (Bayvel and Orzechowski 1993). The first system that I tried, I used largely for the historical reason that our laboratory has had a lot of experience with pneumatic nebulisers. The principle of operation of these nebulisers is very simple; they consist of two capillary tubes, one for liquid, and one for compressed air. Pneumatic nebulisers utilise the Bernoulli effect; the alignment of the two tubes is such that the end of the liquid tube is in the low-pressure region that is generated by the gas exciting the gas tube. The low-pressure region at the end of the tube draws the liquid up through the tube and a jet is generated which upon exiting the tube collides with the gas jet and breaks up into aerosols. The biggest advantage of this sort of nebuliser was the possibility of building them in-house from glass.

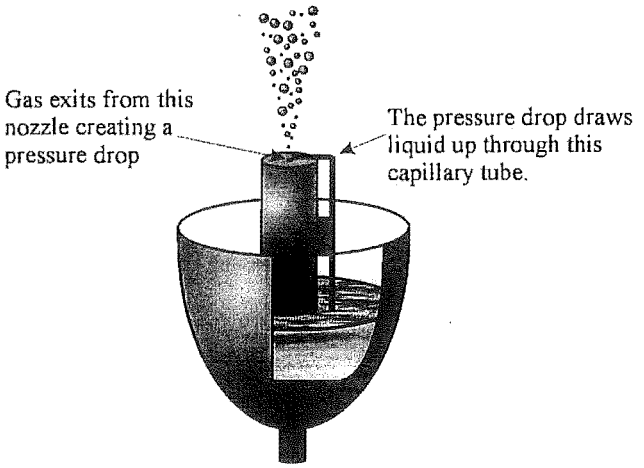

Figure 3.10 The most basic sort of nebuliser

Many, possibly even most, authors would use the word 'atomiser' where I use the word 'nebuliser'. I prefer to use the words nebulise, nebulisation, and nebuliser rather than atomise, atomisation, and atomiser because the double meaning of 'atomise' has caused considerable confusion in discussions about atomic absorption spectroscopy and about aerosol time of flight mass spectrometry. Both of these applications involve the literal atomisation, to atoms, of aerosols.

Previously researchers in my laboratory used this type of nebuliser with a piece of glassware known as the 'turnip'. The turnip is just a turnip-shaped piece of glassware designed to have a nebuliser inserted in one end; from there the aerosol flows into the irradiation cell. I modified the turnip so that it fitted into the irradiation cell, from the first system I built, without modification to the cell. Not only was this less work for me, it also gave the system backwards compatibility. I was still able to use the VOAG delivery system without modifying the system. I continued this modular approach to experimental systems throughout all the work with glass systems. All the glassware I used has quick-fit joints that make the modular approach possible. I used halocarbon wax to seal the joints.

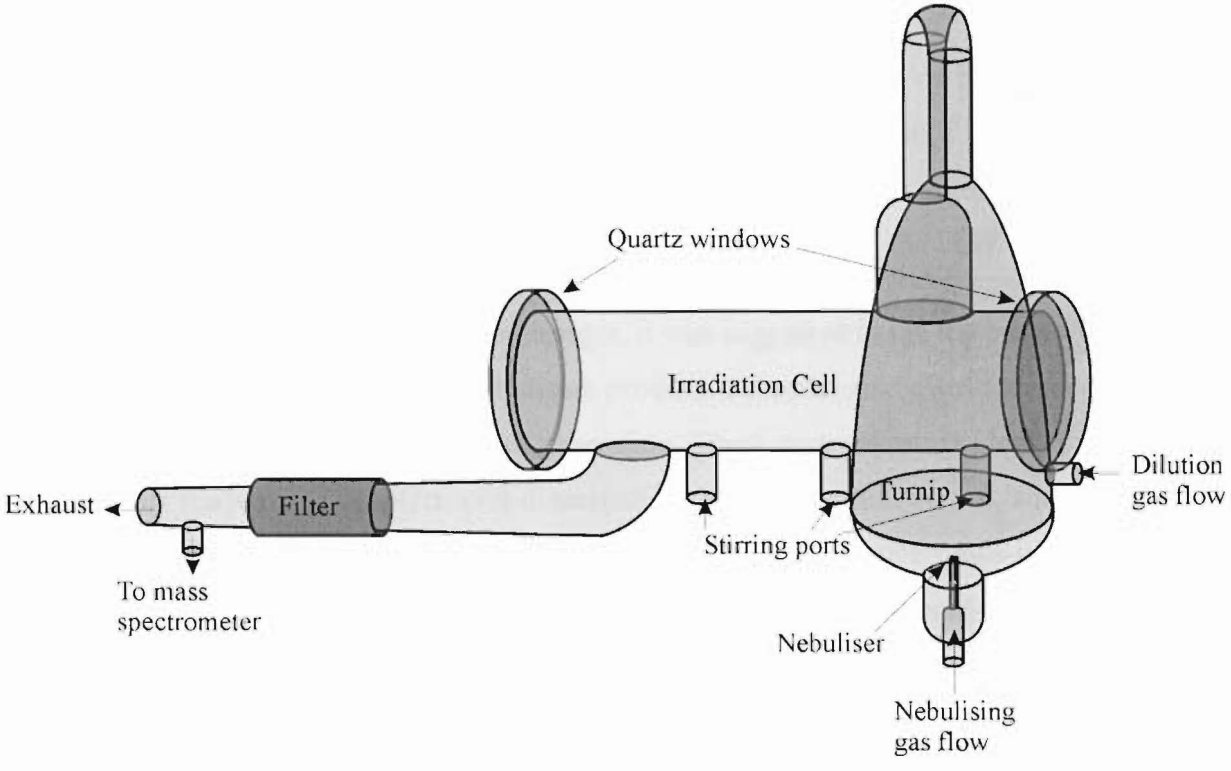

Figure 3.11 The 'turnip' based liquid aerosol photochemistry cell

Unfortunately, trying to make use of previously built equipment, specifically the turnip, was more trouble than it was worth. The most unhelpful feature of the turnip was the quick-fit joint at its base. Either the joint leaked or, when I sealed the joint, the sealant contaminated the liquid. The nebulisers were very fragile, I frequently broke them, and a new nebuliser was never the same as the old one. More importantly, this design of nebuliser (Figure 3.10) proved to be unsuitable for liquid aerosol photochemistry. The particles it produced were too large, and the flow rates required to generate an aerosol were so high that the resultant droplets

flowed so fast that they were resident in the irradiation cell for less than a second. Although a second is sufficient time for a photochemical reaction to occur it is insufficient for the occurrence of a photocatalytic reaction. At this point that I realised that it would be necessary to use a new type of nebuliser.

The turnip system does not really qualify as a liquid aerosol photochemical system because I did not actually use it to do any aerosol photochemistry. In fact, it was really a system for experimenting with different types of nebulisers. While I was working with the turnip system, I realised the necessity of including an impactor in the system. However, because I did not actually get the nebulising aspects of the turnip system working properly I did not include an impactor in the turnip system.

This system was the first successful system for the photochemistry of liquid aerosols that I developed. Incorporating an impactor into the system was vital to its success. Additionally, the use of medical nebulisers provided a relatively reproducible high-volume source of liquid aerosols and the flash lamps delivered substantially more light than the laser.

While I was considering new nebuliser designs, it was suggested to me the possibility of using medical nebulisers. Most medical nebulisers produce a droplet size distribution centred on 2 μm and use a 6 $L \cdot min^{-1}$ flow for aerosol generation. These parameters are ideal as I planned to use aerosols made up of droplets with diameters between 1 μm and 10 μm, and flow rates of between 4 $L \cdot min^{-1}$ and 8 $L \cdot min^{-1}$ ensure reasonable droplet residence times in the irradiation cell. Of the range of medical nebulisers available, the Fisher and Paykel Sidestream nebuliser was chosen, primarily because the local pharmacy sells these nebulisers for less than five dollars.

These nebulisers are also pneumatic nebulisers; they utilise the Bernoulli Effect to produce aerosols. However, their design is considerably more elaborate than the simple two capillary system I had been using (Figure 3.10). The different design enables the production of a finer aerosol with a lower pressure drop across the nebuliser.

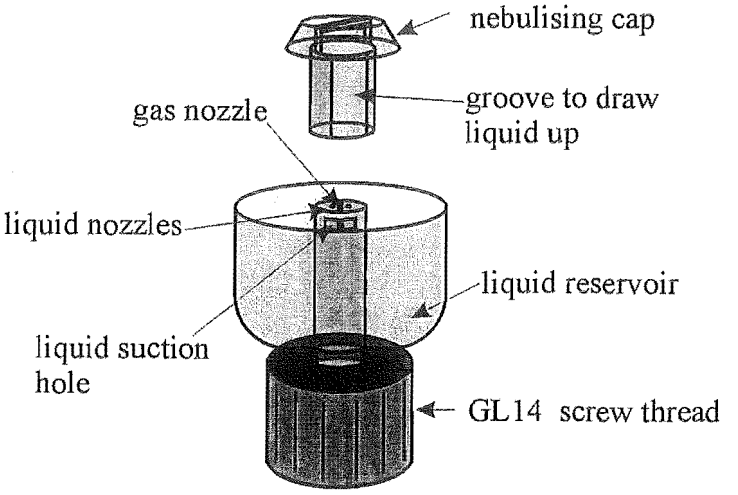

Figure 3.12 The core parts of a Fisher and Paykel Sidestream nebuliser

Fisher and Paykel nebulisers have three parts; Figure 3.12 shows the two important parts. The third part is a baffle that prevents large droplets from leaving the atomiser. The nebulising cap serves a dual purpose. It acts as another baffle and removes any large droplets from the aerosol as they form. More importantly, the stem has internal grooves that leave small gaps between it and the central stem when it is in position. The liquid is drawn up through these gaps and through four nozzles so that four jets of liquid collide with the gas jet to generate the droplets. Figure 3.13 shows the size distribution of decane aerosol produced by a Fisher and Paykel nebuliser

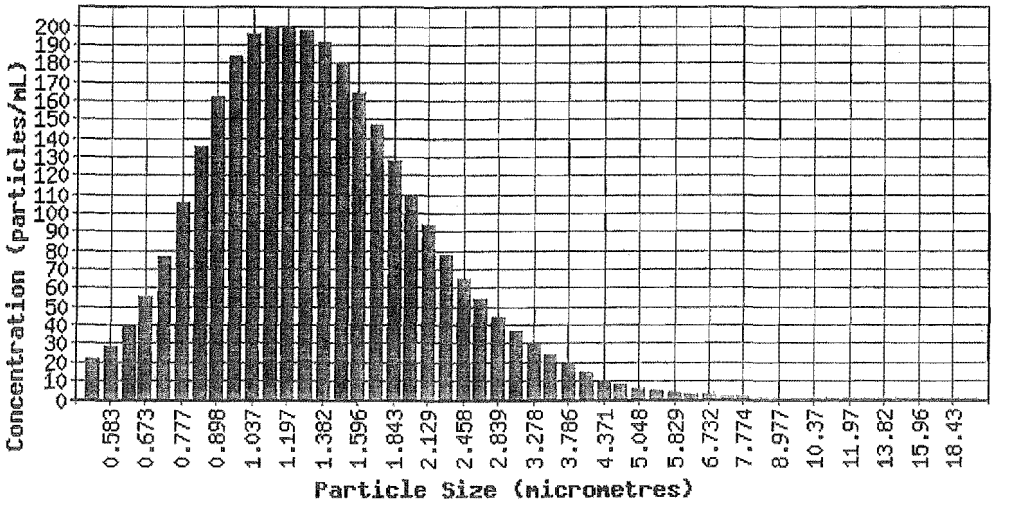

Figure 3.13 Sample output from a Fisher and Paykel nebuliser characterised by the APS

The nebuliser was easily adapted to enable its connection into a glass system. The airflow necessary for nebulisation enters these nebulisers through a ¼" plastic tube at the base of the system. Three pieces that stop the nebuliser from falling over while being filled hindered the airflow port. However, as they were not important to the nebulising function of the nebuliser I cut them off. A ¼" GL14 screw-thread glassware seal was connected to the nebuliser ¼" plastic tube. I tested the quality of this seal, and it only leaked when the pressure was higher than two atmospheres, or when the pressure was lower than a quarter of an atmosphere. Both of these extremes are well beyond my operating conditions.

At the same time as I was investigating alternative nebulisation systems to the turnip, I also decided to stop using the laser as a light source and carry out experiments using broadband irradiation. A number of things motivated this decision. Firstly, Glenn Rowland needed the laser to complete his Ph.D. Secondly, analogous to the decision to switch from monodisperse to polydisperse aerosol, I thought it would be better to first use a thermal lamp to demonstrate that reactions occurred. Once I had a working reaction I could return to the laser and investigate the reaction in more detail. Finally, the work that Glenn did on the laser photochemistry of sulfuric acid aerosol (Rowland 2001) pinpointed a possible danger for my work on the photochemistry of liquid aerosols if I continued to use the laser.

In his work on the laser photochemistry of sulfuric acid aerosol, Glenn observed reactions that were due to multiphoton processes in the aerosol. He had not wanted or even expected multiphoton processes in his system, as he was using an unfocused laser at reasonably low powers. However, an *ab initio* calculation has shown that the longest wavelength radiation that sulfuric acid could possibly absorb is 150 nm. Hence, the requirement for multiphoton processes to explain the photochemical reactions that Glenn observed while irradiating sulfuric acid droplets at 193 nm. The most plausible mechanism for achieving field intensities that were high enough for multiphoton processes to be occurring in Glenn's system invokes morphology dependent resonances. Radiation that is incident on a droplet can be focused inside the droplet if it is resonant with the natural mode of the droplet (Wrenn, Butler, Rowland, Knox and Phillips 1999). Subsequent experimental measurements have determined that the upper limit of the absorption cross-section of sulfuric acid at 195 nm is $< 1 \times 10^{-21}$ cm^2 $molecule^{-1}$ (Burkholder, Mills and McKeen 2000).

Glenn's results were encouraging because he conclusively demonstrated that photochemical reactions occurred in an aerosol system that did not occur in the equivalent liquid phase system. However, because the principle interest of my work is in industrially relevant photochemical reactions in liquid aerosols, the results of his work also suggested that I should not use the laser for my work. In a discussion of applied photochemistry, Donohue (1989) superimposed the operating costs of a krypton fluoride laser and a carbon dioxide laser onto a consumption versus cost plot for a range of commodities and materials. In this analysis, it is only economical to use a krypton fluoride laser in the production of Vitamin D, Marijuana, Ruthenium, Osmium, Palladium, Iridium, Rhenium, Platinum, Gold, Oxygen-18, Cocaine, and Mercury-196. The use of a carbon dioxide laser extends the list to Lithium-7, Silver, D_2O, Uranium-235, and Uranium (Donohue 1989 p. 91). Although this analysis is undoubtedly a little dated, it does make the point very nicely. Lasers are only useful in industry for very high value products. Additionally, the extensive analyses of the laser irradiation of microdroplets have shown that a range of interesting optical effects, including massive intensity enhancements, occur inside the droplets. Therefore, it is not surprising that liquid aerosol laser photochemistry is unique. However, I wanted to demonstrate that liquid aerosol photochemistry with normal light sources was unique. Additionally, when a reactant has a broad absorbance, which essentially all absorbing species in the liquid phase have, thermal lamps can deliver considerably more energy than a laser.

At that time, there was not a suitable continuous emission light source, but there was a Xenon flash lamp system in our laboratory. While I waited for a continuous emission light source, I used the flash lamp system.

The design I used followed a design used previously in our laboratory; I mounted two flash lamps inside a piece of PVC piping that wrapped around the irradiation cell. This meant that the quartz windows were unnecessary, but I did not remove them as I planned to use them again later.

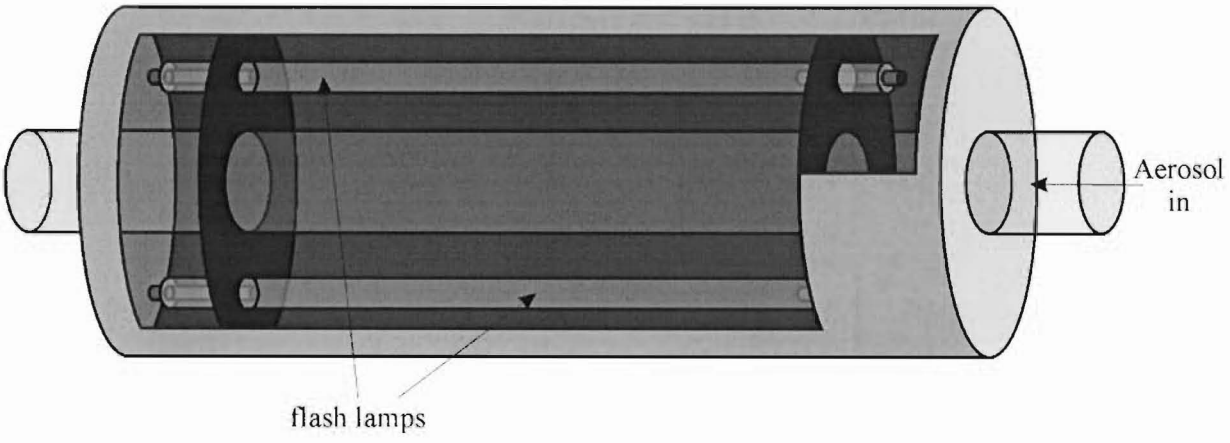

Figure 3.14 Cut-away picture of the flash lamps and the irradiation cell

The first aerosol photochemistry system I built did not have an impactor. Originally, I thought that it would be possible to follow the reaction just using gas phase mass spectrometry. That was not the case and I realised I needed to include an impactor in my system to enable me to collect the aerosol as a liquid and analyse the liquid by the usual techniques that are available to chemists, such as ultraviolet-visible, infrared, and nuclear magnetic resonance spectroscopy.

Most texts on aerosols contain some discussion on techniques of impaction for the collection of aerosols. However, most of these discussions address the impaction of solid or occasionally, involatile aerosols. The requirements for the impaction and collection of liquid aerosol are different to those for solid aerosol.

All impactors follow the same basic design. As their name suggests they are an obstruction in the aerosols' flow path. When the aerosols collide with the obstruction, they are impacted out of the gas flow. Figure 3.15 shows the standard design for most impactors. The gas and aerosol flow impacts upon a plate situated in the middle of the flow.

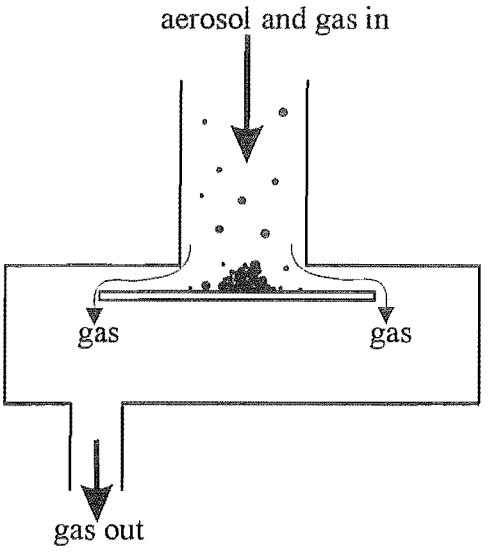

Figure 3.15 The basic design of an impactor

The aerosols' momentum prevents them from turning the corner and so they strike the plate. Gas molecules either bounce off the plate or they avoid it completely. In some systems the plate has a charge in order to ensure that the aerosols stick. The plate configuration is not appropriate for a liquid aerosol impactor. Liquid aerosols not only require impaction out of the gas flow, but also containerisation once they are collected.

Thanks to the highly-skilled glass blowers, I was able to experiment with a number of different impactor designs. Figure 3.16 shows the general design that I used.

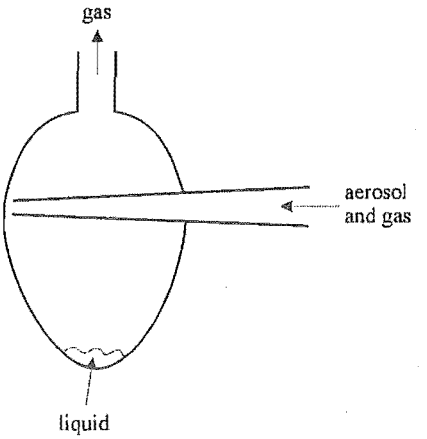

Figure 3.16 Schematic of impactor design that I used.

The body of the impactor is a pear shaped flask. A tapered tube introduces aerosol into the impactor through a tapered tube. The tube finishes as close as possible to the internal wall of

the flask. The aerosol accelerates as the tube tapers and it then collides with the wall. The liquid runs down into the bottom of the flask while the gas flows upwards without forcing the liquid up and out of the flask. This design of impactor is certainly not one hundred percent effective and it is likely that particle bounce resulted in the re-suspension of some particles. However, in general I was able to collect ~80% of the mass that was nebulised and this was sufficient for my analytical work.

The system (Figure 3.17) required extensive changes in order to incorporate the new nebulisers, the flash cell assembly, and an impactor. All that remained from the turnip system was the irradiation cell and its aerosol entry and exit ports.

A 180° turn in a 45 mm internal diameter glass tube replaced the turnip. One end of this connected to the irradiation cell and the other end was a large joint. The Fisher and Paykel nebulisers are full of little holes and leaks so this joint sealed the whole nebuliser inside the system. Any additional dilution or reactive gas that an experiment required entered through a side port that was level with the nebuliser outlet.

It was necessary to remove the stirring ports from the bottom of the irradiation cell so that the flash cell assembly fitted around the cell. However, they were no longer required as there was nowhere in the cell that was not being irradiated. When comparing Figure 3.17 and Figure 3.11 it appears that the irradiation cell is longer in the flash cell system. This is a feature of the drawings and is not actually the case. The irradiation cells were the same length.

The final modification that this system required was the removal of the filter assembly and its replacement with an impactor. The tapered tube and the impactor were a single seal unit that connected to the exit port with a Quik-fit seal. A stopper in the top of the impactor enabled the removal of liquids for analysis. The mass spectrometer sampled the gas stream after the impactor; this configuration prevented aerosols from entering the mass spectrometer and burning the filament out.

I observed a number of promising liquid aerosol photochemical reactions in the flash lamp system. The incorporation of an impactor into the system was a very important development as it greatly extended the range of analytical techniques that I could use to monitor the reactions. The medical nebulisers worked very well and I used that design for the rest of my

work on liquid aerosols with the only major disadvantage being that the nebulisers are plastic and this prevented the use of some solvents.

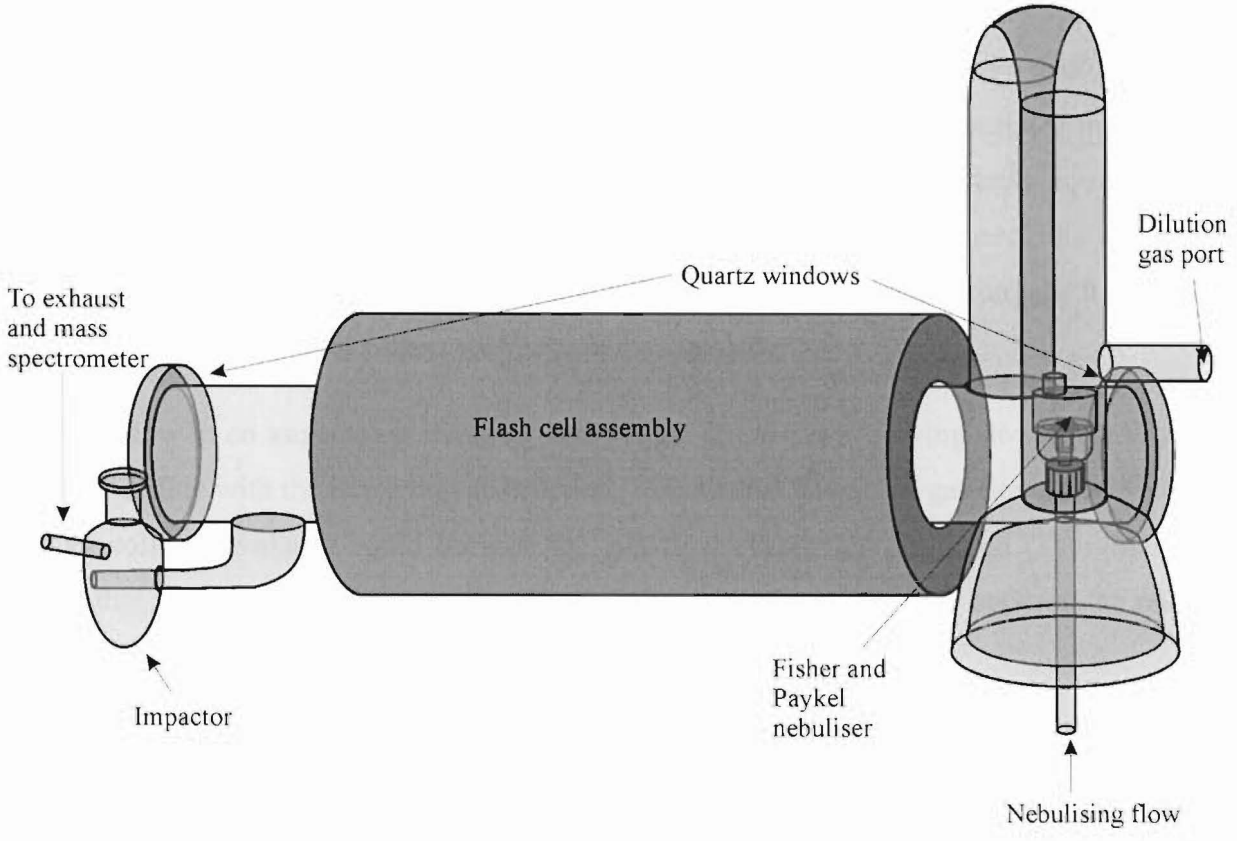

Figure 3.17 The flash cell system

One drawback of the configuration used in the flash lamp system is that the light enters the cell through the glass sides of the system rather than through the suprasil quartz ends. Additionally, the close proximity of the lamps to the cell also means that the lamps heat the cell up. The chemistry that takes place in this system is a mixture of photochemistry and thermal chemistry. This is not a particularly desirable situation as it makes it difficult to understand the reactions that are taking place. The reconstruction of the cell out of quartz with a water-cooling jacket could have solved these problems. However, this would have been both expensive and difficult to construct and an easier solution was to use a different light source in a different configuration.

When the high-pressure xenon lamp arrived, I rearranged the system and returned to the configuration where light source irradiated the aerosols through the suprasil quartz windows at the end of the cell, rather than through its glass sides. To house and power the lamp I used a system that was built for xenon lamps more than thirty years ago. With new wiring and clean electrical connections, it still worked well.

The type of impactor used in the flash lamp system (Figure 3.16) works very well for liquids like decane and glycerol, but is inappropriate for volatile liquids. The process of impacting a volatile liquid aerosol out of the gas flow is no different to that for an involatile liquid aerosol. The difficult part is keeping the volatile liquid after its collection. In general, the volume of volatile liquid the impactor collected was the same in every experimental run, and it was quite independent of the amount of aerosol entering the impactor.

The gas flow in an impactor is inevitably very high. If the gas is moving slowly, the droplets will not collide with the impacting obstruction. Vessels that have high gas flows through them cannot collect a volatile liquid because the gas flow evaporates the liquid. The volume of liquid that an impactor collects represents the formation of a steady state between the rates of liquid collection and liquid evaporation.

One way of handling volatile aerosols is to use gas that is saturated with the liquid before it enters the aerosol system. The vapour pressure of a liquid in a droplet depends on the droplet size complicating the requirements for controlling the saturation. However, even when a saturated gas preferentially stabilises certain droplet sizes, the use of saturated gas is still constructive. Unfortunately, saturated gas does not prevent evaporation in an impactor. When I used water saturated gas the amount of water that the impactor collected was more than that for dry gas, but the volume collected was still independent of the amount of aerosol entering the impactor. The gas flow through the impactor must have been so high that the liquid evaporated anyway. The presence of saturated gas decreases the rate of evaporation, but not enough to prevent the formation of a steady state.

The easiest way to collect volatile liquids is to use a cooled impactor (Figure 3.18). Cooling the impactor to a temperature below the freezing point of the aerosol effectively turns a volatile liquid aerosol into a solid aerosol. Further cooling does not increase the amount of liquid collected. When working with aqueous aerosols, ice, NaCl-ice-water eutectic, and dry

ice-ethanol mixture cooling solutions all result in the same amount of liquid being collected. The most important difference between a cooled impactor and a normal impactor is the position of the tapered nozzle relative to the internal wall of the impactor. Unlike normal impactors, the nozzle should not be close to the wall in a cooled impactor. If the nozzle is too close to the wall, the freezing liquid blocks up the nozzle and stops the gas flow into the impactor. When the only way for gas to get out of the system is through the impactor, the result of a blocked impactor is a broken system.

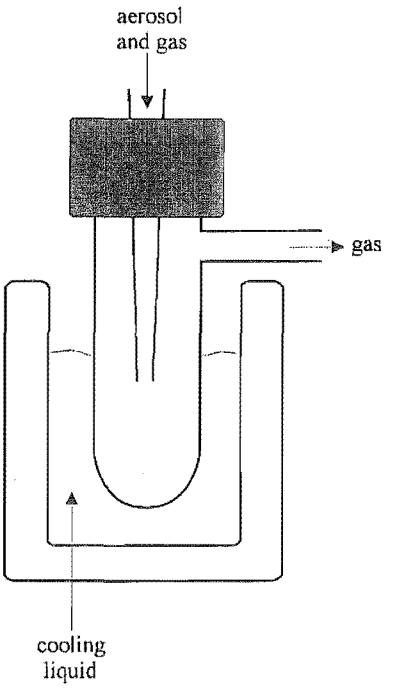

Figure 3.18 Schematic of a cooled impactor.

The use of the high-pressure xenon lamp required the removal of the flash lamp assembly and the replacement of the stirring ports. I doubled the length of the irradiation cell in order to increase the amount of time that aerosols were resident in the irradiation cell. The exit port needed minor alterations for use with the cooled impactor system. A significant modification in this system was a change in position of the mass spectrometer sampling port. When the impactor coolant was dry ice and ethanol, some of the products could freeze in the impactor. This change also enabled the sampling of the gas phase immediately after the irradiation of the aerosol, rather than after it had passed over a reservoir of liquid that it was soluble in.

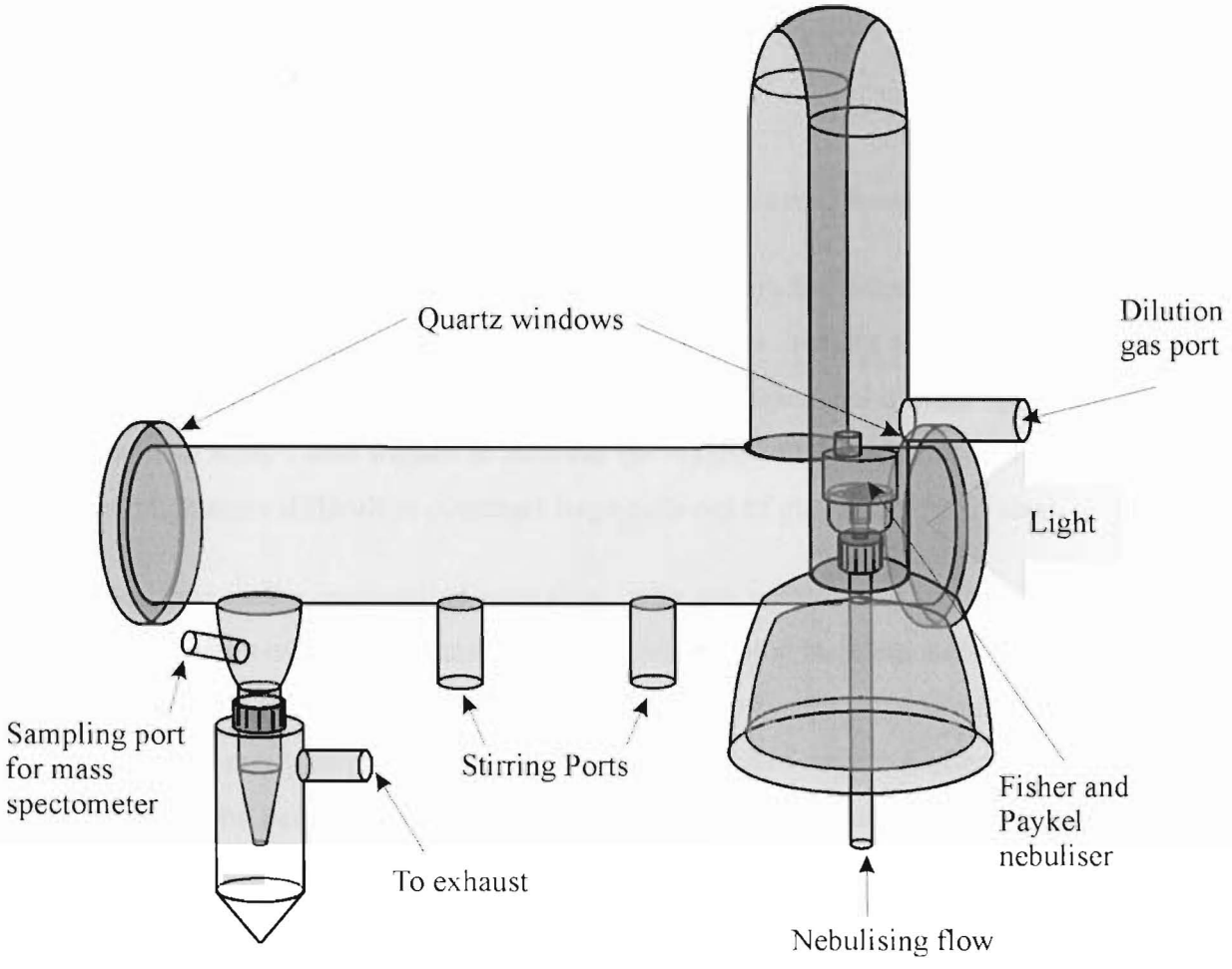

Figure 3.19 The high-pressure xenon lamp and cooled impactor system

The utilisation of a cooled impactor extended the range of solvents that liquid aerosol photochemistry could be carried out it. However, even when it is possible to collect volatile liquid aerosols, in this sort of system it is to determine the parameters that describe what is happening in reactions involving volatile liquid aerosols. Due to evaporation, the concentration of species in the droplets cannot be known. It is also possible that the reactions are taking place entirely in the gas phase. Therefore, although the collection and analysis of volatile liquid that have been nebulised and irradiated is possible, it does not imply that liquid aerosol photochemistry has taken place.

One advantage of aerosol photochemistry is that the droplets scatter a lot of the light that is incident on them. This ensures a more homogeneous distribution of light absorption than is possible in liquid phase photochemistry. Unfortunately, the use of glass irradiation cells for liquid aerosol photochemistry turns this advantage into a disadvantage. Droplets not only

scatter light for absorption by other droplets, but they also scatter it out through the sides of the cell.

3.3.3 A Liquid Aerosol Photochemical System Constructed from Stainless Steel

In order to address the problem of light being lost through the sides of the irradiation cell, I considered silvering the surface of the irradiation cell to create a mirror. However, a more practical approach was to design and build a new photochemical system for liquid aerosols out of stainless steel. I also wanted to increase the residence time of aerosols in the irradiation cell. It is much more difficult to construct large cells out of glass than out of steel.

The technicians in the mechanical workshop, who are very skilled, were able to copy and improve the design of the Fisher and Paykel nebuliser using stainless steel. The use of a steel nebuliser addressed the final weakness of the previous system; it was never possible to be completely sure that plasticizers from the plastic nebulisers were not affecting the chemistry in the system. The performance characteristics of the steel nebuliser are virtually identical to those of the medical nebulisers.

One of the major changes in the steel system was in the orientation of the irradiation cell. In the steel system, the Xenon lamp was mounted above the cell and the light was directed downwards onto the aerosol as it fell down the steel tube. An additional advantage was that the vertical orientation meant there was no longer any concern about aerosol collecting on the bottom surface of the irradiation cell because there was no bottom surface. The internal wall of the irradiation was polished to be as shiny as steel can be. Although this was still an imperfect optical surface, the percentage reflection was much greater than the percentage reflection from a glass surface. It also made it much easier to work in the lab because there was no longer any UV light leaking into the lab and I now knew that virtually all 400 W of light were going into the cell. This also made it much easier to carry out experiments with light sensitive solutions because once the solutions were inside the system I could turn the lights in the lab back on. The internal diameter of the irradiation cell was 95 mm and the cell was 70 cm long. Light entered the cell through a 50 mm quartz window in the top of the cell. Although this was smaller than the internal diameter of the cell, I was not concerned because in this system unlike the horizontal irradiation systems the aerosol cannot sink below the

beam of light. Light entering the cell vertically would be scattered throughout the cell by the aerosol in the cell.

At the bottom of the irradiation cell, the entire diameter of the cell tapers down into a thin nozzle that exits into the impactor. The impactor is vertical to accommodate the cooling of the impactor when using volatile liquid aerosols. To reduce evaporation from the impactor I used a curved jet for the impactor so that the airflow from the nebuliser was not passing directly over the collected liquid reservoir.

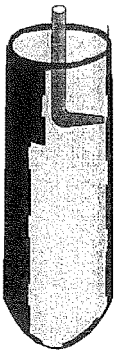

Figure 3.20 Cut-out view of final impactor

Figure 3.21 is a photograph of the steel system. I mounted the whole system on a scaffold on top of a bench. The final height of the nebuliser was about head height. During the irradiation of a non-toxic aerosol I removed the impactor to see how much light was coming out of the irradiation cell and into the impactor. Light from the impactor was only visible when the lights in the laboratory were off.

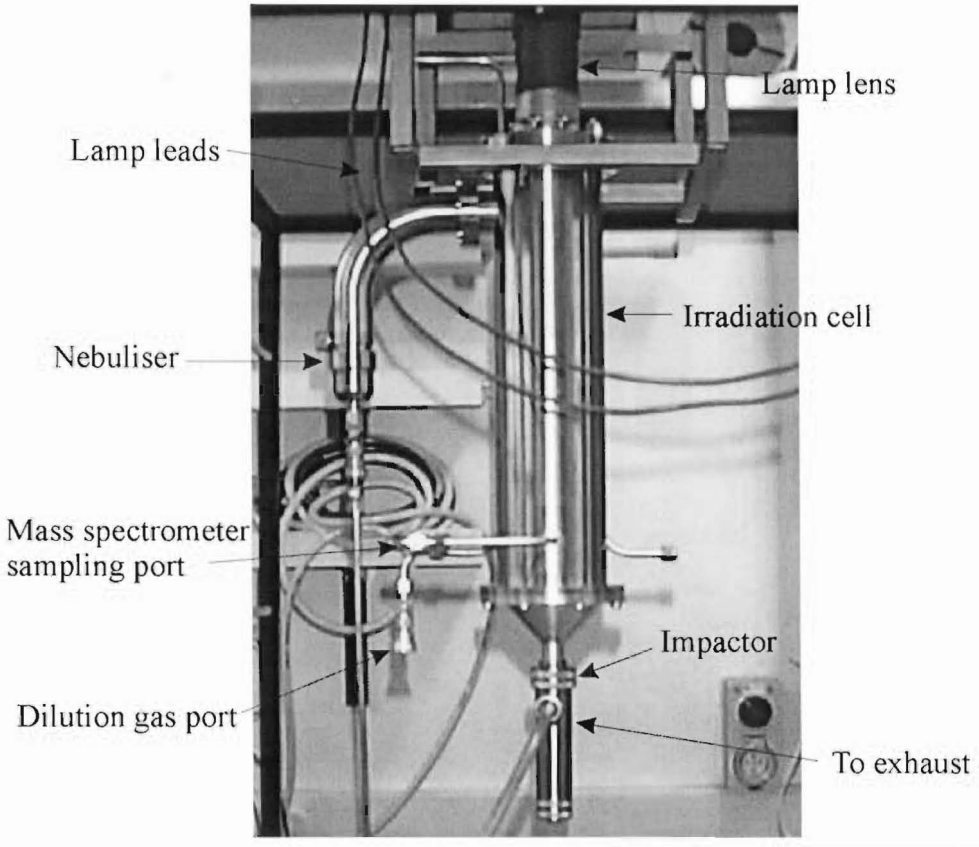

Figure 3.21 A photograph of the Steel System for Studying the Photochemistry of liquid aerosols

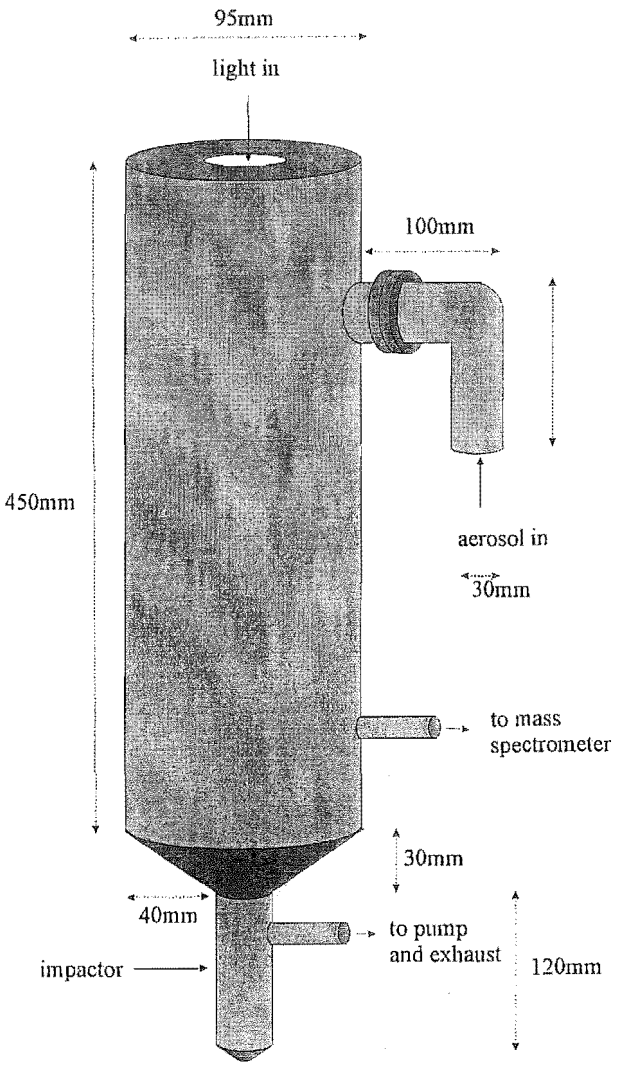

Figure 3.22 Schematic of the steel system

4 The Investigation of Liquid Aerosol Photocatalysis

One of the most promising applications of liquid aerosol photochemistry is in industrial catalysis. The majority of my work has been devoted to the investigation of liquid aerosol photocatalysis. In this chapter, I first outline why liquid aerosol photochemistry has applications in industrial catalysis. Then follows a discussion of the experimental work I carried out on liquid aerosol photocatalytic systems.

4.1 General Discussion of Industrial Catalysis

The role of catalysts and catalysis in the chemical industry is very important. The vast majority of industrial catalytic reactions use surface catalysts. Below is a brief discussion of the reasons for this, and of some of the ways of modifying molecular catalytic processes to make them more suitable for use in industry.

4.1.1 Terminology

In most catalysis literature, the terms homogeneous catalysis and heterogeneous catalysis are unambiguous and therefore suitable for the classification of various types of catalysis. However, this discussion addresses issues such as the heterogenisation of homogeneous catalysis and biphasic catalysis. In this situation, the classification of homogeneous and heterogeneous catalysis loses its meaning and even becomes misleading. Therefore, it is appropriate in this discussion to adopt alternative terminology. Although the majority of the literature that addresses these issues attempts to use the terms 'homogeneous' and 'heterogeneous', I shall use the more accurate terms: molecular catalysis and surface catalysis.

4.1.2 Issues in Industrial Catalysis

Many industrial catalytic reactions involve gaseous reactants. In these reactions gas transfer processes are very important. Ideally a chemical reactor design should ensure that

the transfer of gaseous reactants to a catalyst is not rate limiting unless an excess of reactants at the catalyst results in undesirable products.

It is convenient to classify industrial catalytic reactions by their reaction pressure. Typically, three pressure ranges are used. The high-pressure processes (~ 300-400 bar), the medium-pressure processes (~100-250 bar), and the low-pressure processes (~ 50-100 bar) (for example Weissermel and Arpe 1993 p. 29). The fact that a low-pressure process is one that uses between 50 and 100 bar is testimony to the importance of gas transfer processes. Although it must be remembered that in some processes high pressure is necessary to activate the reaction; i.e. the catalytic species only exits at high pressure. Additionally, some catalysts have longer lifetimes at high reaction pressures. However, in many situations the high pressure is required to ensure reasonable gas-transfer rates. In these cases achieving necessary gas-transfer rates at lower pressures would be very beneficial.

Table 4.1 (reproduced from Cornils and Herrmann 2000 p. 5) lists the important characteristics of an industrial catalytic system and describes the general usefulness of surface and molecular catalysts.

Table 4.1 Comparison of homogeneous and heterogeneous catalysis

	MOLECULAR CATALYSIS	SURFACE CATALYSIS
ACTIVITY (RELATIVE TO METAL CONTENT)	HIGH	VARIABLE
SELECTIVITY	HIGH	VARIABLE
REACTION CONDITIONS	MILD	HARSH
SERVICE LIFE OF CATALYSTS	VARIABLE	LONG
SENSITIVITY TOWARDS CATALYST POISONS	LOW	HIGH
DIFFUSION PROBLEMS	NONE	MAY BE IMPORTANT
CATALYST RECYCLING	EXPENSIVE	NOT NECESSARY
VARIABILITY OF STERIC AND ELECTRONIC PROPERTIES OF CATALYSTS	POSSIBLE	NOT POSSIBLE
MECHANISTIC UNDERSTANDING	PLAUSIBLE	MORE OR LESS IMPOSSIBLE

From the analysis in Table 4.1, it appears that molecular catalysis is superior to surface catalysis in many respects. The conditions required for molecular catalysis are milder, and

they continue to get milder as catalysts improve. Molecular catalysts are more selective, more active, and invulnerable to poisons. It is perhaps surprising then that the ratio of surface to molecular catalysis use in industry is 85:15.

Surface catalytic reactions take place in either fixed bed reactors, where the reagent mixture flows over a fixed catalytic surface, or suspension reactors, which use a suspension of catalytic particles. In a fixed bed reactor there is no need to separate the products from the catalyst, and filtration will separate the reaction mixture from a suspension reactor.

The weakness of molecular catalysis is that techniques for catalyst recycling are either expensive or impossible. The extraction of a molecule for a reaction mixture that it is soluble in has never been an easy process. In many reactions the problem of catalyst recycling outweighs all the other benefits of molecular catalysis. This is especially true of transformations that are possible using both surface and molecular catalysis. Traditionally molecular catalysts have only found use in industry for reactions that are not possible using a surface catalyst. There are of course processes where surface catalysis is simply better than a molecular catalysis. However, resolution of the problem of recycling molecular catalysts would increase their use in industry.

The difficulty of recycling molecular catalysts is actually a two-fold weakness. Firstly, there is the obvious weakness that not recycling catalysts is expensive . This is becoming more important as the cost of elaborate ligands trivialises the cost of the metals in the catalysts. For example, the cost of 2 grams of 99.8% rhodium powder is US$396 and the cost of 2 grams of the rhodium based hydrogenation catalyst $Rh(C_8H_{12})(C_{18}H_{28}P_2)CF_3SO_3$ is US$1104 (Strem 2001-2003). The cost per mole of rhodium is US$20,394 and of the catalyst is US$324,024. The comparison is not quite fair as the expensive catalyst has a much greater activity and selectivity, but it still highlights the importance of catalyst recycling.

From an industrial point of view, continuous processes are preferable to batch processes (Tundo, Moraglio and Trotta 1989). The labour costs and dead time associated with a batch reactor are much higher than for a continuous process. Consequently they are usually only used for low production, high-value products such as specialty chemicals and

pharmaceuticals (Froment and Bischoff 1990 p. 305). Here lies the second problem in recycling molecular catalysts: surface catalytic reactions are innately continuous; it is simply a matter of flowing the reactants and products over the catalyst or through a tank of suspended catalytic particles. However, the difficulty of separating catalysts from products often makes molecular catalytic reactions more like batch or semi-batch reactions rather than continuous reactions. Molecular catalytic reactions are possible in continuous processes if the catalyst is discarded rather than recycled, but this only highlights the problem.

Surface catalytic processes are preferred in industry not only because they facilitate continuous processes, but also because the catalyst is immobilised relative to the continuous process. Immobilisation of a catalyst does not imply making the catalyst stationary. Immobile components are those that remain in, as opposed to passing through, a continuous system. Thus, the surface catalysts in fixed bed reactors are both immobilised and stationary, because the reactants flow over them. Surface catalytic particles in a suspension reactor are immobilised but not stationary; a filter at the end of the suspension reactor ensures that the catalysts remain in the system while the reagents flow through the system. Even when molecular catalytic reactions are adapted for continuous processes the catalysts cannot be immobilised because they are soluble in the reactant mixture.

In addition to cost there is increasing concern about the environmental consequences of the chemical industry (Anastas and Warner 1998). More efficient chemical process design that leads to greater retention of any of the materials used, especially expensive catalytic materials, has both an economic and an environmental benefit.

Systems that contain immobilised catalysts are naturally suited to the industrial requirements for continuous systems and catalyst recycling. By definition, surface catalysts are immobilised. This is why surface catalysts are so prominent in industrial chemistry. It is also why a considerable amount of work has been devoted to the immobilisation of molecular catalysts.

The usefulness of molecular catalysis is sufficiently great that, despite difficulties outlined above, considerable effort has been devoted to resolving the problems of catalyst recycling.

Most of the techniques attempt to immobilise molecular catalysts (Cornils, Herrmann, Horváth, Panster, Wieland, Basset, Niccolai, Schmind and Bahrmann 2000).[i]

There are two principle ways of immobilising molecular catalytic systems: biphasic liquid immobilisation and anchored immobilisation. Anchored immobilisation is the physical anchoring of a catalyst to an inert material, making it much more like a surface catalyst. Ideally, the attachment process does not destroy any of the properties that make the catalyst a good molecular catalyst. Some of the inert materials used are polymers, colloids, or fixed surfaces. Anchored immobilisation attempts to create systems that combine the advantages of molecular catalysis, particularly steric control and selectivity, with the ease of industrial application of surface catalysts. Anchoring molecular catalysts to fixed surfaces and colloids allows the use of anchored catalysts in the same sort of system as that used for surface catalysts. Anchored immobilisation is a challenging chemical problem and is more complicated and therefore less successful than biphasic immobilisation.

Biphasic liquid immobilisation is the use of a system consisting of two immiscible liquid phases; one in which the reactants and products are soluble and the other in which the catalyst is soluble (Fish 1999, Cornils and Hermann 1998). Many authors simply call this biphasic immobilisation or biphasic catalysis, but these terms are not adequate for the present discussion. Cornils and Herrmann (Cornils et al. 2000 p. 578) define biphasic liquid immobilisation systems as only those systems

1) which use no additional measures – except for moderate temperature gradients – to ensure the phase separation (e.g., the application of solvents or co-solvents, chemical derivatisation), and

2) which make possible the immediate start of new catalyst cycles in the same phase and without any additional steps.

The two phases are usually water and an organic liquid. The catalyst is generally an aqueous phase catalyst, and the reactants and products are organic (Cornils and Hermann 1998). Two factors dictate the use of the aqueous phase as the catalytic phase. Firstly, it is

---

[i] The immobilisation of molecular catalysts is often called the heterogenisation of homogeneous catalysis.

necessary to modify the majority of organometallic catalysts to make them stable in the presence of even tiny amounts of water. Once modifications to the catalyst begin, it makes sense to continue and make the catalyst soluble in water as well. Ultimately, the choice of the phase depends on the solubility of the products and reactants. If they are soluble in organic liquids and insoluble in water then the aqueous phase is the catalytic phase and vice versa. The second reasons most biphasic catalytic systems use water as the catalytic phase is that most of the products produced in the chemical industry are soluble in organic liquids.

The ease of molecular catalyst recycling in biphasic liquids means that the technique is not only useful in continuous industrial processes, but also in laboratory-scale batch reactions. Thus, it is helpful to make a distinction between biphasic liquid catalysis and biphasic liquid immobilisation. The use of biphasic liquids in batch process molecular catalysis is defined as biphasic liquid catalysis. The system is catalytic but not immobilised, because the term is only meaningful in a continuous process.

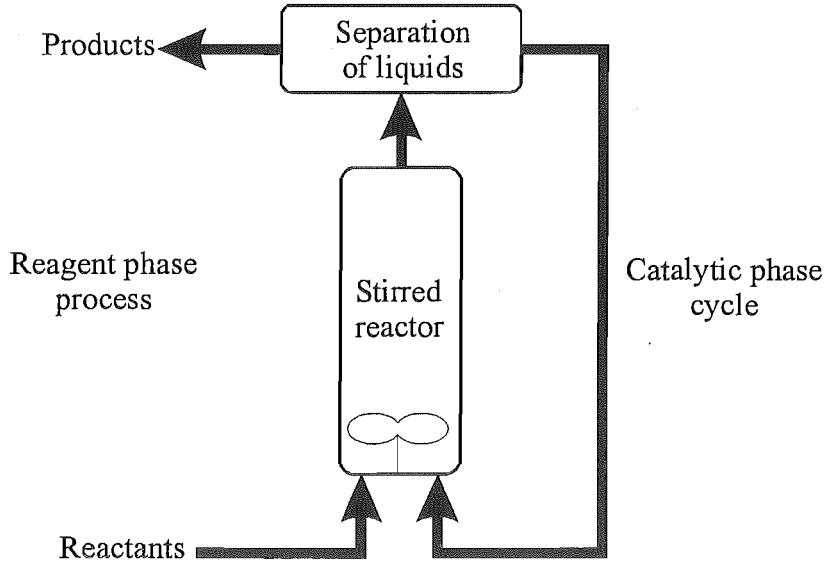

Figure 4.1 Schematic of biphasic immobilisation process

It is possible to convert biphasic liquid catalysis into biphasic liquid immobilisation by using what is essentially two continuous processes (Cornils and Hermann 1998 pp. 167-168). The catalytic process is cyclic; the catalyst flows through the stirred reactor, into a separation vessel, and then returns into the reactor. The catalytic cycle can contain catalytic regeneration if necessary. In the reagent process, reactants enter the reactor and react to

become products. After the separation of the products and the catalytic phase, the products leave the system. A decanter separates the liquid phases (Figure 4.1).

Biphasic liquid immobilisation has been so successful that only ten years passed between the first demonstration of the method and the construction of a biphasic liquid immobilisation plant with an annual output of 100000 t of formaldehyde (Cornils and Hermann 1998 back cover).

Very few authors make a distinction between biphasic liquid immobilisation and biphasic immobilisation, because until now they have been virtually synonymous. However, liquid aerosol catalysis is a biphasic immobilisation technique that uses gas and liquid phases, rather than two liquid phases.

4.1.3 Liquid Aerosol Catalysis

In liquid aerosol catalysis, as distinct from the solid aerosol catalysis of Glikin (1996) and Weber et al. (2001), a molecular catalyst is dissolved in a liquid and the liquid is then nebulised into an aerosol. The reactants enter into the system as gases or vapours or they are included in the liquid prior to nebulisation. When the reaction is photocatalytic, an appropriate light source irradiates the liquid aerosol. The use of a liquid aerosol system for catalysis fits within the definition of process aerosol chemistry. In liquid aerosol catalysis, the morphological properties of aerosols are used, not to influence the structure of the product, but to alter the reactivity of the system.

Liquid aerosol catalytic systems are not necessarily immobilisation systems. Whether or not a particular aerosol system is also an immobilisation system will depend on the volatility and solubility of the products. Thus, liquid aerosol catalysis is not as versatile an immobilisation technique as biphasic liquid techniques are. Liquid aerosol catalysis is not an alternative to biphasic liquid immobilisation, but rather it is useful in situations were biphasic liquid immobilisation is not appropriate. Liquid aerosol catalysis not only addresses issues of molecular catalyst recycling, but the properties of aerosols also offer additional enhancements for aerosol catalytic systems. For example, aerosol systems provide access to reactivity that is not generally available in liquid phase systems. The superior rates of gas-liquid transfer in aerosol systems enable the reduction of the operating

pressure of catalytic systems. Furthermore, the nature of the interaction of light with microdroplets improves photocatalytic systems.

One could argue that while liquid aerosol catalysis is a biphasic immobilisation technique, this is simply a case of giving a fancy name to an obvious process; there is nothing special about separating products from the catalyst when the products are a gas and the catalytic phase is a liquid. However, the existence of gaseous products still does not guarantee that product separation will be simple. Liquid aerosol catalysis utilises the physical properties of aerosols to enhance the gas-liquid transport processes. In many industrial processes, high pressures are necessary because the rate of gas-liquid transfer is kinetically, rather than thermodynamically limited. It is therefore quite likely that the liquid-gas transfer rate will also be slow. Additionally, liquid aerosol catalysis extends the range of the gas phase; volatile liquid species are effectively vaporised in liquid aerosols systems.

The physical properties which allow liquid aerosol catalysis to separate products from the reaction phase are the enhanced rates of gas-liquid and liquid-gas transfer that characterise aerosol systems. The most common way to separate volatile species from reaction mixtures is to heat the mixture. However, aerosol systems can facilitate the evaporation of volatile components without heating, which decrease the energy requirements of the process, or remove the requirement for heat stable catalysts.

The vapour pressure of volatile components that are generated inside an aerosol droplet is very large. Provided that the reaction is not extremely fast the vapour pressure will remain high and the volatile components become effectively gaseous. Thus, in a liquid aerosol immobilisation system the droplet phase is the immobilised catalytic phase and the gas/vapour phase is the continuous phase.

This enables a very simple separation of products from the reactant mixture. Impaction or filtration of the aerosol is sufficient to recover the catalyst. This is a simple technique; therefore, aerosol catalysis is a 'true' biphasic immobilisation system according to Cornils and Hermann's definition. However, I do not want to include aerosol catalysis under the umbrella definition of biphasic immobilisation catalysis because the separation of the catalyst from the products in aerosol systems makes use of different physical properties.

If the reaction used a volatile aerosol, this would be ineffective, but liquid aerosol catalysis uses involatile solvents like decane and glycerol. If the product were something like methanol then it would be relatively easily to separate from glycerol. Of course, if the products of a reaction were involatile then the aerosol phase would not be useful for assisting in the separation of the products from the catalyst. In considering catalysis and separation techniques, aerosol catalysis is not going to replace techniques like aqueous/organic biphasic or fluorous/non-fluorous biphasic catalysis, but rather it will be useful in situations where these already established techniques are not suitable. This might include systems where the reaction is not possible in two liquid phases and the products are both volatile and soluble in the reaction phase.

Liquid aerosol catalysis is not just another technique for the immobilisation of molecular catalysts. One of the other benefits of liquid aerosol catalysis is the possibility of enhanced reactivity at the gas-liquid interface.

Liquid aerosol catalysis uses molecular catalysts, although catalysis in liquid aerosol systems is not necessarily restricted to catalysis by molecular species. Studies of atmospherically relevant aerosol chemistry reactions have suggested that reactions are occurring at and being influenced by the gas-liquid interface itself (Finlayson-Pitts and Pitts 2000 pp. 158-163). Unfortunately, very little is known about liquid-surface specific reactivity; for instance it is not known whether this type of reaction is peculiar to the water-air interface, or whether it is a general property of liquid surfaces. Even if surface reactions are not a property of liquids like decane, it is conceivable that the reactivity of an organometallic catalyst dissolved in decane could be different at the surface than in the bulk.

4.1.4 Liquid Aerosol Photocatalysis

The promise of liquid aerosol catalysis increases even more when liquid aerosol photocatalysis is considered. Liquid aerosol photocatalysis takes advantage of the photochemical properties of liquid aerosols as well as the physical properties.

Obviously, in a photocatalytic system increased light intensity is a good thing. One limitation in liquid phase photochemistry is the relatively small penetration depths of light

into the liquid. If all the light that is absorbed is used for reactive processes then this is not a problem. However, a significant absorption of light in the first few millimetres of a liquid will result in a high concentration of reactive excited state species in that region, but other reactants will be evenly distributed throughout the liquid and will not present sufficient concentration in the irradiated area to react with the excited state species. This will result in a considerable portion of the excited state reactants relaxing back into their non-reactive ground state before encountering a reactant. In an irradiated aerosol the motion of the aerosol droplets and the scattering of light from the surface of aerosol droplets should make the distribution of light absorption by the liquid far more.

4.2 Hydrogenation

Having decided that liquid aerosol catalysis was a good idea the first thing that I wanted to do was demonstrate that liquid aerosol photocatalysis worked for a well-known and relatively well-characterised reaction. Reactions catalysed by transition metal carbonyls are one of the most studied classes of photocatalytic reaction (Roundhill 1994 p. 248). Transition metal carbonyls catalyse a large range of reactions, in both the liquid and gas phase, including hydrogenation, hydrosilation, isomerisation, polymerisation, and metathesis of alkenes and alkanes (Ibid. p. 221, Szymanska-Buzar 1997).

I chose to try hydrogenation of ethylene in the presence of molybdenum hexacarbonyl and ultraviolet light in a liquid aerosol system.

$$C_2H_4 + H_2 \xrightarrow[Mo(CO)_6]{h\nu} C_2H_6 \qquad (19)$$

It is more common to use iron pentacarbonyl to hydrogenate ethylene; however, because iron pentacarbonyl is quite volatile I chose to use molybdenum hexacarbonyl. In addition, molybdenum hexacarbonyl is easier to obtain and to handle and I wanted to keep the emphasis of the work on the aerosol photochemistry rather than getting too involved in the organometallic chemistry.

The group 6 transition metal carbonyls $M(CO)_6$ (M = Cr, Mo, W) have been extensively studied because they catalyse the selective hydrogenation of dienes to monoenes

(Nasielski, Kirsch and Wilputte-Steinert 1971, Wrighton and Schroeder 1973). Both of the reactions shown in Figure 4.2 produce no other observable products.

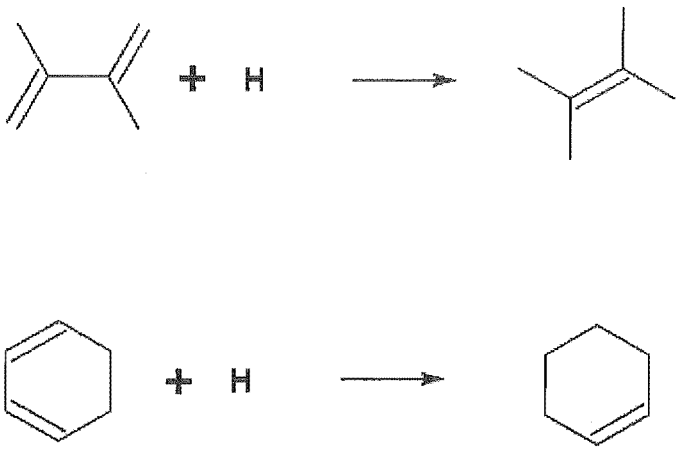

Figure 4.2 Examples of the selective hydrogenations of dienes possible using group 6 transition metal carbonyls.

However, I was only interested in demonstrating the simple hydrogenation of a monoenes (ethylene) and assumed that molybdenum hexacarbonyl would work. A considerable amount of work has been done on the mechanism of photocatalytic hydrogenation of olefins by transition metal carbonyls and the accepted mechanism for iron pentacarbonyl, which is generally applicable, is shown in Figure 4.3 (Kutal 1997 p. 154).

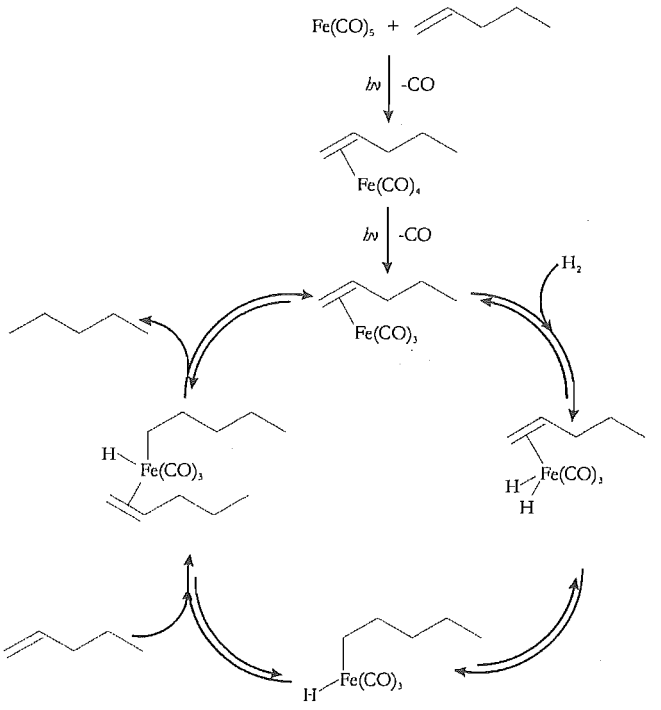

Figure 4.3 The mechanism of photocatalytic olefin hydrogenation by iron pentacarbonyl

It should be mentioned that there are a number of definitions of what actually constitutes a photocatalytic reaction (Chanon and Schiavello 1997, Hennig, Billing and Knoll 1993). The class of reactions represented by the transition metal carbonyl hydrogen of alkenes in the presence of light can be found under a number of different labels: a photoassisted reaction, photogenerated catalysis, catalysed photoreactions, and photoinduced catalytic reaction (Szymanska-Buzar 1997, Chanon and Schiavello 1997 pp. 5-6). However, the range of definitions and classifications seem to be converging towards a common ground which I outline below (Chanon 1997, Kutal 1997, Hennig et al. 1993).

The most common and sensible approach is not to try and increase the precision with which the word photocatalysis is used, but rather to develop precise definitions of the classes of reaction loosely referred to as photocatalysis. The usual approach to this is to make a major distinction between the two classes of reaction, represented in Figure 4.4.

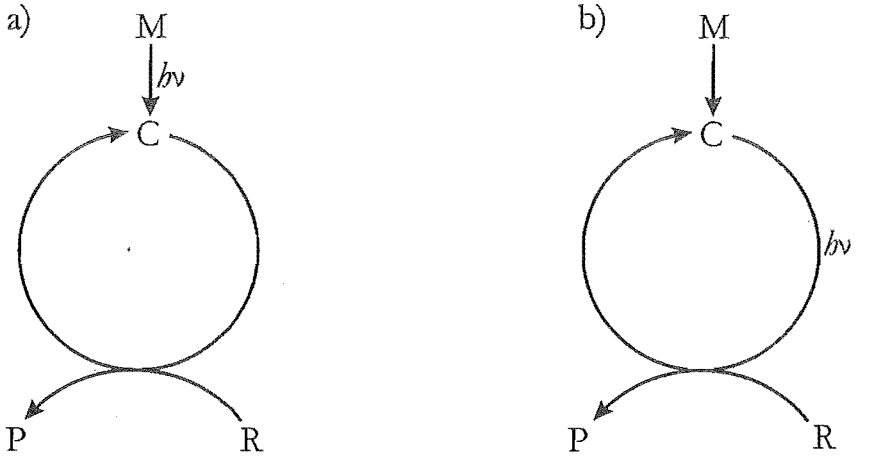

Figure 4.4 Classes of Photocatalysis: a) photogenerated catalysis, b) catalysed photochemistry

The first class of photocatalytic reactions (Figure 4.4a) are reactions that are catalytic in photons; the quantum yield is greater than one. The hydrogenation of alkenes by irradiated transition metal carbonyls falls into this category. Light transforms a precatalyst, a transition metal carbonyl, into a catalyst, an unsaturated transition metal carbonyl, which undergoes many catalytic cycles without further irradiation. As indicated above, this class of photocatalytic reactions has a number of different names, some of which are used by different authors to refer to the second class of reaction. I use the term suggested by Salomon (1983): photogenerated catalysis to refer to the reaction indicated by Figure 4.4a.

The second class of photocatalytic reactions (Figure 4.4b) are those that require a photon to complete each catalytic cycle; the quantum yield must be less than one. Hennig et al. (1993 pp. 58-9) refer to this class of reactions as photoassisted reactions. However, this is how Wrighton (1984) describes photogenerated catalysis. Therefore, I use the name suggested by Kutal (1985): catalysed photochemistry. Catalysed photochemistry, can itself be split into sub-classes to classify processes like photosensitisation (Chanon and Schiavello 1997 p. 7), however, elaboration of these subclasses is not necessary for my work.

In summary, the definitions I use are as follows:

1) Photocatalysis is any catalytic reaction that involves light. If it is necessary to go beyond this loose definition two classes of reaction are defined:

2) Photogenerated catalysis are reactions where light generates the catalyst and is not part of the actual catalytic cycle (Figure 4.4a).

3) Catalysed Photochemistry describes reactions where light is necessary to complete each catalytic cycle (Figure 4.4b).

4.2.1 Hydrogenation of Ethylene with a Molybdenum Hexacarbonyl in Decane Aerosol

The role of the solvent is more significant in liquid aerosol chemistry than in liquid chemistry and it needs to be selected with care. Beyond the usual solubility requirements is the need for a stable aerosol that enhances gas-liquid transport.

The choice of solvent for aerosol catalysis is a matter of balancing two properties: volatility and viscosity. On one hand, solvents like cyclohexane, which are usually used for catalytic hydrogenations, are inappropriate because of their volatility. The use of a volatile solvent would result in a demonstration of the already known ability of gas-phase transition metal carbonyls to hydrogenate gaseous alkenes. The natural solution was to use a higher molecular weight alkane as the solvent. Nevertheless, I also wanted to avoid using a solvent that was so viscous that the rate of hydrogen and ethylene diffusion to the catalyst was impossibly slow. I also wanted to avoid a solvent that, at room temperature, is close to the solid-liquid phase transition. When a liquid is nebulised, it cools and I did not want to try photocatalysis in wax.

It was easiest to try a solvent that might be too volatile rather than a solvent that might be too viscous. If the solvent was evaporating then I would be able to detect it using the mass spectrometer, and I could not think of a simple way to check rate of diffusion of hydrogen and ethylene in a viscous solvent. I decided to start with the two solvents n-decane and decalin (decahydronaphthalene). According to their material safety data sheets (MSDS) the vapour pressures of decane and decalin are 133 Pa at 16.5°C and 5.6 kPa at 92°C respectively. Unfortunately, the vapour pressures at the same temperatures are not available. For comparison, the vapour pressure of water at 16.5°C is 1.88 kPa and at 92°C, it is 75.6 kPa. Decane and decalin were the most volatile liquids I was prepared to try. Fortunately, when I carried out experiments, the mass spectrometer did not detect either of these solvents.

Aerosol catalysis is restricted to relatively viscous solvents and I was expecting the viscosity of the solvent to play an important role in aerosol catalysis. Therefore, I wanted to see if the molecular structure of the solvent affected the diffusivity, and consequently the reactivity, of the reactants. Decalin and n-decane are both ten carbon hydrocarbons but they have quite different molecular structures. Decalin is two fused six-membered rings and n-decane is linear hydrocarbon. I wanted to see if the hydrogen and ethylene would diffuse and react more readily when the solvent molecules were long linear chains or when they were rings.

Decalin (b.p. 190°C) and n-decane (b.p. 174°C) were vacuum distilled. It was necessary to exclude dissolved oxygen from the solvents. This prevented the formation of a brown solid which I attributed to oxidative side reactions. I used two different vacuum distillation techniques: firstly, I distilled the solvents under vacuum with a small flow of argon bubbling through the liquid. The argon flow made it unnecessary to stir the solution or to use boiling chips. However, vacuum distillation with a gas flow is very tricky and as I was obliged to use others' distillation apparatus, more than once what I thought was an argon flow was actually airflow into the system via a leak in the argon hose. Fortunately, the distillation of the solvents under straight vacuum followed by argon bubbled through the solution for 10 – 15 minutes proved to be sufficient. The reason that I tried to exclude oxygen from the samples was that during the first experiment a large amount of brown solid formed in the aerosol. Repeating the reactions with oxygen-free decalin prevented the formation of the brown solid.

Solutions irradiated in the flash lamp system were much more sensitive to inadvertent oxygen exposure than solutions irradiated in the high-pressure xenon lamp system. Both lamp types used a xenon gas discharge to generate the light. However, the light from the flash lamps entered the cell through its glass sides, whereas the light generated by the high-pressure xenon lamp entered the cell though the suprasil quartz windows. Thus, the greater propensity for side reactions in the flash lamp irradiated solutions cannot be (as I initially suspected) due to greater ultraviolet absorption. I (now) believe that the formation of the brown solid is due to heating of the aerosol. In the flash lamp system, the lamps are very close to the cell, and during an experimental run, the cell got very hot, whereas in the high-pressure xenon lamp system the lamp is a lot further from the cell, and during a run the cell

did not increase in temperature. I concluded that the brown solid was the result of a heat-induced reaction between oxygen and molybdenum hexacarbonyl and possibly decane or decalin. Molybdenum hexacarbonyl was definitely involved, while the decane of decalin was only possibly involved, because the brown solid went blue after standing for a couple of days and blueness is a more common characteristic of transition metals than it is of hydrocarbons.

When I switched to the high pressure xenon lamp system the formation of the brown solid virtually ceased. While using the high-pressure lamp system, the bubbling of argon through distilled inadvertently air-exposed solutions prevented the formation of the brown solid. When I was using the flash lamp system, the same solution would have required re-distillation.

I prepared solutions by dissolving a measured amount of $Mo(CO)_6$ into a known amount of solvent, decane or decalin, bubbling argon through the solution for 5 to 10 minutes to expel any oxygen, and leaving the solution to sit for at least 4 hours to ensure that the $Mo(CO)_6$ was completely dissolved. Concentrations ranged from 1×10^{-6} molL^{-1} to 1×10^{-4} molL^{-1}.

The experiment was monitored by real-time mass spectrometry of the gas-phase of the irradiation zone and by collecting the aerosol as a liquid by impaction. The mass spectrometer recorded partial pressure versus time data. I chose what mass values I wanted to follow and the instrument plotted the variation of the partial pressure of those mass units during the course of the experiment. The technique used to analyse the liquid was normally ultraviolet-visible spectroscopy.

Unfortunately, I was unable to use decalin in the medical nebulisers. Before deciding to use the plastic nebulisers, I soaked one in decalin and one in decane to check to see if the plastic was appropriate for those solvents. Surprisingly, the decane soaked nebuliser was unchanged, but the nebuliser that was soaked in decalin dissolved. I stopped using the two solvents and worked with just decane. I also checked to see if the ultraviolet-visible spectrum of the decane had changed after having had the nebuliser soaked in it and it had not.

Between five and ten millilitres of molybdenum hexacarbonyl in decane solution was poured into the nebuliser and the flask containing the solution was flushed with argon to

remove the air that had got into it. Although it was impossible to prevent contact between the solution in the nebuliser and the air, I minimised the air exposure whenever possible. The nebuliser was placed inside the cell and the B55 joint that housed the nebuliser was heated with a hot air gun. Once the wax had melted and a good seal formed in the joint, it was then necessary to wait about fifteen minutes for the wax to solidify and seal the joint.

Once the system had been assembled, and prior to carrying out the experimental run, I flushed the system with argon to remove air that might be present. I adjusted the argon flow rate and the exhaust-gas pumping rate so that the pressure in the cell was between 17 and 18 psia.

While the system was being purged, I turned on the mass spectrometer so that the recorded mass spectrum trace would show a background level. The mass spectrometer was set to record the variation of the masses of relevant species during the course of the experiment. The mass to charge ratios that I monitored were 2 (hydrogen), 28 (nitrogen/ethylene), 30 (ethane), 32 (oxygen), and 40 (argon). On some runs I recorded the change over the course of the experiment of the full mass spectrum, from mass 0 to mass 200. I then checked for any significant changes in peaks that were not being monitored.

It is unfortunate that ethylene and nitrogen have the same mass. Generally, I assumed that if any nitrogen was present it had to be from the air and so oxygen would be present. Therefore, when the mass 28 peak changed and the mass 32 peak did not, the change in mass 28 was due to ethylene. When both the mass 32 and mass 28 peaks changed, the change in mass 28 was due to nitrogen. If cost was not a factor this problem would be avoided by the use of ^{13}C labelled ethylene.

Once the mass spectrometer showed that the system no longer contained air I turned on the hydrogen and ethylene flows, adjusted the exhaust rate so that the pressure did not change, and waited until the flows had balanced and the mass spectrometer showed no change in the partial pressure of argon, ethylene, and hydrogen.

When the gas flows were stable, I switched on the lamp and then switched the gas flow from the sheath flow to the nebulising flow. Typically, the nebulising flow rate was between 3 and 4 $L \cdot min^{-1}$. I balanced the nebulising and sheath flows and the exhaust gas so that the pressure in the cell changed as little as possible. It was necessary to avoid pressure

changes in the irradiation cell because they affected the pressure inside the mass spectrometer. If the pressure in the cell rose too quickly, the pressure in the mass spectrometer would rise above the maximum level of 10^{-4} torr and the filament would turn off automatically. The aerosol flow through the irradiation cell was turbulent for the first half of the cell. Depending on the nebulising flow rate and the volume of solution in the nebuliser it took between 15 and 30 minutes to nebulise and irradiate the contents of the nebuliser.

The software that controlled the mass spectrometer saved the data in an ascii text file. I used Microsoft Excel and Python to carry out the majority of the data analysis and handling. The mass spectrometer does not record data at regular time intervals, but it does save the acquisition time of each data set in the data file. I wrote a short Visual Basic for Applications (VBA) programme that rearranged the data into a suitable format. Having done this, the analysis of the pressure versus time data was generally a matter of plotting the variation of partial pressures with time. If I thought that there might be a significant result in the data I recalculated all the partial pressures as fractions of the total pressure to check that the 'result' was not an artefact of the fluctuations of the total pressure. Sometimes I also recalculated a partial pressure at one mass as a fraction of the partial pressure at another mass. For example, I often calculated the partial pressure of mass 32 as a fraction of mass 28 as a way of distinguishing between nitrogen and ethylene.

The mass spectrometer software was definitely not designed with the task of recording the variation of the whole mass spectrum with time in mind. However, I found it easier to check and see if any peaks other than those that I was monitoring were promising by extracting the relevant information from the data file, than by watching the 0 to 200 mass spectrum for any changes in real time. The mass spectrometer software saves each 0 to 200 mass spectrum in three lines. I wrote another short VBA programme that removed all the extra information, rearranged the data so that each data set took up one line, and ensured that plotting the values in any column would display the variation of a particular mass with time. To check for any unexpected changes, I plotted the 200 different columns and then looked to see if any mass units rose above the background noise significantly. I always checked mass 142 (decane) and mass 132. Molybdenum hexacarbonyl has mass 264 which is beyond the upper limit of the mass spectrometer, but if there was any $Mo(CO)_6$ present

in the gas phase it would be reasonably likely that it would form doubly charged species when ionised. I never observed any increases in mass 142 or mass 132, so I was reasonably certain that the decane was not evaporating significantly and neither was the $Mo(CO)_6$ escaping into the gas phase.

I used the flash lamps for what was essentially continuous irradiation and in general, the flash system was not appropriate for my work, so when the high-pressure xenon lamp arrived I stopped using the flash system. However, while using the flash lamps I observed a number of hints that that the system was working and the ethylene hydrogenation was occurring.

When I finished a run, I shut off the exhaust flow and the gas flow, completely sealing the system. One of the difficulties of aerosol systems is that, while they have the potential for very high gas-liquid exchange rates, there is also the potential for no gas-liquid exchange to occur at all. I was concerned about the possibility of ethane generation inside the decane without any ethane transfer out of the decane. Consequently, if I had done a run the previous day and left the system sealed, before I started another experiment I turned on the mass spectrometer and sampled the gas in the system to see if it had changed overnight. I was looking for any gases that might have been slowly out-gassing from the decane solution. I often observed significant but not reproducible or consistent increases, sometimes as high as twenty fold, in the partial pressure of mass 30. I did not view the rise in the partial pressure of mass 30 as particularly strong evidence, but it did indicate that the experiments were going in the right direct.

The hydrogenation that I was studying is a photogenerated catalytic reaction, which means that the actual reaction, the hydrogenation of ethylene by an unsaturated molybdenum carbonyl species, does not require light. In fact, this sort of reaction can continue for several hours after the light source has been removed (Roundhill 1994 p. 249). With this in mind, I constructed a series of glass tubes that could be inserted in a spiral-like manner between the irradiation cell and the impactor. Using this system, I could add an aerosol flow path, without irradiation, of up to ~1.2 metres. It obviously did not take several hours for aerosol to pass through this section of tubing, but I hoped that it would be sufficient to observe any significant dark reactions that might be taking place. I did not observe anything significantly different to when the additional aerosol path was not there. Adding

the 'dark' aerosol flow path complicated the experiment and made the mass spectrometer response time even worse than it already was, so I only spent a small amount of time investigating dark aerosol reactions, and I did not try to observe any dark reactions in any of the other irradiation systems.

One of the most promising results I obtained came from the flash cell system. During some runs I observed a dramatic decrease in the partial pressure of ethylene in the system when the lamp was turned on and when the lamp was switched off the partial pressure of ethylene rose again.

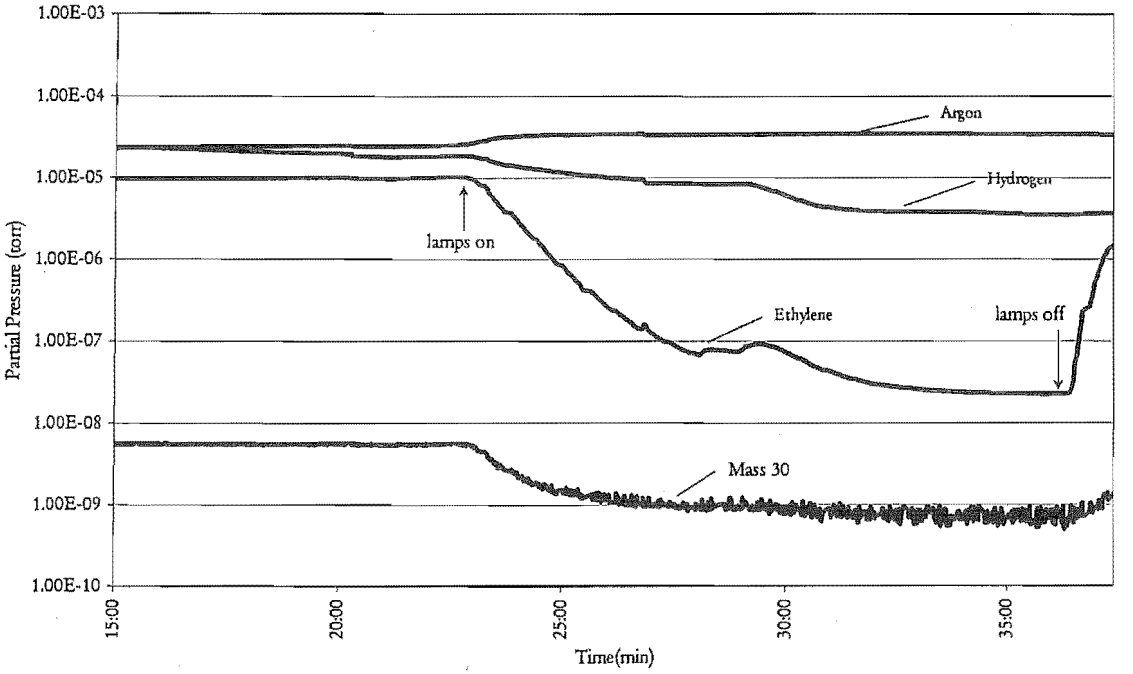

Figure 4.5 The partial pressures of argon, hydrogen, and ethylene during the irradiation of a $Mo(CO)_6$ in decane aerosol.

Figure 4.5 shows the pressure vs. time trace of the reactive gases hydrogen and ethylene, and the carrier gas argon, during the irradiation of a molybdenum hexacarbonyl in decane aerosol in the presence of these gases. When irradiation began, there was a dramatic decrease in the partial pressure of mass 28 and the level of mass 32 did not change, making it almost certain that the mass 28 line was due to ethylene. Although it does not look like it from figure 4.5, because of the logarithmic scale, the fall in hydrogen partial pressure is sufficient for a reaction with ethylene to be taking place. Unfortunately, the mass 30 peak,

which corresponds to ethane, also decreases, and then drops off to the background noise level.

The fact that an increase in the mass 30 peak was not observed does not imply that the ethylene was not reacting. Transition metal carbonyls can catalyse olefin reactions other than hydrogenation, for example, oligomerisation. Alternatively, as mentioned above, ethane could be forming, but not leaving the droplets. The day after reactions in which a drop in ethylene occurred, the partial pressure mass 30 had usually increased in the system. Although oddly the overnight increases in mass 30 partial pressure were not as large as on occasions when no decrease in ethylene was observed.

Again, on its own these results were not particularly good evidence that a reaction was taking place. However, combined with the other observations of the increases in mass 30 partial pressure overnight the results gave me confidence that the hydrogenation of ethylene was taking place some of the time, but that it was necessary to understand what was causing the irregularity of the results.

I carried out many different runs, varying the flow rate (1 $L \cdot min^{-1}$ to 10 $L \cdot min^{-1}$), reaction pressure (½ atm to 2 atm), catalyst concentration (1×10^{-6} $molL^{-1}$ to 1×10^{-4} $molL^{-1}$), and the relative partial pressures of hydrogen and ethylene (1:9 to 9:1). I also increased the residence time of the aerosol in the irradiation zone by doubling the length of the glass cell. Despite all this, I was unable to observe any indications that hydrogenation was taking place.

The selection of the hydrogenation of ethylene using a molybdenum hexacarbonyl catalyst as the reaction to demonstrate the viability of liquid aerosol photocatalysis was not a good direction for this research.

After I became more familiar with the literature and realised that photocatalytic reactions often take hours, I wondered about the appropriateness of the molybdenum hexacarbonyl reaction. However, at the same time the flash lamp system provided promising results, so I decided to continue with the molybdenum hexacarbonyl reaction.

In compiling the results of my investigations into liquid aerosol photocatalysis, I have recognised that the heating of the flash lamp cell probably played a greater part in the results I observed than I realised at the time.

4.2.2 Hydrogen, Acetylene, $Mo(CO)_6$ and Decane

There are reports of transition metal carbonyls catalysing the trimerisation of acetylene to benzene, the hydrogenation of acetylene, and the polymerisation of acetylene by molybdenum hexacarbonyl. On an occasion when I had no ethylene I decided that, although I did not expect a reaction, I would use acetylene instead of ethylene and see what happened.

I prepared molybdenum hexacarbonyl in decane solutions in just the same way as I prepared them for the ethylene hydrogenation reaction. Acetylene cylinders contain acetone so it was necessary to pass the ethylene through an acetone/dry ice trap to remove the acetone. This meant that the flow meters did not work. The range of delivery pressures was also more restricted than in other experiments, because it is dangerous to pressurise acetylene higher than 15 psi.

The principle instrument used to monitor this series of experiments was the mass spectrometer. I also looked at the ultraviolet spectra of the molybdenum hexacarbonyl-decane liquid before and after nebulisation and irradiation.

During the experiment, the mass spectrometer sampled the gas phase. After irradiation, an impactor in the flow line collected the aerosol. Ultraviolet spectra of the collected liquid provided additional monitoring of the reaction.

The first time I tried acetylene in my system I recorded changes in partial pressure of all the mass unit channels below one hundred. Using Excel, I generated a plot of partial pressure variation of the channels that rose above the background noise. In subsequent experiments, I monitored only the significant channels.

The initial results for the acetylene experiments were very promising. The first time I tried the experiment there were indications that the dimerisation of acetylene was occurring in the reaction. Figure 4.6 shows a typical successful result for the irradiation of acetylene,

hydrogen, and decane-molybdenum hexacarbonyl aerosol. When the irradiation began, the partial pressures of species with masses 56 and 58 increased. When the irradiation ceased, the partial pressures of these species decreased.

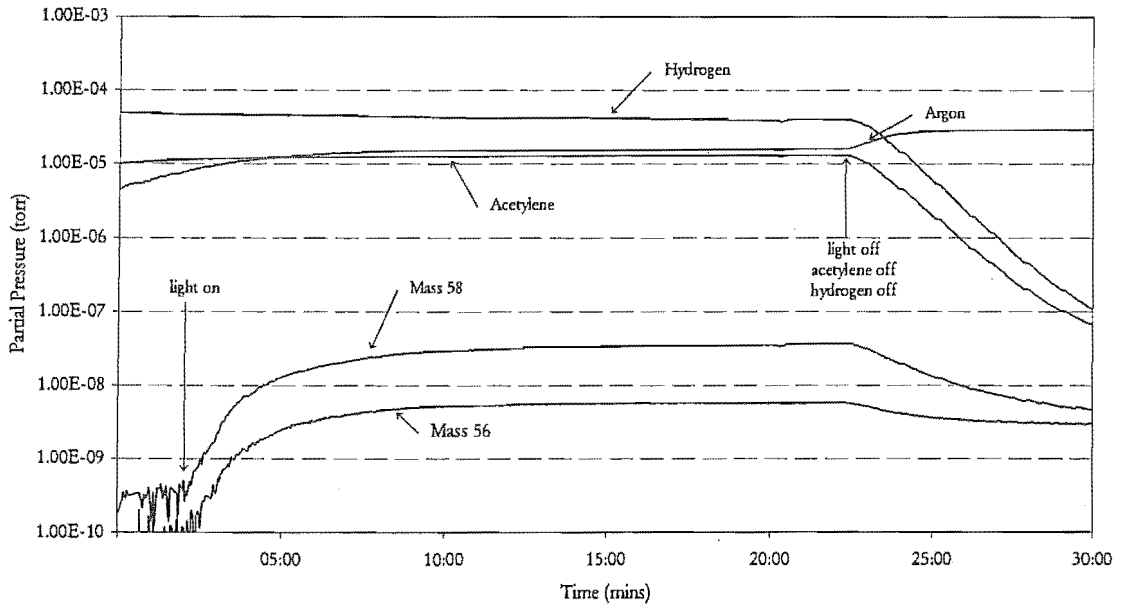

Figure 4.6 Typical partial pressure versus time result for an acetylene run

I tentatively concluded that the species whose partial pressure increased were the products of acetylene dimerisation. One would expect the initial product of the dimerisation of acetylene to be 1,3-butadiene, $CH_2CHCHCH_2$, which has a mass of 54. No increase in the partial pressure of mass 54 occurs. However, irradiated molybdenum hexacarbonyl is an excellent catalyst of the hydrogenation of 1,3-butadiene to 2-butene (see Figure 4.2). 2-butene has a mass of 56 and 2-butene can undergo further hydrogenation to become butane, which has a mass of 58. Given these considerations, a possible mechanism that explains the observed increase in the partial pressure of mass 56 and mass 58 is that the acetylene is dimerised to form 1,3-butadiene. The 1,3 butadiene is rapidly converted to 2-butene, which is hydrogenated more slowly to butane.

If this mechanism is to withstand any scrutiny at all, it is necessary to discount the possibility that the increase in partial pressure observed could be the result of the possible presence of acetone in the system. As mentioned above, acetylene cylinders contain

acetone and I used a dry-ice/acetone trap to remove the acetone before the acetylene entered the system. In addition, I always checked to see if the mass spectrometer detected any acetone before beginning an experiment. However, the mass of acetone is 58, so despite these precautions I could not discount the role of acetone altogether. I was reasonably certain that I not observing an increase in acetone in the system, because the increases were only observed during irradiation of the aerosol in the presence of hydrogen and acetylene. Additionally, in most experiments the rise and fall of mass 56 and 58 intensities did not show any correlation with the change in ethylene intensity.

Unfortunately, as with the ethylene experiment, the behaviour of this system was very erratic. In fact, on one occasion, after getting a good result that showed a significant increase in the amount of butane and 2-butene I decided to repeat the experiment straight away while things were working. The only change I made to the system was to refill the nebuliser and wait for the seal to set. In the second run, no more than half an hour after the finish of the first, nothing happened: none of the partial pressures I monitored changed during the irradiation.

The ultraviolet spectra of the nebulised and irradiated solutions were of limited utility. There was very little variation from spectrum to spectrum; even the spectra of cyclohexane-diluted solutions were not useful. All that I could really conclude from ultraviolet spectra was that the absorptivity of the solution after irradiation, within the error of my dilution, was 5-10% less than that of the unirradiated solution.

4.2.3 1-Decene, Hydrogen and Molybdenum Hexacarbonyl

In order to simplify the experimental systems and isolate more of the variables that were affecting the results I decided to try hydrogenating 1-decene. In this system, there was only one gaseous reactant, which simplified its delivery and removed the possibility of competitive solvation. However, it was necessary to mix argon with the hydrogen in order to nebulise the decane mixture[i]. The principle technique used to follow this reaction was

[i] I observed an interesting effect that I did not have time to follow up in this work. Argon will nebulise the liquid with a pressure drop of around 5 psi and a flow rate of 1 $L \cdot min^{-1}$. However in the same nebuliser

FTIR spectroscopy of the liquid portion of the aerosol. ^{1}H and ^{13}C NMR were used to detect small amounts of organic products. UV-Visible spectroscopy was also tried, but there were no useful peaks in that region. Gas phase mass spectrometry was used, with all the usual difficulties associated with mass spectrometry of aerosols.

A definite and reproducible reaction was observed, but it was clearly not hydrogenation of the 1-decene to decane, because the product solution was brown.

I carried out these experiments in the stainless steel reaction cell. The 1-decene was distilled under vacuum at 30°C and after being checked for purity by FTIR and NMR was stored in the dark in the flammable goods cabinet in a round bottomed flask sealed with a Suba seal. For some reactions, argon was bubbled through the 1-decene. When this was the case, the solution was only handled through Suba seals with syringes.

This system did not demonstrate the sensitivity to oxygen that was observed in the ethylene system. Consequently, most of the time I took no special precautions to exclude air from the liquid and the system. This confirmed the supposition that the formation of the brown solid was due to heat. The steel system was a better heat sink than the glass system and the cell did not heat up at all.

At the same time as the steel system was constructed, the department acquired a new accessory for the FTIR spectrometer. The new accessory was a horizontal attenuated total reflection (HATR) cell. Previously, obtaining FTIR spectra of small amounts of liquid was very difficult and rarely produced useful spectra. However, the HATR cell made the routine acquisition of FTIR spectra of nebulised, irradiated, and impacted solutions much easier and more helpful. FTIR spectroscopy proved to be a more effective probe of liquid aerosol photochemical systems than either mass spectrometry or ultraviolet-visible spectroscopy.

---

hydrogen would not nebulise the liquid. I increased the flow rate to more than 10 $L \cdot min^{-1}$ and the pressure drop over 30 psi and it still did not nebulise the liquid. I did not increase the flow rates and pressure in more for fear of damaging my reaction cell. But when I mixed a small amount of Argon with the Hydrogen the liquid nebulised as usual. Consequently I was unable to carry out the reaction in a pure hydrogen atmosphere.

The FTIR spectrometer was a Shimadzu FTIR 8201-PC spectrometer interfaced with a 486 PC using the standard software provided by Shimadzu. No special modifications were made to the instrument or the software.

The attenuated total reflection (ATR) method, also known as the multiple internal reflectance (MIR) method, is very useful for carrying rapid FTIR spectroscopy on liquid samples. The spectra obtained were of much higher quality than those obtained using the sealed liquid cells.

The refractive index must be higher than that of the sample to ensure total internal reflection in the prism. This technique makes use of the not quite 'total' internal reflection of light from the external wall of a prism (Figure 4.7) made of a material with a large refractive index. Some of the light penetrates a small distance into the sample and this is light is used to measure the spectrum.

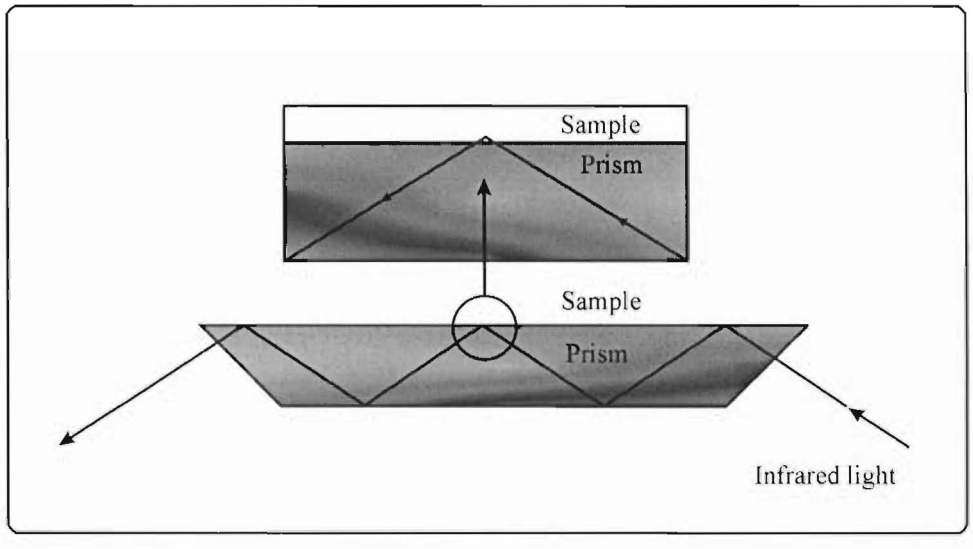

Figure 4.7 A schematic of attenuated total reflection.

The penetration depth is expressed by:

$$d_p = \frac{\lambda}{2\pi\sqrt{\sin^2\theta - m_{21}^2}} \qquad (20)$$

Where λ is the wavelength, θ is the incident angle and $m_{21} = m_2/m_1$ is the relative refractive index of the sample (m_2) and the prism (m_1). The cell used was a PIKE

technologies horizontal attenuated total reflectance trough cell with a 45° ZnSe crystal (see Figure 4.8).

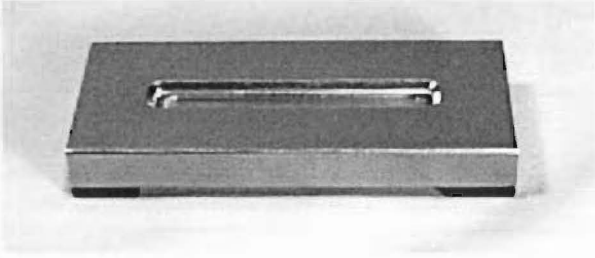

Figure 4.8 The PIKE HATR trough cell

After each irradiation, I recorded a horizontal attenuated total reflection Fourier transform infrared spectrum (HATR FTIR) of the irradiated and un-irradiated sample. These were compared to determine if a reaction had taken place, and to try to determine what the reaction might have been. If the sample appeared to have undergone a significant change then a 500 MHz ^{1}H NMR spectrum of the sample was obtained. Initially I took 300 MHz spectra but the greater noise in this instrument masked the products that I was trying to observe.

The spectrum of 1-decene, Figure 4.9, was obtained using the HATR cell. This was compared with the spectrum catalogued in the Aldrich FTIR spectra library (Pouchert 1985). The spectra were the same, implying that the HATR cell would be suitable for work with 1-decene solutions.

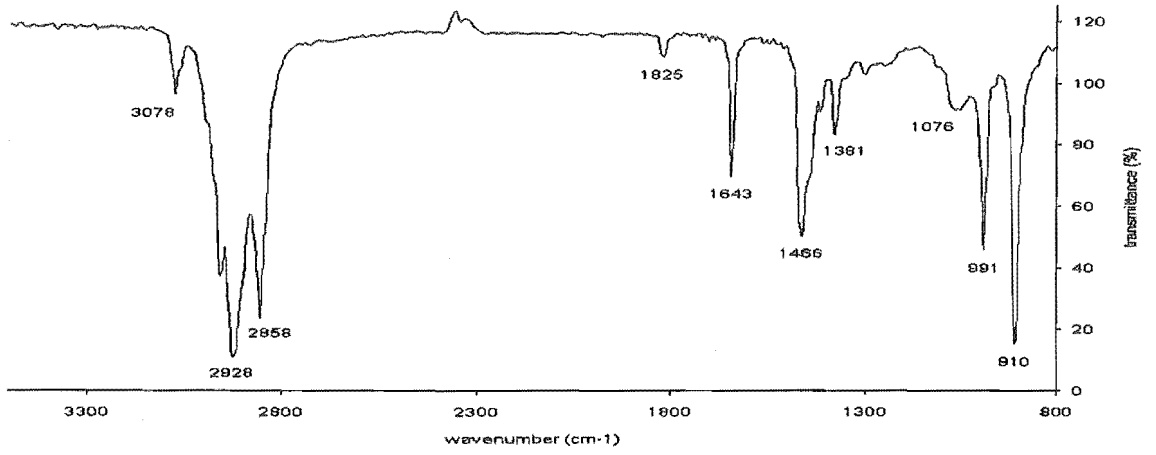

Figure 4.9 The FTIR spectrum of 1-decene.

The peaks between 2800 cm^{-1} and 3000 cm^{-1} are due to C-H modes and the prominent peaks at 1643, 1466, 991 and 910 cm^{-1} are due to stretching mode of the double bond and the bending modes of the hydrogen atoms bound to double bonded carbons. The peak at 3078 is due to the C-H stretch of the hydrogen atom attached to double bound carbons. I expected the peaks associated with the double bond to decrease in intensity as the decene was hydrogenated.

The spectrum of $Mo(CO)_6$ in 1-decene (Figure 4.10) shows only one real difference from that of neat 1-decene; a very intense peak at 1987 cm^{-1}. Gas-phase $Mo(CO)_6$ has three vibrational modes around 2000 cm^{-1}: two Raman-active modes at 2121 $cm^{-1}(A_{1g})$ and 2025 cm^{-1}(Eg), and one infrared-active mode at 2000 cm^{-1} (F_{1u}).

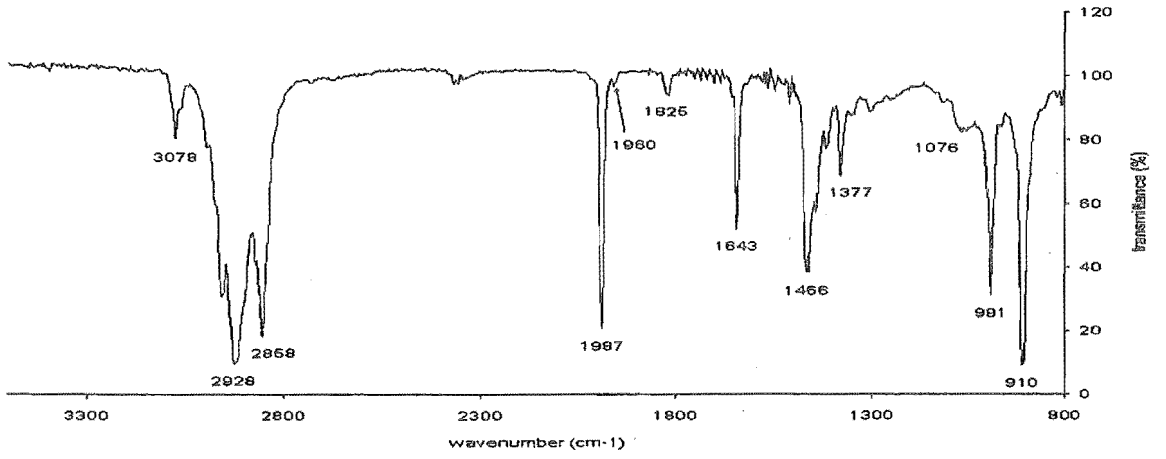

Figure 4.10 The FTIR spectrum of $Mo(CO)_6$ dissolved in 1-decene.

The three modes vibrational modes around 2000 cm^{-1} are all assigned to the carbonyl stretch ν(CO) (Nakamoto 1997 p. 28, Hawkins, Mattraw, Sabol and Carpenter 1955). There are other peaks for the ν(MoC), ν(MoCO) and ν(CMoC) modes, but they occur below 650 cm^{-1} which is the lower limit of the ZnSe cell. Infrared spectra have been reported for $Mo(CO)_6$ in various solvents (Clark and Crociani 1967), but not decane or 1-decene. In n-hexane and cyclohexane the ν(CO) peak is shifted to lower energy by 12 cm^{-1}, to 1991 cm^{-1}. All the shifts are to lower energies and the largest shift that Clark and Crociani measured is 23 cm^{-1} for dibromomethane.

It seems reasonable that in a more viscous and higher molecular weight solvent the shift would be a slightly lower energy, however, when the spectrum of $Mo(CO)_6$ in cyclohexane is obtained on our instrument the ν(CO) peak occurs at 1987 cm^{-1}. Therefore, within the accuracy of our instrument, the ν(CO) peak occurs at the same frequency in 1-decene as it does in cyclohexane and the difference between our results and those of Clark and Crociani is 4 cm^{-1}, which was the spectrometer's resolution.

In the spectrum recorded in 1-decene there is a small shoulder at 1960 cm^{-1}, but I am not certain what this is. Its intensity seems to increase upon aerosol irradiation in the presence of hydrogen or in the liquid phase regardless of the gas present, see Figure 4.12 and Figure 4.14, and upon aerosol phase irradiation in the presence of argon it decreases, see Figure 4.11. It is also present in the $Mo(CO)_6$ spectrum in cyclohexane and remains after irradiation in liquid phase cyclohexane. It is possible that this peak is due to some sort of $Mo(CO)_5X$ species or a dimeric molybdenum carbonyl species, but its intensity in the unirradiated solution, Figure 4.10, suggests that it is probably not. It is possible that it is an impurity in the $Mo(CO)_6$.

After nebulisation and irradiation in the presence of Ar, that is, using argon as the carrier gas and the nebulising gas, two major changes are observed in the FTIR spectrum of the aerosol irradiated product, see (Figure 4.11). The 1987 cm^{-1} peak virtually disappears.

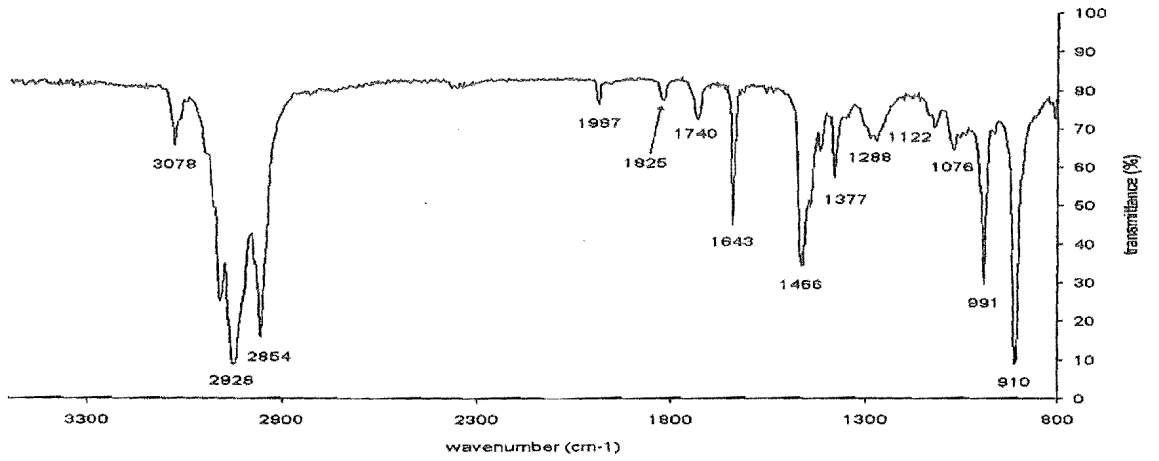

Figure 4.11 The FTIR spectrum of $Mo(CO)_6$ in 1-decene aerosol nebulised and irradiated in the presence of argon.

A number of new peaks form at 1740 cm^{-1}, 1289 cm^{-1} and 1123 cm^{-1}. The substantial decrease in intensity of the ν(CO) peak is consistent with photolysis of the Mo—CO bond.

The spectrum (Figure 4.12) observed after nebulisation and irradiation in the presence of hydrogen and argon had only one significant difference from that irradiated in just argon. The small peak/shoulder present in the original solution at 1956 cm^{-1} does not disappear; if anything, it increases in intensity. This behaviour does nothing to clear up the puzzle of what this peak might be.

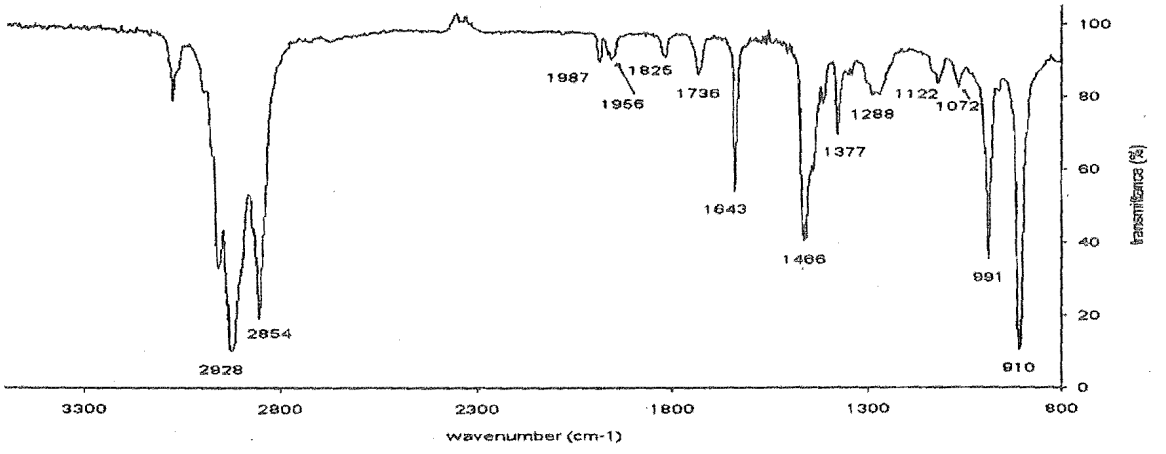

Figure 4.12 The FTIR spectrum of $Mo(CO)_6$ in 1-decene aerosol nebulised and irradiated in the presence of hydrogen and argon.

When the $Mo(CO)_6$ in 1-decene aerosol is irradiated in the presence of hydrogen and carbon monoxide (Figure 4.13), the intensity of the ν(CO) peak does not decrease as much as when no carbon monoxide is present. This is consistent with the disappearance of the ν(CO) peak being due to photolysis of the Mo—CO bond in the aerosol. The presence of the carbon monoxide allows the possibility of the reformation of the Mo—CO bond and a smaller decrease in the intensity of the ν(CO) peak is observable.

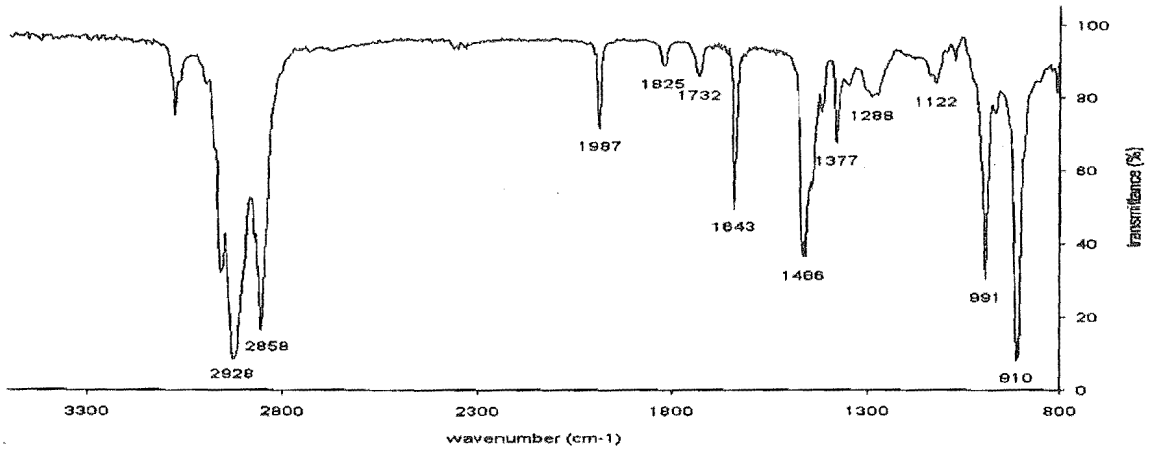

Figure 4.13 The FTIR spectrum of $Mo(CO)_6$ in 1-decene aerosol nebulised and irradiated in the presence of carbon monoxide and hydrogen.

While it was a relatively easy task to assign the reactant; 1987 cm^{-1} peak to the ν(CO) mode and recognise that its disappearance was due to photolysis of the Mo—CO bond, it was somewhat more difficult to assign the product peaks. Upon irradiation, peaks appear at 1740 cm^{-1}, 1289 cm^{-1} and 1123 cm^{-1}, for example (Figure 4.11). These peaks do not seem particularly affected by the presence or absence of the reactive gases hydrogen and carbon monoxide; compare (Figure 4.11) with (Figure 4.12) and (Figure 4.13). The lack of a free carbon monoxide peak (~2150 cm^{-1}) in Figure 4.13 implies that all the carbon monoxide out-gasses between the reaction and the acquisition of the spectra. Thus, the lack of a free carbon monoxide peak in other product spectra does not rule out carbon monoxide as a reaction product.

No appreciable changes in the intensity of the bands associated with the C—H stretches or the stretching or bending modes of the carbon-carbon double bond associated atoms are observable. Therefore, the peaks that we are observing in the infrared spectrum are likely

to be associated with changes in the $Mo(CO)_6$ rather than the 1-decene. This does not preclude the possibility of a small amount of reaction product originating from the 1-decene and present in such a small concentration that it is not detectable by infrared spectroscopy. In order to check this and to try to shed more insight on the reaction, ^1H NMR spectra were taken.

The NMR spectra showed the presence of a very small amount of material that had ^1H NMR multiplets at 7.5 ppm and 4.2 ppm in the irradiated solution. There was also an almost undetectable amount of the same material in the original solution. The increase in this material in the irradiated-nebulised solution varied from twenty to fifty fold. Initially, I believed that I was observing the product of a reaction that was able to go very slowly under thermal conditions and that was photochemically enhanced. Unfortunately, the same NMR spectrum was producible by soaking the plastic tubing from the impactor or the plastic cap of the volumetric flask in 1-decene. The material was a plasticizer and the two different plastics also had the same plasticizer. This is what prompted the redesign of the steel cell impactor so that it contained no plastic.

Aside from the plasticizer species, there were no other species that could be detected in the ^1H NMR spectra. Therefore, the reaction I was observing did not involve hydrogen. This is consistent with the unimportance of hydrogen gas in the reactivity of the system.

In order to compare the reactivity of liquid phase systems with the reactions I was observing in the liquid phase I carried out some liquid phase reactions. I irradiated solutions of molybdenum-hexacarbonyl in 1-decene under an atmosphere of argon, hydrogen, or hydrogen and carbon monoxide. The irradiation cell contained 10 mL of solution and was irradiated for between half-an-hour and one hour in order to provide the fairest possible comparison with the aerosol system. All the spectra of the liquid phase irradiated solutions looked the same and were significantly different to the aerosol phase solutions.

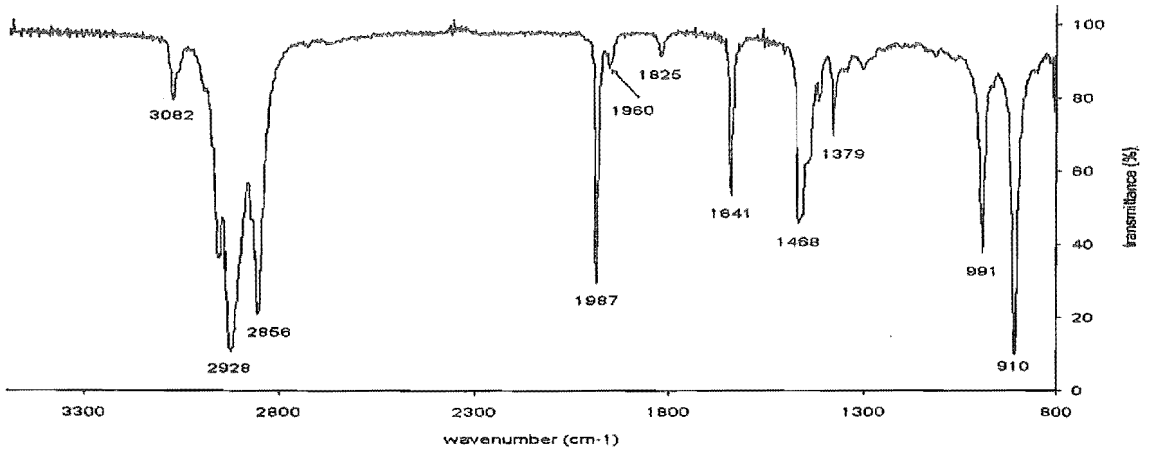

Figure 4.14 Typical FTIR spectrum of liquid phase irradiated $Mo(CO)_6$ in 1-decene

As can been seen from Figure 4.14, no detectable decrease in the intensity of the 1986.5 cm^{-1} peak occurs. This demonstrates a dramatic difference in photochemical lability between identical liquid phase and aerosol phase systems.

I did not think that the decrease in ν(CO) intensity in the nebulised-irradiated solutions was due to the evaporation of $Mo(CO)_6$. The absorption intensity in the ultraviolet spectrum of nebulised-irradiated solutions did not show any decrease, and evaporation would not explain the new peaks in the product spectra. Nevertheless, I carried out a number of aerosol runs without irradiation in order to confirm this. The decrease in the intensity of ν(CO) due to nebulisation was less than 10%.

The aerosol droplets were resident in the irradiation cell for between thirty and sixty seconds. In this time a photochemical reaction, which did not even show indications of starting in the liquid phase after one hour, went to completion. Although this reaction has not been characterised, as neither the rate nor the products are known, it still represents a remarkable increase in reactivity.

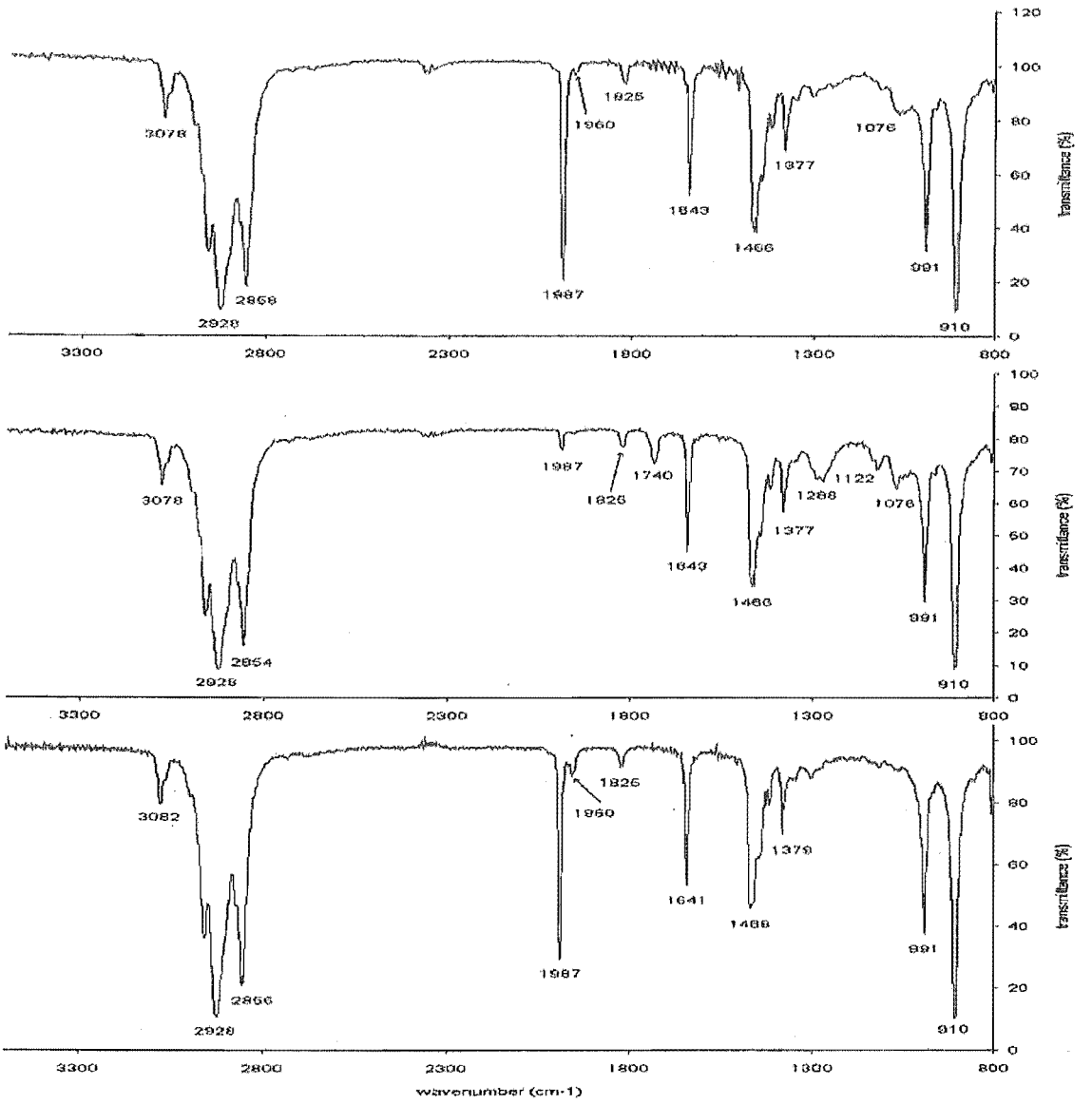

Figure 4.15 Comparison of unirradiated, aerosol phase irradiated and liquid phase irradiated $Mo(CO)_6$ dissolved in decene

Figure 4.15 clearly demonstrates the extent of the enhanced reactivity of the photolysis of molybdenum hexacarbonyl in the aerosol phase and it is shows the lack of reactivity of the 1-decene. The middle spectrum is that for the aerosol phase irradiation and it is quite different to the other two spectra, while the unirradiated and liquid phase irradiation spectra are almost identical.

Using liquid aerosol photocatalysis for the hydrogenation of olefins proved somewhat more difficult in practice than I initially expected. Although I was unable to demonstrate

conclusively the application of liquid aerosol photocatalysis to hydrogenation, I did discover significantly enhanced photolytic reactivity of molybdenum hexacarbonyl in the aerosol phase.

4.3 Other Experiments

4.3.1 Wastewater treatment

The use of photo-Fenton chemistry for wastewater treatment is an important application of homogeneous photocatalysis. The use of a liquid aerosol photocatalysis system to carry out photo-Fenton wastewater treatment is a promising application of liquid aerosol photochemistry.

One of the most significant industrial uses of photocatalysis, both homogeneous and heterogeneous, is probably in the area of wastewater treatment. The treatment of wastewater in photocatalytic systems is part of a general class of wastewater treatment technologies called advanced oxidation processes. Advanced oxidation processes are processes that generate hydroxyl radicals in aqueous solution. The generation of hydroxyl radicals initiates a series of radial processes, sometimes called mineralisation, that oxidise organic material to carbon dioxide and water. A number of other compounds form, depending on the elemental composition of the original organic material.

There are a number of chemical systems that are suitable for the generation of the hydroxyl radicals: ozone and ultraviolet light, hydrogen peroxide and ultraviolet light, titanium dioxide and ultraviolet light, hydrogen peroxide and ferrous iron, and photo-Fenton chemistry (Kim and Vogelpohl 1998). In general, the best system is the one that produces the most hydroxyl radicals for the least cost. In practice, this translates into a system that utilises sunlight and produces hydroxyl radicals catalytically.

There is considerable interest in using advanced oxidation processes for the decontamination of polluted water. The pollution comes from sources as diverse as insecticide use (Malato, Caceres, Agueera, Mezcua, Hernando, Vial and Fernandez-Alba 2001), industrial dye (Herrera, Lopez and Kiwi 2000), landfills (Kim and Vogelpohl 1998), and military rocket fuel disposal (Nadtochenko and Kiwi 1998). The ozone and ultraviolet

light process and the hydrogen and ultraviolet light process are not suitable for large-scale pollution treatment because they are unable to utilise natural light.

The hydrogen peroxide and ferrous iron system does not require irradiation. This system, Fenton chemistry, uses the decomposition of hydrogen peroxide by ferrous ions to produce hydroxyl radicals. The description of this reaction is a little confusing. Some papers describe this process as catalytic, even though the reaction (21) is clearly not a catalytic reaction.

$$Fe(II)+H_2O_2 \rightarrow Fe(III)+OH^- + {}^{\bullet}OH \qquad (21)$$

The confusion results from ambiguous descriptions of the process under discussion. The reaction (21) that produces hydroxyl radicals is stoichiometric; each ferrous ion reacts to produce one hydroxyl radical. However, the overall oxidation process is catalytic because the steps in which the organic molecules are oxidised regenerate the ferrous ions from the ferric ions (Walling 1975). Thus, advanced oxidation processes that use Fenton chemistry are catalytic, but they do not utilise the catalytic production of radicals.

Of the five methods for the production of hydroxyl radicals mentioned above, only two fit the ideal requirement and produce radicals catalytically. Fortunately, both photo-Fenton and titanium dioxide chemistry can also utilise solar radiation. Both of these systems have aroused considerable interest in the possibility of their use in wastewater treatment.

The titanium dioxide system is a heterogeneous photocatalytic system. The irradiation of titanium dioxide in aqueous solution at a sufficiently short wavelength produces hydroxyl radicals at the 'titania' surface. Because the generation of radicals requires ultraviolet radiation, the energy requirement for this system is very high. However, unlike the pure hydrogen peroxide system, titanium dioxide can produce hydroxyl radicals upon the absorption of natural light. The major limitation of this system is that it does not work well when the pollutant species also absorb ultraviolet radiation. In addition, comparative studies have shown that, under identical conditions, photo-Fenton systems are faster than titanium dioxide system at oxidising organic material (Malato et al. 2001). A major advantage of the titanium dioxide system is that it is possible to recycle the catalyst.

Photo-Fenton chemistry is just a photochemical extension of Fenton chemistry. The same basic processes are utilised. The ferrous-iron-facilitated breakdown of hydrogen peroxide produces hydroxyl radicals. The additional step in photo-Fenton chemistry is the photochemical reaction of Ferric ion with water to produce a hydroxyl radical and a ferrous ion.

$$Fe^{3+} + H_2O + h\nu \rightarrow Fe^{2+} + {}^{\bullet}OH + H^{+} \qquad (22)$$

The photochemical reaction has a two-fold effect on the rate of hydroxyl radical production. The reaction itself produces another hydroxyl radical, and subsequently, reactions (21) and (22) combine to produce hydroxyl radicals catalytically. The use of coloured iron salts such as iron chloride (Nadtochenko and Kiwi 1998) or iron oxalate (Kim and Vogelpohl 1998) increases the range of wavelengths that drive (22), so that visible light is also effective. At higher wavelengths, reaction (22) may proceed without the production of a hydroxyl radical, but the existence of a catalytic cycle is more important than two radical producing steps. In addition, both ferric and ferrous salts are effective initial reagents in a photo-Fenton system. A disadvantage of photo-Fenton systems is that the ferric ion concentration must always be minimised because ferric ions catalyse the dismutation of hydrogen peroxide to oxygen and water.

$$2H_2O_2 \xrightarrow{Fe^{3+}} 2H_2O + O_2 \qquad (23)$$

The significance of reaction (23) is probably not as great as some authors fear. Walling (1975) has shown that this reaction is almost certainly occurring by a radical mechanism (24), so the side reaction does not represent a complete loss of radicals from the system.

$$\begin{aligned}
&H_2O_2 + Fe^{3+} \rightarrow Fe^{2+} + H^{+} + HO_2^{\bullet} \\
&Fe^{2+} + H_2O_2 \rightarrow Fe^{3+} + HO^{-} + HO^{\bullet} \\
&HO^{\bullet} + H_2O_2 \rightarrow H_2O + HO_2^{\bullet} \\
&HO_2^{\bullet} + Fe^{3+} \rightarrow O_2 + Fe^{2+} + H^{+} \\
&HO_2^{\bullet} + Fe^{2+} \rightarrow HO_2^{-} + Fe^{3+}
\end{aligned} \qquad (24)$$

The photo-Fenton advanced oxidation process is an ideal system to which to apply liquid aerosol photocatalysis. I carried out a brief series of experiments to see how easy this

would be. I had no initial success, and concluded that the glass experimental system that I was using at the time was inappropriate for photo-Fenton chemistry.

Frequently the pollutants that advanced oxidation processes treat are involatile species. Volatile contaminants are reasonably easy to remove from water because they evaporate. Of course, evaporation is not a suitable technique for highly toxic materials. Unfortunately, many conventional techniques for decontamination, like air stripping or activated carbon treatment, are only processes for transferring contaminants into a phase where they are less harmful; the process does not destroy the contaminant. Ideally, all pollution treatment processes should be, like advanced oxidation technologies, destructive rather than transfer processes. However, the combination of liquid aerosol and photo-Fenton techniques is particularly suited to the treatment of involatile contaminants.

Photo-Fenton oxidation processes have many of the characteristics of systems that would work well in the aerosol phases. Firstly, the principle reactants are involatile, while the products are volatile or gaseous, although the system is simpler because the products are not isolated. Secondly, gas-transfer is important; the oxidation reaction requires oxygen and generates carbon dioxide. Finally, most commercial photo-Fenton chemistry uses the sun's radiation, and the focusing of light by aerosol droplets will concentrate solar radiation, making the process more efficient.

It is worthwhile considering how an aerosol photo-Fenton process would work in an industrial situation because this clearly demonstrates some of the advantages of the aerosol process. Assuming that the problem of generating sufficient aerosol, cheaply and consistently, for a commercially feasible process has been solved, there are two approaches, depending on the ease of oxidation of the pollutant, to an aerosol photo-Fenton process. In both approaches, the actual irradiation would take place outdoors. This avoids the expensive requirement for windows that do not attenuate ultraviolet radiation. It also means that the carbon dioxide produced does not have to be vented because it can just diffuse way.

The first approach would be utilised in situations where it was certain that all the organic material would be oxidised before the aerosol droplets evaporated. This situation would be the simplest to implement; the process only requires the generation of the hydrogen

peroxide, iron, and wastewater aerosol, and a subsequent release into the environment sufficiently remote, possibly from the top of a chimney, that the oxidation is complete before the aerosol interacts with anything else. Of course, a thorough study of the potential side effects of hydroxyl-radical-containing aerosols in the environment is required before the implementation of this process.

The second approach requires a more complicated reactor system, but it is probably more environmentally sound. This approach would be utilised in a situation where the oxidation would not necessarily be complete before the aerosol entirely evaporated, leaving involatile aerosol that was essentially pure pollutant. Aerosols would be generated downwards inside a sheath flow similar to that used inside the aerodynamic particle sizer. The production of aerosol inside a sheath flow would ensure that the aerosol is guided into an impactor system, rather than escaping into the environment.

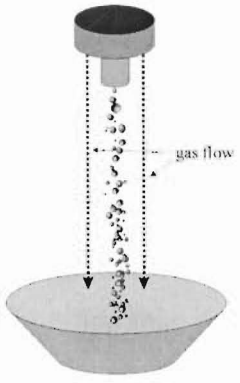

Figure 4.16 Schematic of Aerosol Photo-Fenton System

As the aerosols fall downwards, the sun irradiates them, converting the involatile pollutant into carbon dioxide and water. Impactors at the bottom of both reactor types collect the remaining involatile material and iron. A flow system returns the collected material to the original reactant reservoir for re-nebulisation. Catalyst recycling, which is not possible in conventional photo-Fenton systems, occurs almost by default in this system. Even though the cost of iron salts is relatively small, any recycling of chemicals is beneficial. This also opens up the possibility of using iron-based catalysts that absorb more of the solar spectrum, although I doubt that it would be economically feasible to develop a ligand that is resistant to hydroxyl radicals. A better approach, that utilises more of the solar spectrum, is the use of ferrioxalate (Safarzadeh-Amiri, Bolton and Cater 1996).

I have carried out a small number of preliminary investigations in order to try and determine if liquid aerosol photo-Fenton advanced oxidation processes are worth pursuing. The first group of experiments I carried out in the high-pressure xenon lamp glass system. This system was inappropriate for photo-Fenton chemistry, so the results were inconclusive. However, further work using the stainless steel system indicated that liquid aerosol photo-Fenton chemistry warrants further investigation.

I tried to oxidise three model pollutants: phenol, dyes, and ethylene glycol. None of the species were oxidised in the liquid aerosol photo-Fenton system. The problem with the glass system was that it was necessary to wait at least twenty minutes once the sample had been loaded into the system before it could be nebulised and irradiated. During this time, the ferric iron caused the hydrogen peroxide to decompose via a route that does not produce many radicals. Because the liquid aerosol system was only designed for small amounts of liquid, by the time the liquid was nebulised there was no hydrogen peroxide left.

An additional difficulty with trying aerosol photo-Fenton chemistry is in accessing the amount of change of the pollutant concentration. Thus, in a system without impactor cooling, regardless of any reaction that might have taken place, the collected solution is more concentrated than the original solution, and in one with impactor cooling, the collected solution is considerably more dilute than the original solution. Unfortunately, the magnitudes of the concentration changes are not reproducible.

Because the steel system did not require a wait between sample loading and nebulisation, I decided to carry out some rough experiments to see if the time lag had been the limitation of the previous experiments. The system tested was an ethylene glycol, potassium ferrioxalate, and hydrogen peroxide system. Although, ethylene glycol is not usually considered a pollutant, it is used in sufficiently large amounts to de-ice runways that there is concern about its environmental effects. Consequently, photo-Fenton chemistry has been investigated as a possible method for disposing of ethylene glycol (McGinnis, Adams and Middlebrooks 2000). Additionally, the use of ferrioxalate increases the amount of visible light that photo-Fenton systems can utilise (Safarzadeh-Amiri et al. 1996).

One advantage of using volatile/involatile solutions like water and ethylene glycol in aerosol systems is that most of the water evaporates. I realised that I could see if ethylene glycol was oxidised in irradiated ethylene glycol-ferrioxalate-hydrogen peroxide aerosols by comparing the amount of liquid collected during an irradiated and a dark run. I made up 2×10^{-3} molL^{-1} potassium ferrioxalate solutions in 20% ethylene glycol solution by volume. I combined this solution with 50% hydrogen peroxide in a 1:1 ratio in the nebuliser. Compressed air was used to nebulise the liquid. When the gas-flow rates and the run times were identical, I found that after irradiation between 5% and 10% less material was collected. The amount of material collected from the nebulisation and irradiation of a water and ethylene glycol solution was slightly more than for the unirradiated solution. Assuming that this decrease was due to the oxidation of ethylene glycol, this is actually quite a reasonable rate of oxidation.

These experiments are very rough and the results should be treated with caution. However, I believe that they have served their purpose and demonstrated that aerosol photo-Fenton chemistry has a great deal of potential for the treatment of involatile pollutant containing water.

4.4 Discussion of Liquid Aerosol Photocatalysis

Despite the difficulties I experienced in getting any liquid aerosol photocatalytic system to work, I still think that liquid aerosol photocatalysis has a great deal of potential. The principle reason that liquid aerosol systems are so promising is that they are very complex. This is also the reason why they are so difficult to work with. Before liquid aerosol systems are used in applied systems this complexity needs to be unravelled. In many ways, the approach I have taken to liquid aerosols systems has involved largely ignoring the possibility of understanding the complexities. Instead, I tried to develop systems by trying many different configurations. I do not think that this approach is ineffective; however, it would benefit from closer collaboration with people who are approaching aerosols in a more precise way, such as in single droplet reactivity studies.

5 The Investigation of Optical Effects in the Photochemistry of Liquid Aerosols

5.1 Computational Investigation

In Section 2.2.2, I outlined the mathematical theory, Mie theory, for the interaction of electro-magnetic radiation with microdroplets. I wanted to use Mie theory to calculate the distribution of light intensity in an irradiated aerosol droplet in my system. There is no shortage of computer programs designed to calculate the interaction of electromagnetic radiation with small particles; there are at least two large online listings of scattering codes (Flatau 2000, Wriedt 2002). However, there is a considerable bias towards scattering of radiation by particles as opposed to the absorption of radiation by particles, both in the literature published about, and in the computer programmes written for, the interaction of electromagnetic radiation with small particles. Even in Bohren and Huffman's book entitled *The Absorption and Scattering of Light by Small Particles*, the Mie theory code they provide is only for calculating the scattering of light by a droplet (1983 pp. 477-482). Of course, most researchers working with small particles are interested in the scattering of light for the particles rather than the absorption of light by the particles, so this bias is not particularly surprising.

Although this bias exists, it does not mean that there are no investigations of the absorption of light by small droplets, just that they are harder to find. I thought that I already knew roughly what the distribution of light inside the droplets was going to look like; however, I was wrong. Additionally, the majority of computational studies focus either on the absorption of light by atmospheric droplets, or on the absorption of laser light by droplets. The nature of the photochemistry of liquid aerosols falls somewhere between these two extremes. The light comes from an un-polarised thermal light source, but the composition, and to some degree the size, of the droplets are well characterised. I found the process of carrying out the numerical calculations to play an invaluable part in understanding some of the physical interactions involved in the photochemistry of liquid aerosols.

5.1.1 Computational Investigation of Ultraviolet and Visible Light Absorption by Microdroplets

The majority of investigations on the interaction of light with microdroplets have focused on the scattering and the external field. Often the only parameter related to absorption and the internal field calculated is the absorption cross-section, and this is calculated as the difference between the extinction cross-section and the scattering cross-section.

There have been two major groupings of studies of the absorption of light by small droplets. There is interest in the absorption of infrared radiation by droplets, and a number of studies have also been carried out which aim to model the intensity distributions inside droplets in an engine (Lage and Rangel 1991, Mackowski 1989, Tuntomo, Tien and Park 1991). However, the size parameters and complex refractive indices associated with the absorption of infrared radiation are quite different from those that are relevant when considering the absorption of ultraviolet and visible radiation.

One paper has been published entitled 'Effect of Optical Resonances on Photochemical Reactions in Microdroplets' (Ray and Bhanti 1997). The introduction to this paper contains references to a number of other papers that have examined the absorption of light by small droplets. These papers mention that the enhancement of light intensity due to optical resonances, particularly at the surface of the droplet, might be important in the photochemistry of atmospheric aerosols. However, Ray and Bhanti present the only investigation of the effect of optical resonances on photochemistry. They note that the rate of photochemical reaction in a droplet is proportional to two opposing variables: concentration and intensity. The enhancement of internal intensity is greater for smaller complex parts of the refractive index, but the complex part of the refractive index increases as the concentration of absorbing species increases.

In their book, *Light Scattering by Particles: Computational Methods*, Barber and Hill include some graphs of the light intensity distribution inside droplets. However, these graphs are for droplets with complex parts of the refractive index that are significantly higher than are relevant for the absorption of ultraviolet and visible light.

In addition, Ruggaber et al. (1997) have calculated the actinic flux inside droplets with a range of atmospherically relevant size distributions and particle compositions. They have

shown that the internal actinic flux is on average more than twice the external actinic flux and at certain size parameters very large enhancements are observed. However, they derived the internal actinic flux from the external actinic flux. Consequently they were limited to the calculation of the droplets absorption cross-sections and they were unable to investigate the structure of the internal intensity distribution.

I have calculated the internal energy distribution inside droplets containing photochemically and photocatalytically relevant concentrations of absorbing species. I have also examined the effect of optical resonances on the intensity distribution of broadband irradiation inside droplets, and the effect of species that have varying absorbances across this range.

This investigation is based primarily on the techniques outlined in chapter four of Barber and Hills' book. I have summarised the important mathematical equations here. The internal electric field for parallel incident polarisation is

$$E_r = n(n+1)\frac{1}{mkr} j_n(mkr)\cos\varphi \frac{P_n^1(\cos\theta)}{\sin\theta}\sin\theta d_{e1n} \tag{25}$$

$$E_\theta = j_n(mkr)\cos\varphi \frac{P_n^1(\cos\theta)}{\sin\theta} c_{o1n} + \left[j_{n-1}(mkr) - \frac{j_n(mkr)}{mkr} \right] \cos\varphi \left[n\cos\theta \frac{P_n^1(\cos\theta)}{\sin\theta} - (n+1)\frac{P_{n-1}^1(\cos\theta)}{\sin\theta} \right] d_{e1n} \tag{26}$$

$$E_\varphi = -j_n(mkr)\sin\varphi \left[n\cos\theta \frac{P_n^1(\cos\theta)}{\sin\theta} - (n+1)\frac{P_{n-1}^1\cos\theta}{\sin\theta} \right] c_{o1n} - \left[j_{n-1}(mkr) - n\frac{j_n(mkr)}{mkr} \right] \sin\varphi \frac{P_n^1(\cos\theta)}{\sin\theta} d_{e1n} \tag{27}$$

In equations (25), (26), and (27) the usual convention for spherical coordinates is used: j_n is the spherical Bessel function of the first kind, P_n^1 is the associated Legendre function, m is the complex refractive index and k is the wavenumber. The incident wave propagates in the $+z$ direction. The internal field coefficients c_{o1n} and d_{e1n} can be re-expressed from equations (5) and (6) using

$$\left[xz_n(x) \right]' = xz_{n-1}(x) - nz_n(x) \tag{28}$$

They become

$$c_{o1n} = i^n \frac{2n+1}{n(n+1)} \left\{ \frac{\frac{i}{x}}{\left[j_n(mx) h_{n-1}^{(1)}(x) - m h_n^{(1)}(x) j_{n-1}(mx) \right] x} \right\} \tag{29}$$

and

$$d_{e1n} = -i^{n+1} \frac{2n+1}{n(n+1)} \left\{ \frac{\frac{mi}{x}}{x\left[m^2 j_n(mx) h_{n-1}^{(1)}(x) - m h_n^{(1)}(x) j_{n-1}(mx) \right] - n(m^2-1) h_n^1(x) j_n(mx)} \right\} \tag{30}$$

The expressions for perpendicular incident field polarisation differ from those for parallel polarisation only by the switching of the cosϕ and sinϕ terms. However, I only considered unpolarised incident light. The internal intensity distribution is unaffected by the polarisation of the incident light, but I was unsure how to modify the equations to reflect this. Therefore, I initially calculated the internal energy distribution for both parallel and perpendicular polarisation, and then added the two distributions together and divided the sum by two. This produced three identical distributions, and thereafter I only calculated the distribution for parallel incident polarisation and assumed it was the same as that for unpolarised incident radiation. The papers cited above, which consider the absorption of infrared radiation by droplets, set ϕ equal to ¼π when the incident light is unpolarised. Unfortunately, the origin of this technique is unclear, so I did not use it. It is also unclear why ϕ equals ¼π in the XZ axial plane when it should equal zero. I did carry out some calculations with ϕ = ¼π, and the internal energy distributions had the same qualitative features as when ϕ varies.

The majority of internal energy distributions calculated were slices through the y = 0 plane, and consequently the ϕ = 0 plane. When ϕ = 0, so does equation (27), and equations (25) and (26) are simplified because the cosϕ term is equal to one.

The first spheres for which I calculated the internal intensity distributions had x = 20 and m = 1.5, 1.5+0.05i, and 1.5+0.10i. The complex part of the refractive index is related to the absorbance by:

$$m_i = \frac{\lambda A}{4\pi} \tag{31}$$

Barber and Hill provide sample numerical data for these spheres. Following Barber and Hill, and in order to simplify the images, I have set the intensity outside the sphere to zero. Unless stated otherwise, the intensity distributions have been calculated in the $\phi = 0$ plane.

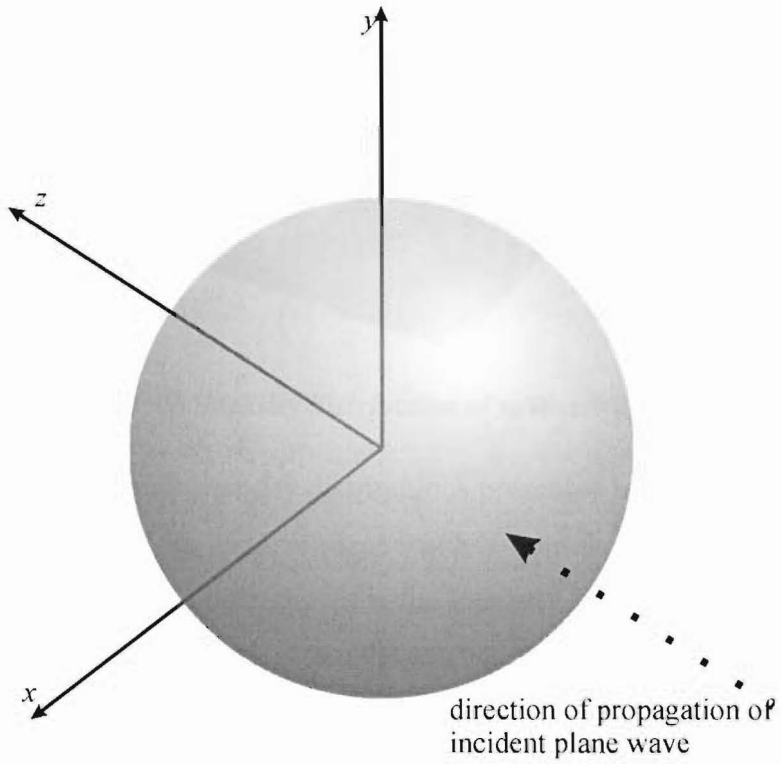

Figure 5.1 The axis system used for internal intensity calculations

Figure 5.1 indicates the orientation of the axis system used for internal intensity calculations. All the internal intensity distributions images below display the internal intensity in the $y = 0$ plane. These images are oriented in the same way as Figure 5.1; the incident plane wave propagates in the $+z$ direction.

The incident field intensity is equal to one, and the droplet radii have all been normalised to one. My calculations produced the same numerical results as those of Barber and Hill, and the intensity distribution images have the same features.

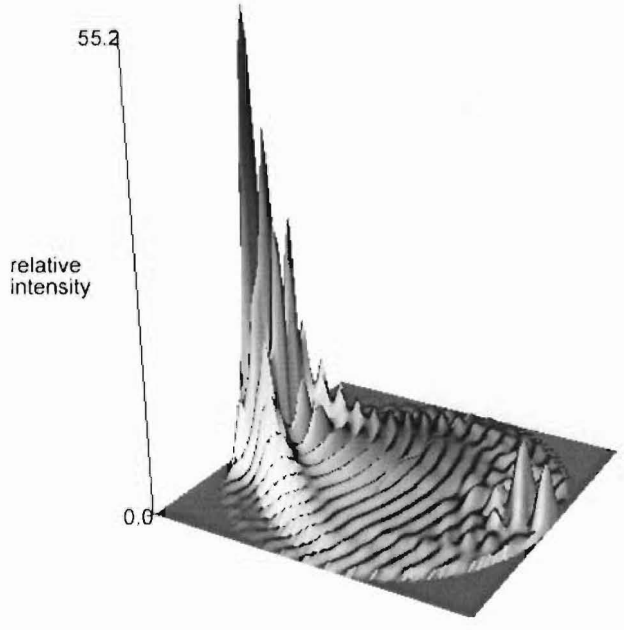

Figure 5.2 Internal intensity distribution of sphere with $x = 20$, $m = 1.5$

All of the images of internal intensity distributions presented here are oriented so that the direction of propagation of the incident plane wave is from the right hand side of the page. The relative intensity enhancement shown is the intensity relative to an incident intensity of one. Figure 5.2 is an image of the internal energy distribution of a non-absorbing sphere. The majority of the intensity inside the sphere is concentrated on the shadow side of the droplet. The average intensity enhancement, relative to an incident intensity of one, is 2.04 throughout the droplet's $\phi = 0$ plane.

Figure 5.3 and Figure 5.4 are images of the intensity distribution inside absorbing spheres. When the complex component of the refractive index is 0.05, some shadow side enhancement is still observable. However, the enhancement is twenty-fold smaller than for a non-absorbing sphere, and considerably more intensity is present on the illuminated side of the droplet. The average intensity change relative to the incident intensity in Figure 5.3 is 0.32.

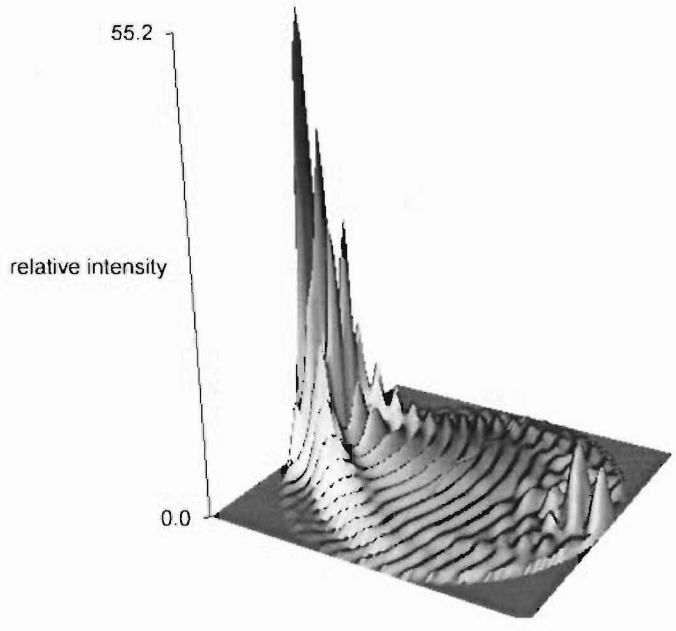

Figure 5.3 Internal intensity distribution of a sphere with $x = 20$, $m = 1.5 + 0.05i$

When the complex component of the refractive index is as high as 0.1, the shadow side enhancement has virtually disappeared and although some resonances are present, the intensity distribution does not look very different to what would be expected if no resonance conditions existed. Additionally, at no point in the droplet is the internal field intensity higher than the incident intensity, and the average intensity enhancement is only 0.14.

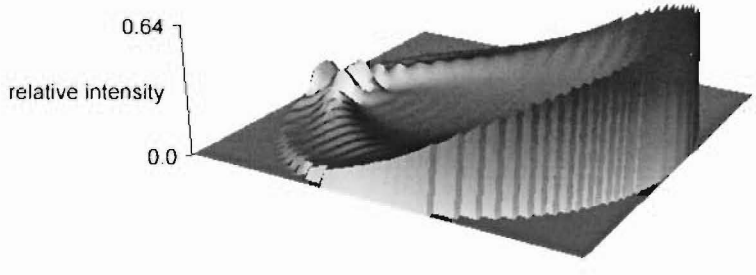

Figure 5.4 Internal intensity distribution of a sphere with $x = 20$, $m = 1.5 + 0.1i$

Because the bulk of the internal field intensity is located on the irradiated side of the droplet and is distributed in an unsurprising way, it might be concluded from these images that Mie absorption is not particularly important in the photochemistry of aerosols. However, a complex component of the refractive index of 0.1 is not particularly relevant to real photochemistry situations. To obtain a complex component of the refractive index of

0.1 for 500 nm radiation requires a 1 $molL^{-1}$ solution of a species, with a molar extinction coefficient of 2.5×10^6 $L \cdot mol^{-1} \cdot cm^{-1}$ and 200 nm irradiation requires a 1 $molL^{-1}$ solution of a species, with a molar extinction coefficient of 6.2×10^6. Both requirements are well beyond usual operating conditions.

Shown below are the internal intensity distribution images of 1 μm droplets irradiated at 500 nm. The droplets are made from solutions that have absorbances of 2, 200, 20000, and 2000000. At 500 nm, these absorbances correspond to values of m_i of 7.96×10^{-8}, 7.96×10^{-6}, 7.96×10^{-4}, and 7.96×10^{-2} respectively. Because the field varies more rapidly in the z direction, all calculations were carried out on a grid with 202 points in the z direction and 51 in the x direction. Throughout this section, a droplet described as a one-micron droplet is a droplet with a radius of one micron.

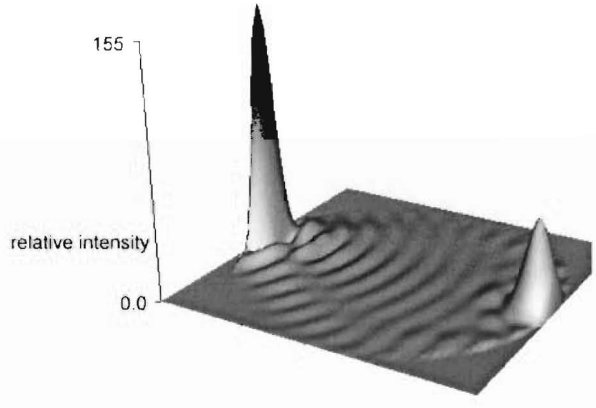

Figure 5.5 Internal intensity distribution; $m = 1.5 + 7.96 \times 10^{-8}$, $a = 1$ μm, $A_{500} = 2$

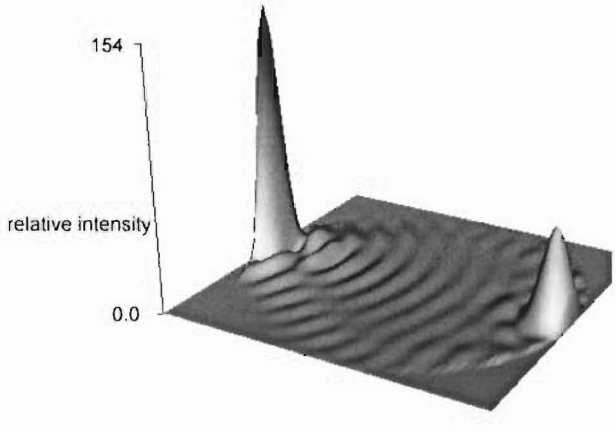

Figure 5.6 Internal intensity distribution; $m = 1.5 + 7.96 \times 10^{-6}$, $a = 1$ μm, $A_{500} = 200$

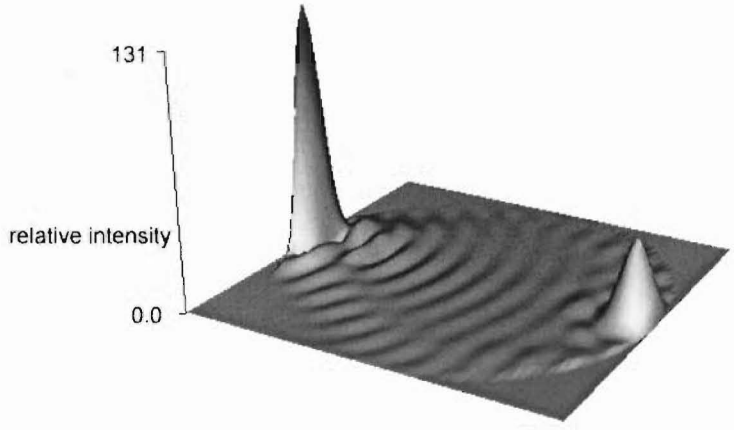

Figure 5.7 Internal intensity distribution; $m = 1.5 + 7.96\times10^{-4}$, $a = 1\ \mu m$, $A_{500} = 20000$

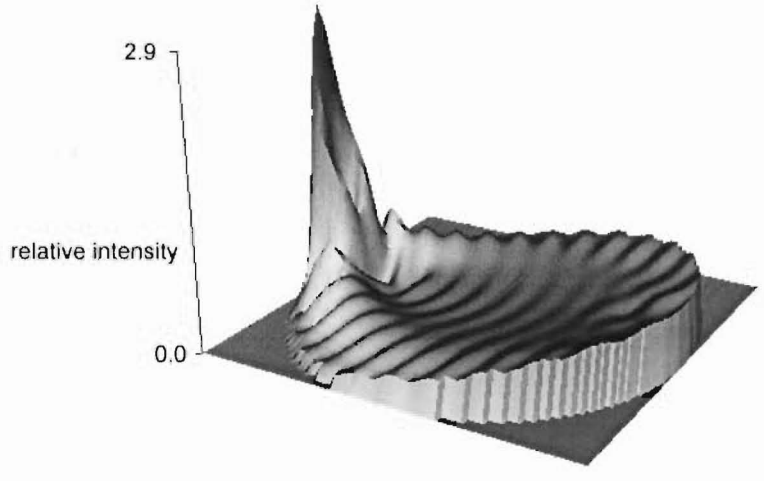

Figure 5.8 Internal intensity distribution; $m = 1.5 + 7.96\times10^{-2}$, $a = 1\ \mu m$, $A_{500} = 2000000$

Both Figure 5.5 and Figure 5.6 show an internal intensity distribution that is virtually identical to that of a sphere with $x = 12.57$ and $m = 1.5$. Even if this similarity is the result of a lack of precision in my programme and a more accurate calculation may reveal more detailed structure, it is not going to produce a significantly different intensity distribution. Consequently, the intensity inside droplets with solution absorbances of between approximately 2 and 200 is the same as for a non-absorbing sphere. These droplets have an average energy enhancement of 3.03 over the incident intensity in the ϕ=0 plane. Additionally, the large shadow side peak has an average intensity enhancement of approximately 50 and is located within 150 nm of the surface. The maximum enhancement shown in Figure 5.5 of 154, is located 52 nm from the surface, and the surface enhancement is 146 where $\theta = 0$. Therefore, the molecules in the interfacial region on the shadow surface of the droplet will be exposed to very large field intensities.

When the solution absorbance reaches 20000, Figure 5.7, the height of the major enhancement peak starts to drop, and average intensity enhancement decreases to 2.67. Solutions with absorbances of 2000000, Figure 5.8, exhibit far more familiar internal intensity distributions, with an average intensity enhancement of 0.34.

When 10 μm droplets irradiated at 500 nm are considered, the results are qualitatively similar. Unsurprisingly, the same independence of concentration is observed for solution absorbencies of 2 and 200. However, the size parameter for a 10 μm droplet irradiated at 500 nm is 125.7.

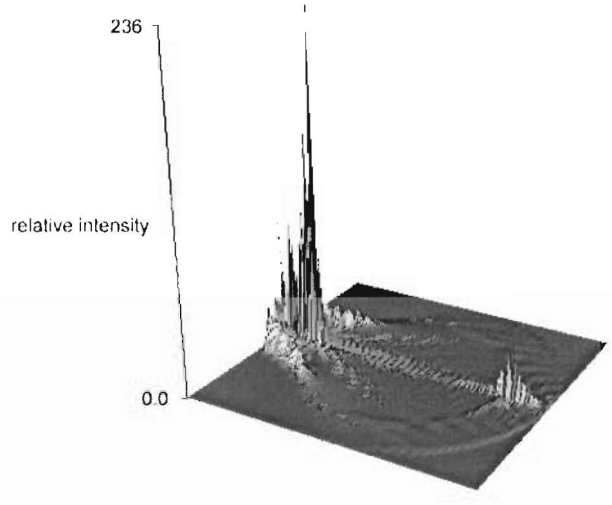

Figure 5.9 Internal intensity distribution; $m = 1.5 + 7.96\times10^{-8}$, $a = 11$ μm, $A_{500} = 2$

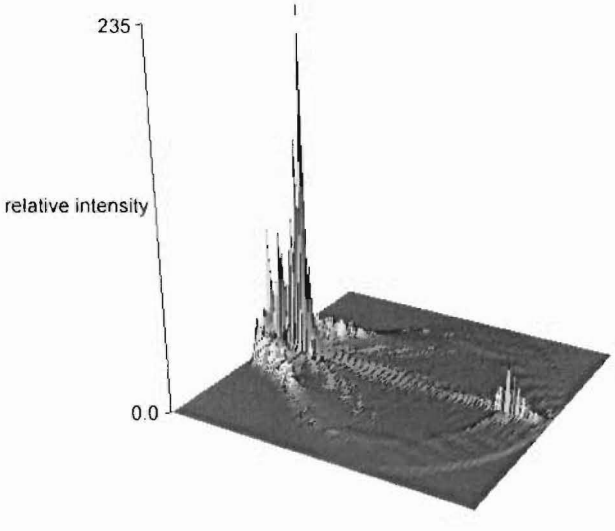

Figure 5.10 Internal intensity distribution; $m = 1.5 + 7.96\times10^{-6}$, $a = 11$ μm, $A_{500} = 200$

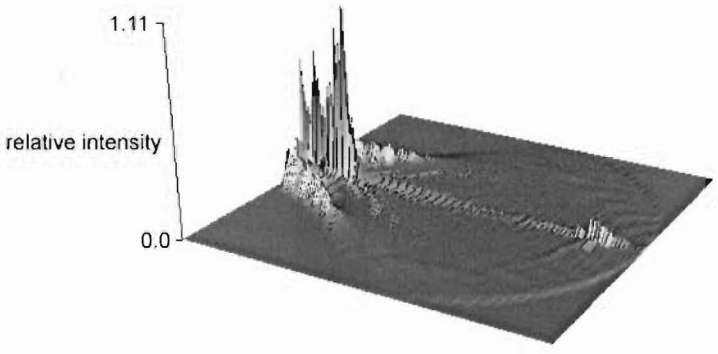

Figure 5.11 Internal intensity distribution; $m = 1.5 + 7.96\times10^{-4}$, $a = 11$ μm, $A_{500} = 20000$

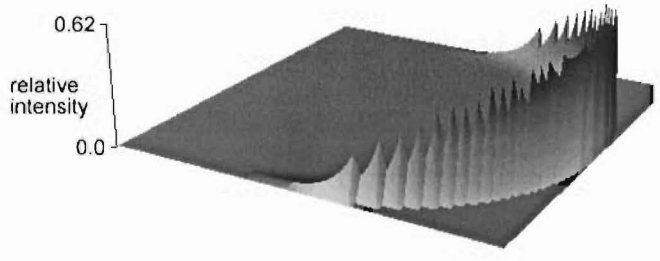

Figure 5.12 Internal intensity distribution; $m = 1.5 + 7.96\times10^{-2}$, $a = 11$ μm, $A_{500} = 2000000$

Larger droplets, and by implication larger size parameters, have more complicated internal intensity distributions and exhibit greater sensitivity to increases in the complex part of the refractive index. Figure 5.12, the image of the internal intensity distribution for $x = 125.7$ and $m = 1.5 + 0.0796$, exhibits no resonance structure at all. The peak-like features are an artifact of the resolution of the calculation. Figure 5.11 exhibits a drop of maximum intensity enhancement relative to the non-absorbing sphere of more than half, while the equivalent drop for a droplet with $x = 12.57$ is approximately 10%. Furthermore, the average enhancement in Figure 5.9 and Figure 5.10 is 1.88 relative to the incident wave, while the equivalent enhancement for a 1 μm drop is 3.03. The intensity enhancement for larger droplets is also located deeper inside the droplet than it is for smaller droplets.

I calculated the internal energy distributions for droplets with radii (a) between 0.1 μm and 10 μm, which were irradiated at 500 nm.

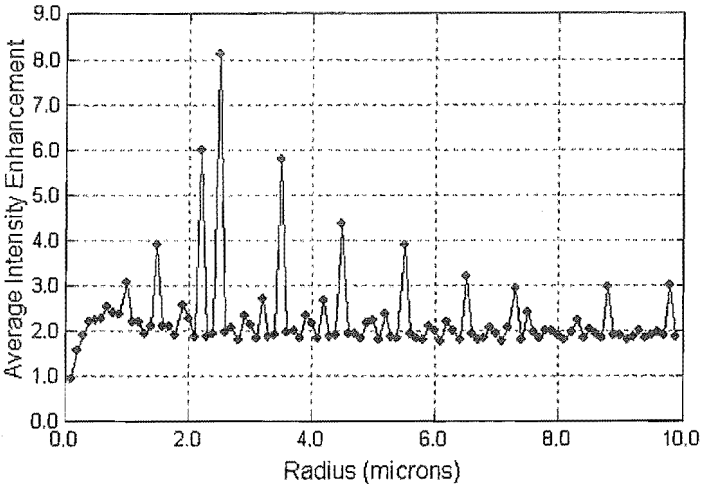

Figure 5.13 Average Intensity Enhancement in the $\phi = 0$ plane

Figure 5.13 shows the average internal intensity enhancement in the $\phi = 0$ plane. The internal intensity distributions were calculated for droplets with a refractive index of 1.5. Thus, the results are applicable to both non-absorbing spheres and to absorbing spheres with concentrations in the region of photochemical interest. It is clear from Figure 5.13 that there is some sort of periodicity in the dependence of the internal field enhancement on the size parameter or droplet radius. This is not surprising, and many books about light scattering discuss the dependence of the absorption cross section on the size parameter (x) (for example Barber and Hill 1990 p. 213). It is important to note that I have not calculated the absorption cross-sections.

In Figure 5.13, the maximum intensity enhancement occurs when $x = 10\pi$. Given that the size parameter is equal to $2\pi a/\lambda$ it is not surprising that the optimum size parameter is a multiple of π. To investigate this resonance condition further, I recalculated Figure 5.13 with a $\pi/4$ separation between size parameter values. In comparison, Figure 5.14 shows this result for a range of droplet sizes irradiated at 500 nm.

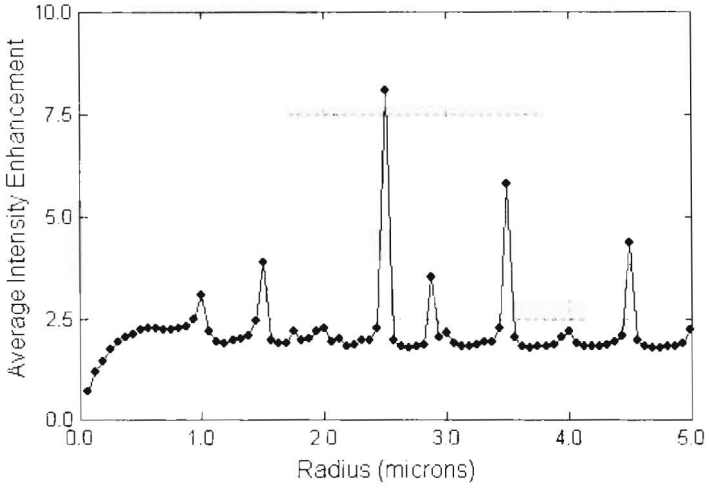

Figure 5.14 Average intensity enhancement; $x = n\pi/4$, n = 1,2,3...

It can be seen from both Figure 5.13 and Figure 5.14 that droplets with radii smaller than ~0.5 μm do not enhance the internal intensity. This is not surprising and could be stated as the general condition that internal intensity enhancement is not observed for $a \leq \lambda$. The most prominent internal intensity enhancements are observed for $x = 6\pi$, 10π, 14π, 18π...etcetera and the maximum enhancement is observed for 10π. A curious feature of both Figure 5.13 and Figure 5.14 is that, although the maximum enhancement varies significantly, the minimum enhancement when $a > \lambda$, remains constant at 2. This is consistent with previous results that only calculated the absorption cross section (Ruggaber et al. 1997).

Shown below are a series of internal energy distributions of droplets in the range discussed above.

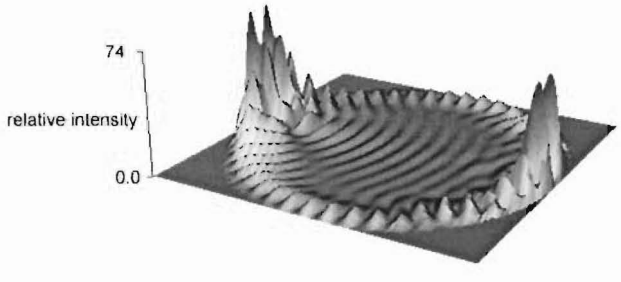

Figure 5.15 Internal intensity distribution, $x = 6\pi$

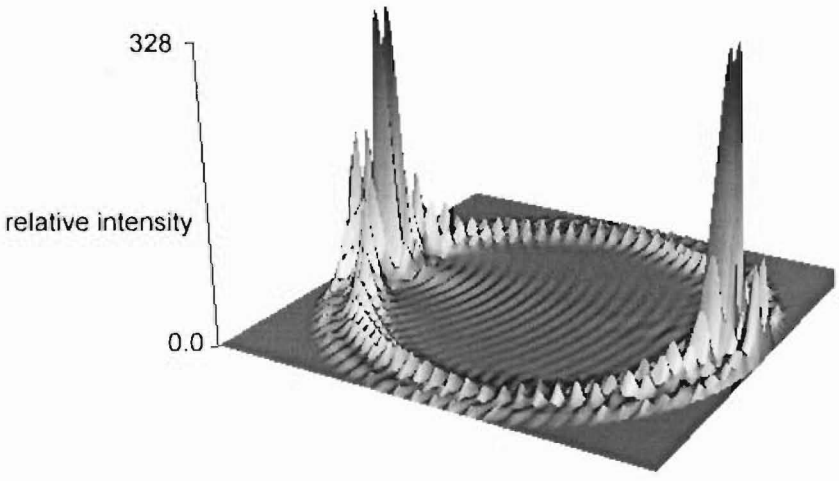

Figure 5.16 Internal intensity distribution, $x = 10\pi$

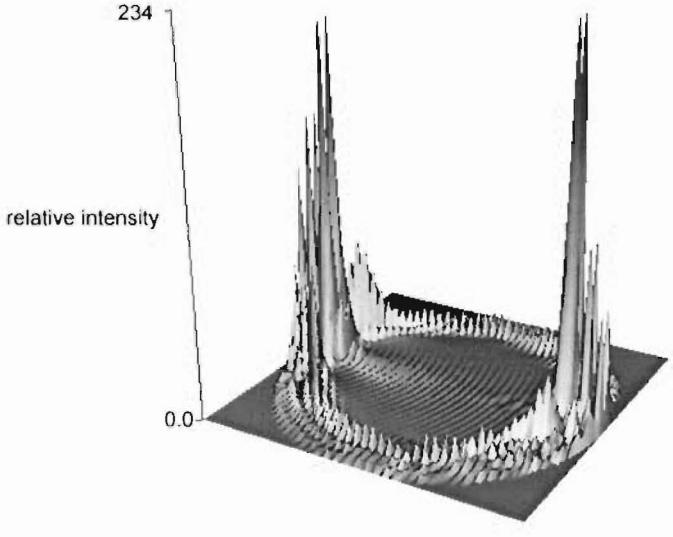

Figure 5.17 Internal intensity distribution, $x = 14\pi$

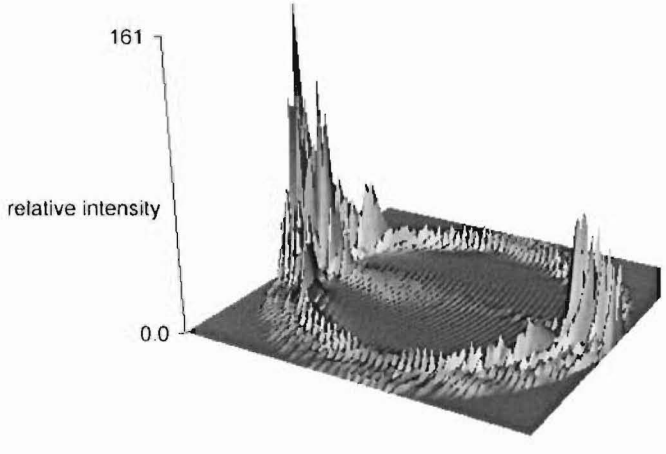

Figure 5.18 Internal intensity distribution, $x = 18\pi$

As has previously been observed, the internal intensity distributions become more complicated with increasing size parameter. The intensity enhancement also becomes more spread throughout the droplet. Furthermore, note that in the size parameter ranges between 6π and 16π, the peak on the irradiated side of the droplet is as intense as the peak on the shadow-side, and is located just as close to the surface. The equal intensity of the two peaks appears to be only a feature of the strongly resonant size parameters.

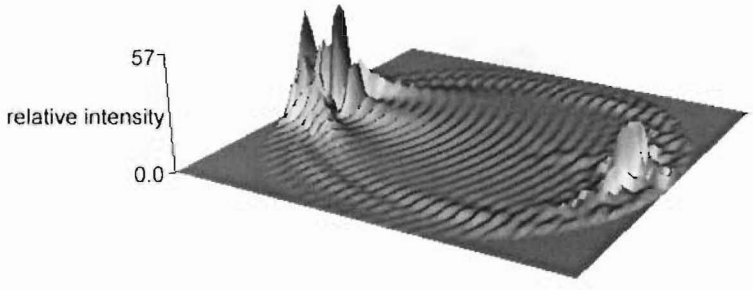

Figure 5.19 Internal intensity distribution, $x = 9¼\ \pi$

Figure 5.19 shows the internal intensity distribution of a droplet with a size parameter that is $¼\pi$ less than 10π. The peak on the irradiated side is significantly smaller than the peak on the shadow side. Clearly, one of the conditions for very high internal intensity enhancement is the resonance of the irradiated side peak as well as the shadow-side peak.

Significantly, Figure 5.14 does not reproduce all the strongly resonant peaks observed in Figure 5.13. The second most intense peak in Figure 5.13 is not present in Figure 5.14, and the size parameter of that peak is equal to 8.80π. The internal energy distribution of this peak is reproduced in Figure 5.20.

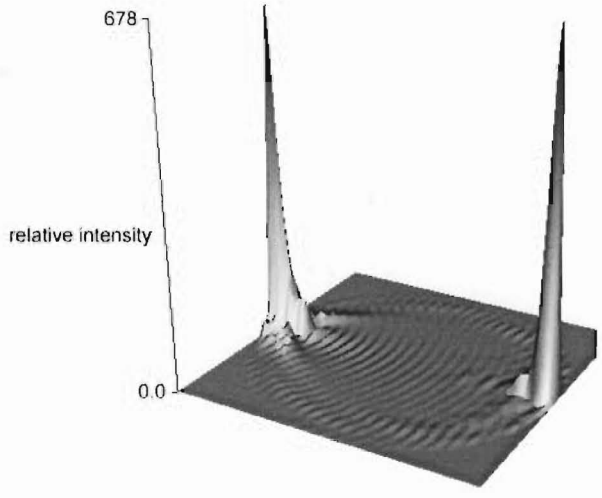

Figure 5.20 Internal intensity distribution, $x = 27.65$

Although the size parameter of 27.65 in Figure 5.20 is not far from that of 31.14 in Figure 5.16, the appearance of the two internal intensity distributions is quite different. Figure 5.20 is a much simpler distribution that is qualitatively more like the distributions for $x = 4\pi$ which feature prominently in this chapter (for example Figure 5.5). In addition, the intensity enhancements in Figure 5.20 are much more concentrated than those in the $(4n+2)\pi$ series. The maximum enhancement in Figure 5.20 is approximately 680, which is considerably greater than the enhancement of 330 observable in Figure 5.16 and Figure 5.17.

Having calculated the internal intensity distributions of droplets irradiated at 500 nm, I wanted to consider droplets irradiated by a broadband source. I wanted to be certain that the superposition of the internal intensity distributions for many wavelengths was not going to average out the intensity enhancements.

In order to avoid complications in the results, I considered a one micron droplet irradiated by plane waves, all with intensities of one, and wavelengths from 800nm to 200 nm. Furthermore, the droplets consisted of a solution which absorbed evenly across the entire wavelength range. Again I considered absorbances of 2, 200, 20000, and 2000000. The images shown below are the averages of the internal intensity distributions taken every 5 nm across the 800 nm to 200 nm range.

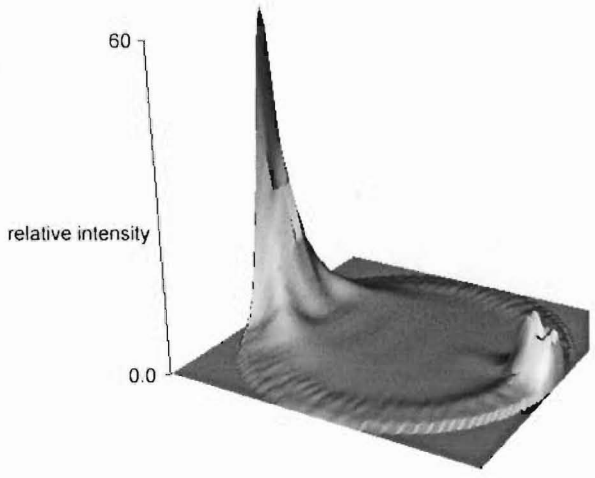

Figure 5.21 Internal intensity distribution; 1 μm droplet, 800 nm $\geq\lambda\geq$200 nm, A = 2

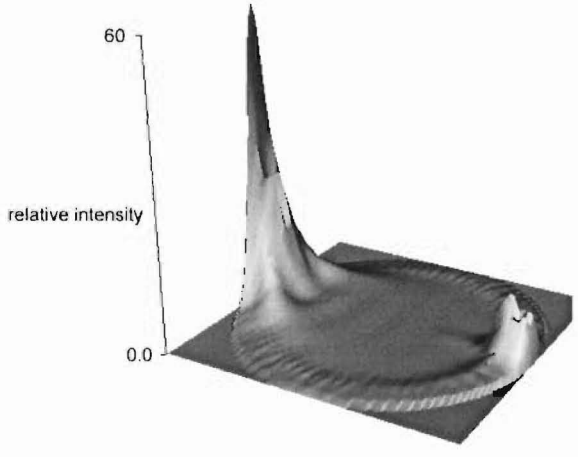

Figure 5.22 Internal intensity distribution; 1 μm droplet, 800 nm $\geq\lambda\geq$200 nm, A = 200

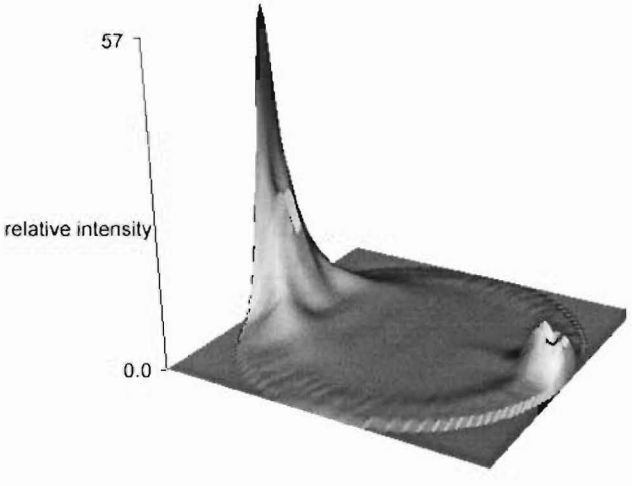

Figure 5.23 Internal intensity distribution; 1 μm droplet, 800 nm $\geq\lambda\geq$200 nm, A = 20000

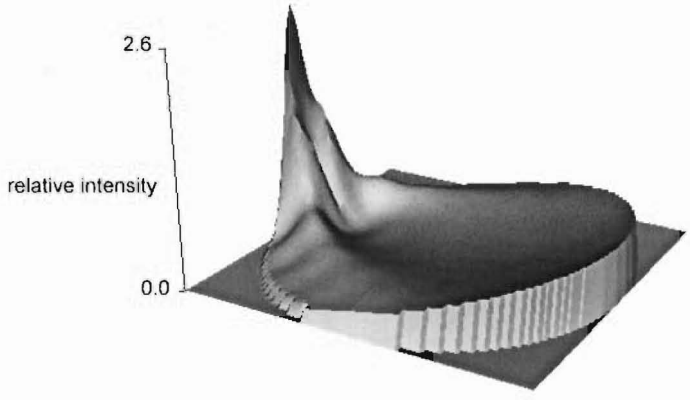

Figure 5.24 Internal intensity distribution; 1 μm droplet, 800 nm $\geq\lambda\geq$200 nm, A = 2000000

Note that the intensity in Figure 5.24 is thirty-fold smaller than that of the other three images. From Figure 5.21, Figure 5.22, and Figure 5.23 it is clear that internal intensity enhancements are possible even when a droplet is irradiated by a broadband thermal light source. The maximum intensity enhancements are approximately sixty-fold, and the average intensity enhancements are 2.5 for A = 2 and A = 200, and 2.3 for A = 20000. Furthermore, most of the enhanced intensity is located close to the surface of the droplet.

Having established that the light intensity is enhanced inside droplets irradiated over a range of wavelengths, I wanted to see if any particular wavelengths were absorbed significantly more than others were. Figures 5.24 to 5.29 show the variation of the intensity enhancement averaged throughout the droplet with wavelength.

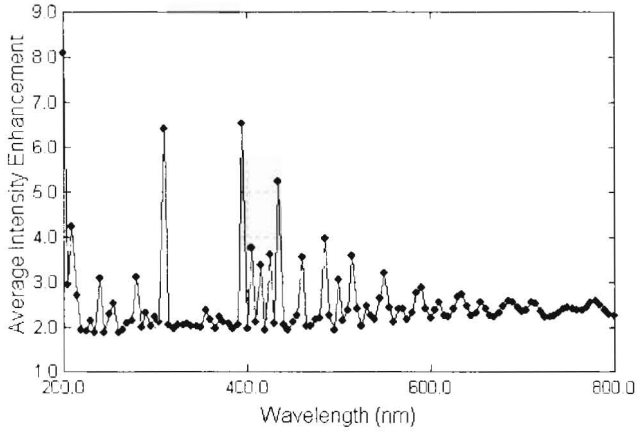

Figure 5.25 Wavelength vs Enhancement, A = 2, a = 1 μm

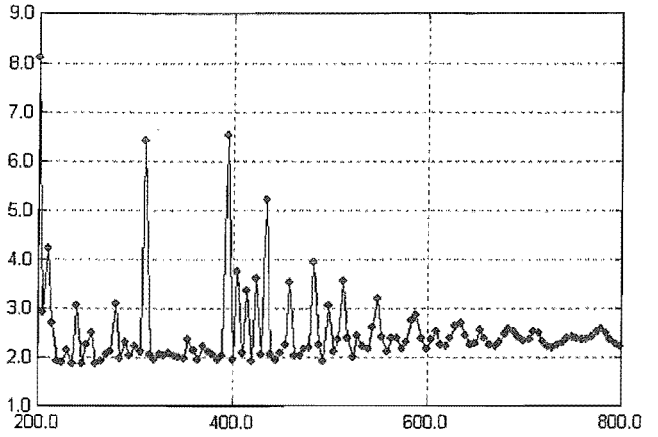

Figure 5.26 Wavelength vs Enhancement, A = 200, $a = 1$

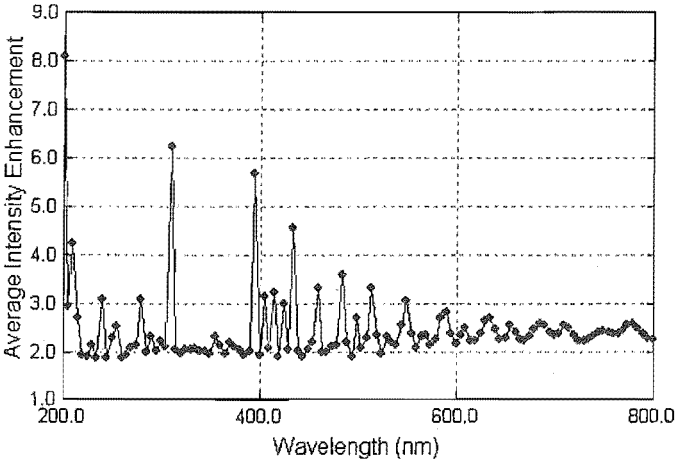

Figure 5.27 Wavelength vs Enhancement, A = 20000, $a = 1$ μm

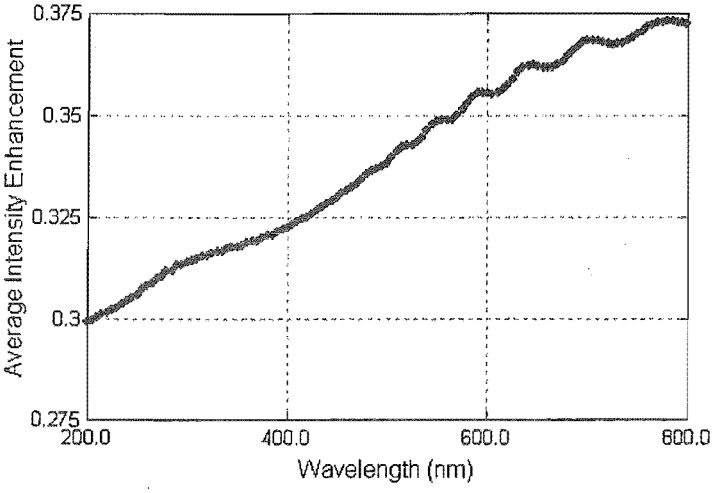

Figure 5.28 Wavelength vs Enhancement, A = 2000000, $a = 1$ μm

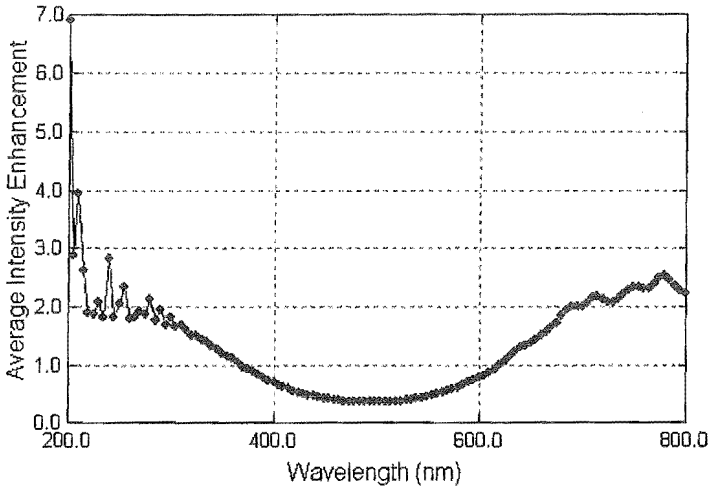

Figure 5.29 Wavelength vs Enhancement, A = 2000000 (Gaussian), $a = 1$ μm

Figure 5.25, Figure 5.26, Figure 5.27, and Figure 5.28 show the wavelength versus average intensity enhancement for constant absorbances across the entire wavelength range. The first three are identical and the fourth represents absorbances beyond any reasonable operating conditions. I also calculated the intensity distributions for solutions that contained a species whose absorbance was characterised by a Gaussian centred on 500 nm with a half linewidth of 100 nm (Figure 5.29). The absorbances at 500 nm were set to A = 2, 200, 20000, and 2000000 respectively. However, only the last of these was any different to the constant absorption distribution, and, in any case, this is the unreal absorption range.

The resonances in Figure 5.25, Figure 5.26, and Figure 5.27 revealed another resonance internal intensity distribution that was different to the two types of distributions already observed. Figure 5.30 is an image of this distribution for the size parameter of 20.27, which corresponds to a wavelength of 310 nm in a one-micron droplet. Note that there are double peaks on both the shadow and irradiated sides.

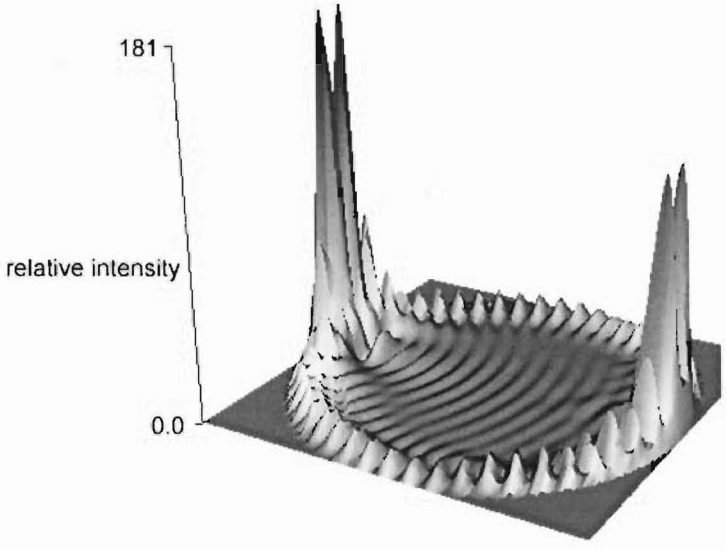

Figure 5.30 Internal intensity distribution, x = 20.27

When considering one-micron droplets, the range of size parameters accessible at reasonable wavelengths is limited. However, this limitation can be overcome by increasing the droplet radius.

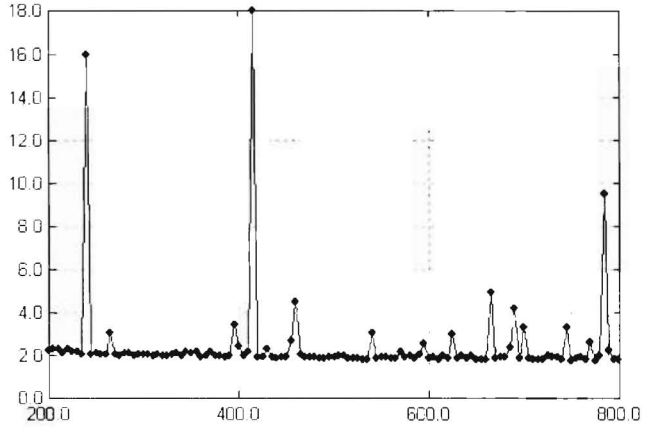

Figure 5.31 Intensity vs Wavelength for an 11 μm droplet

Figure 5.31 shows the presence of some dramatic resonances in the average intensity versus wavelength plot for an eleven-micron droplet. Figure 5.32 shows an image of the internal intensity distribution for the 425 nm peak.

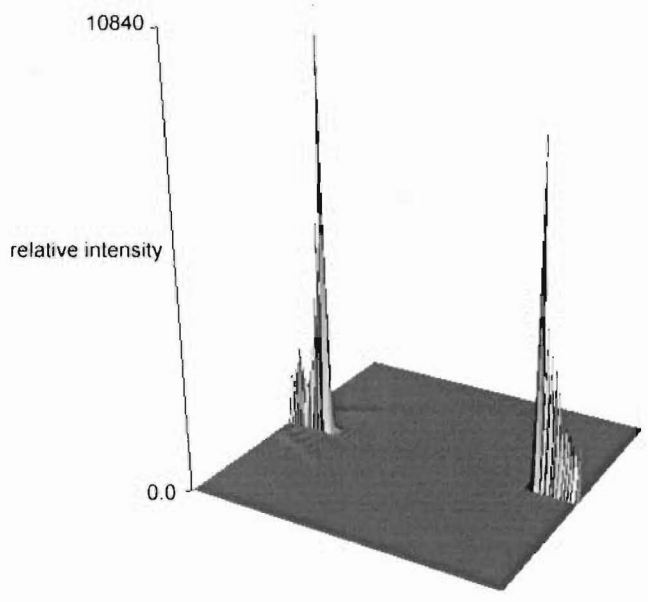

Figure 5.32 Internal intensity distribution, x = 166.54226115

All three of the strong peaks in Figure 5.31 had the same qualitative appearance, although the peaks are so intense that it is difficult to make out any features. These peaks are much narrower than those observed in one-micron droplets. Carrying out the calculation with x = 166.54 instead of x = 166.54226115 results in a thirteen fold decrease in the total intensity, and a reduction of the average intensity enhancement to 2.9. Furthermore, these resonances are much more sensitive to the complex part of the refractive index. The maximum intensity for a droplet with $x = 166.54226115 + 7.96\times10^{-6}i$ is seven fold smaller than for the non-absorbing sphere, and the average enhancement is reduced to 4.11. Nevertheless, a maximum intensity enhancement of over 10000 fold is phenomenal.

Enhancements in the absorption cross-section of droplets considerably greater than the average intensity enhancements I calculated have been reported (Ruggaber et al. 1997). Pure water droplets with radii between 3 μm and 10 μm irradiated at 550.5 nm have enhancement factors > 40. However, enhancements in the absorption cross-section are not directly comparable with the average intensity enhancement in these calculations.

5.1.2 Summary of Computational Investigation

The ultraviolet-visible spectrometer that I used was unable to produce reliable measurements for solutions with absorbances greater than 2. In order to measure the

absorbance of the solutions I was working with I frequently had to dilute them 10 or 100 fold, and occasionally I had to dilute them 1000 fold. Thus, although the solutions I worked with were photochemically and photocatalytically active they can be regarded, within the accuracy of my calculations, as having no complex component of their refractive index. Consequently, my initial assumption that before carrying out the calculations I knew what the internal intensity distribution was going to look like, was a false one. I expected that it would look somewhat like Figure 5.3 and Figure 5.4, the sample distributions provided by Barber and Hill for absorbing droplets.

The computed internal intensity for photochemically relevant droplets has demonstrated the plausibility of the mechanism proposed in the previous chapter for the enhanced photolytic reactivity of $Mo(CO)_6$. It has been shown that large enhancements in internal intensity near the surface of the shadow side are a characteristic feature of droplets that have the size parameters and concentrations of absorbing species present in liquid aerosol photochemical systems. The intensity of these on and near the shadow side surface of the droplets means that it is quite likely photolysis will take place almost exclusively near the surface, resulting in a significant decrease in the time required for carbon monoxide to diffuse out of the solvent cage.

These calculations have demonstrated a range of interesting features in the internal intensity distributions of droplets, and phenomenal enhancements in light intensity have been observed. The accuracy of these calculations is dependant on the applicability of equation (32) for n_c. The number of terms required for a Mie summation. x is the size parameter

$$n_c = x + 4.05\sqrt[3]{x} + 2 \qquad (32)$$

If the number of terms used is 3 or 4 times the value defined by (32), then all of the structure observed disappears and the internal intensity distributions average out. Every discussion of Mie scattering mentions the instability of the Bessel functions used in the calculations. Equation (32) is the standard equation for ensuring that sufficient terms have been used. Because my computations reproduced the sample distributions provided by Barber and Hill, I am confident that they are accurate, and that the distributions I have

computed are not the result of insufficient terms. However, I was not so confident that I felt it was unnecessary to mention this possible limitation.

The results of these calculations are relevant beyond the realm of liquid aerosol photocatalysis. They are naturally important in atmospheric photochemistry. In particular, photochemical processes close to the surface of small (1 μm) droplets are much more important than has been previously recognised.

5.2 Experimental Investigation

I wanted to measure the actinic flux into an aerosol system as a way of determining the light available for reaction in the aerosol system.

5.2.1 Introduction to Chemical Actinometry

Chemical Actinometry can be used to determine the light intensity in a particular photochemical experiment (Calvert and Pitts 1966). A chemical actinometer is a photochemical system for which the quantum yield has been accurately measured. The system is also relatively insensitive to changes in temperature, concentration of reactant, light intensity and the wavelength of absorbed light.

A 1987 report lists 37 different chemical systems for liquid phase actinometry (Braslavsky and Kuhn 1987). However, photochemical texts (Calvert and Pitts 1966, Gilbert and Baggott 1991) consistently describe the Potassium Ferrioxalate system, first reported by Parker (1953, Hatchard and Parker 1956), as being the best or most useful system. Potassium Ferrioxalate is a light green compound. Sulfuric acid solutions of $K_3Fe(C_2O_4)_3$ readily react upon irradiation, with light from 250 nm to 577 nm, to produce ferrous ions. The ferrous ion concentration is then easily analysed by the addition of 1,10-phenanthroline which forms an intensely coloured red complex with Fe^{2+}. $K_3Fe(C_2O_4)_3$ is easy to prepare from $FeCl_3$ and $K_2C_2O_4$. Calvert and Pitts (1966 pp. 784-6) provide a detailed method for carrying out actinometric analysis.

5.2.2 Summary of Actinometry in Aerosols

There appear to be no reports in the literature of any experiments designed to analyse the actinic flux into aerosols, although there are many publications about the effect of aerosols on the sun's actinic flux into a particular area. In order to characterise our system, it was necessary to measure the amount of light in the aerosols that was available for photochemical reactions. This also allowed us to make comparisons between our theoretical predications of the light intensity inside droplets and experimental reality, which was helpful because there are many factors that our theoretical models do not take into account, particularly the effect of scattering from a large number of particles.

5.2.3 Experimental Design

Actinometry was carried out in our aerosol reactor using a high-pressure xenon lamp. The use of the high-pressure xenon lamp meant that we needed an actinometer with a wide wavelength range, of which there are very few. A further complication was that no actinometric system has been designed for involatile solvents such as decane, ethanediol or glycerol. We decided to use the $K_3Fe(C_2O_4)_3$ system as it is usually used; in aqueous dilute sulfuric acid solution. This solution was nebulised, irradiated and impacted, and then the concentration of Fe^{2+} was determined by measuring the absorbance of the Fe^{2+}-1,10 phenanthroline complex at 510 nm. While it might be possible to dissolve $K_3Fe(C_2O_4)_3$ in acidified glycerol of ethanediol, this is almost certain to change the quantum yields of the photochemical reaction of $K_3Fe(C_2O_4)_3$ and we did not want to have to re-characterise an actinometric system. This increased the complexity of the experimental system, because handling aerosols made of volatile solvents is considerably more difficult than handling involatile solvents.

The greatest difficulties I encountered were associated with the impaction and collection of the aerosol. If dry gas was used to nebulise the solution and then as a carrier gas, an unquantifiable amount of evaporation occurred while the solution was in the aerosol phase. This meant we could not determine the concentration of droplets during irradiation. Further evaporation occurred when the sample reached the impactor. No matter what volume was nebulised, or how long is was nebulised for, I always collected the same volume. I think that the relative rates of evaporation and impaction caused the formation of a steady state.

A common technique used to overcome the evaporation of droplets is to use water-saturated gases. However, uncertainties about temperature and the effect of dissolved electrolytes means the concentration in the droplets cannot be known. Unfortunately, saturated carrier gases were of little benefit in the problem of evaporation from the impactor and a similarly small, volume and time independent, amount of liquid was collected.

To overcome the problem of evaporation in the nebuliser I decided to use a cooled impactor. The impactor was dipped in ice, ice/salt eutectic or an ethanol/dry ice bath. The impacted droplets then froze to the surface and were prevented from evaporating significantly. This meant that it was necessary to return to using dry carrier gasses, otherwise the water from the saturator was frozen into the impactor, considerably diluting the aerosol solution.

In conventional potassium ferrioxalate liquid phase actinometry, the total volume of the liquid and the total amount of iron in the system do not change in the course of the reaction. However, in aerosol actinometry this is not the case. It is not known what the concentration of iron in the droplets is while they are being irradiated, nor is the concentration of iron necessarily constant throughout the irradiation. Even with the dry ice/ethanol cooled impactor, less iron was collected in the impactor than left the nebuliser. The concentration of the liquid in the impactor was more dilute than the concentration of droplets during irradiation because the cooled impactor caused the condensation of water vapour as well as preventing the evaporation of the collected liquid. The additional water vapour that condensed in the impactor came from the nebuliser in the first place because I used dry gases.

The only quantity that it is useful to measure in liquid aerosol actinometry is the percentage transformation of ferric iron into ferrous iron. To obtain this it is necessary to the measure not just the concentration of ferrous ion in the irradiated solution, but also the total concentration of iron in the irradiated solution, so that the percentage transformation can be calculated.

I tried three different ways of measuring the total iron concentration in the nebulised, irradiated, and impacted solution: Atomic absorption spectroscopy, the reduction of all the

iron to ferrous iron, and direct spectrophotometric determination of ferric iron alongside the ferrous iron. After trying all the methods, I used the direct spectrophotometric method.

The first method I tried was atomic absorption spectroscopy (AA). The AA spectrometer that the department has is an acetylene flame spectrometer. The instrument draws the sample liquid up through a capillary tube and sprays into the flame where the molecules are atomised. Iron does not emit at the temperature of the flame, so it was necessary to use absorption spectroscopy with an iron lamp as the light source. To calibrate the spectrometer I used the same solutions as those I used to determine the extension coefficient of the iron(II)-1,10-phenanthroline complex, because these solutions each contained a known amount of iron.

Unexpectedly, the AA spectrometer was not sensitive enough and did not even measure the concentration of the calibration solutions consistently. They day after I used the AA spectrometer it stopped working, and it was un-repairable. It was older than I was, and it had been playing up for sometime and I suspect that this was why I did not get any consistent results. The demise of the AA spectrometer prompted me to think about spectrophotometric methods for the determination of ferric iron concentrations. Spectrophotometry has one considerable advantage over atomic absorption methods in that it is not necessary to recalibrate the instrument each time it is used.

Initially I thought that the ferric iron concentration could be determined using thiocyanate because it forms a brightly coloured complex with ferric ions. Unfortunately, the extinction coefficient of the ferric thiocyanate complex is a lot lower than the extinction coefficient of the phenanthroline-ferrous complex. This meant that the thiocyanate technique was not sensitive enough to use in the same system as the phenanthroline technique.

It is possible to detect ferric iron with the same sensitivity as I could detect ferrous iron. I used two solutions, and in one of them reduced all the iron to ferrous iron and then measured the ferrous iron concentration in both of them. After all, I actually wanted to know the total iron concentration, not the ferric iron concentration. Ascorbic acid reduces ferric iron to ferrous iron.

I modified the experimental procedure and made up two solutions for every measurement I wanted to make, one of which contained ascorbic acid. I also tested the technique by

measuring solutions that contained a known amount of ferrous and ferric iron. This technique worked well and I used it for a number of experimental runs. The disadvantage of this method was that it required the collection of twice as much aerosol and the preparation of twice as many solutions.

I began to use the final and best technique for measuring ferric iron concentration when I read that at 396 nm the molar absorptivities of iron(II)-phenanthroline and iron(III)-phenanthroline are identical (Marczenko 1976 pp. #310-311). This makes it possible to determine the concentration of ferric iron simultaneously with the determination of the ferrous iron concentration. All that is necessary is an additional absorbance measurement at 396 nm.

5.2.4 Experimental Results

After developing a technique for measuring the light intensity inside droplets, I applied it to an aerosol system and found that this was not a good technique at all. The problem was reproducibility. I measured percentage transformations of $K_3Fe(C_2O_4)_3$ to Fe^{2+} anywhere between 100% and 2%. I was unable to find any correlation between the conditions inside my system and the percentage transformation.

5.2.5 Discussion

The assumption that I could take a standard liquid phase technique and apply it to the aerosol phase was flawed. I thought that the instability of aqueous aerosol would be a problem, but I did not think it would prevent the acquisition of any meaningful results.

I think that an improved approach to liquid aerosol actinometry would be to develop an actinometric system in a relatively involatile solvent such as glycerol. One way to do this would be to take a well characterised system, such as the $K_3Fe(C_2O_4)_3$ system, and measure the light intensity of a lamp. This lamp could then be used to calibrate $K_3Fe(C_2O_4)_3$ in a glycerol system, which could in turn be used for aerosol Actinometry. In this way the aerosol would be stable and better characterised.

6 The Capillary Wave Model of Interfacial Transport at the Gas-liquid Interface

6.1 The Importance of the Interfacial Region in Aerosol Chemistry

In Chapter 2 the nature of the interfacial region and processes at the interface were used as a justification for the importance of aerosol chemistry. The increase in surface area that accompanies the nebulisation of a liquid is expected to provide greater access to surface reactions and enhance gas-liquid transport rates. The flip side of this discussion is that the gas-liquid interfacial region is probably the least well understood, and therefore the most interesting, 'state' of matter. Of the three phases, liquid is the most difficult to treat theoretically and experimentally, while gases and solids are reasonably well understood. An interface is usually less well understood than the bulk. Of the three types of liquid interface: liquid-liquid, solid-liquid and gas-liquid there is, at least, agreement about the physical nature of the liquid-liquid and solid-liquid interfaces. There is debate about whether the gas-liquid interface is a discrete interface, analogous to a gas-solid interface (that moves), or a continuous transition from bulk liquid through a dense, gas-like region to the gas phase. Given the poor characterisation of the gas-liquid interface, it is not surprising that there is no generally accepted molecular scale model of the transfer of a solute molecule from the gas phase to the liquid phase, even if the solute is the solvent.

It is clear that if aerosol chemistry is to be understood then there are problems, such as the nature of the gas-liquid interface and the mechanism of gas-liquid interfacial transport, that extend far beyond the realm of aerosol chemistry, and which need to be solved.

In trying to understand all of the processes that make up aerosol chemistry, I spent some time looking at various models of gas-liquid interfacial transport. I concluded that none of the models available was adequate and so we decided to try developing our own.

The most recent model of gas-liquid interfacial transport, and consequently the model that most of our attention was directed towards, was proposed by Davidovits and co-workers

(1991). The central point of disagreement between Davidovits et al. and ourselves is alluded to above; that is, the physical nature of the gas-liquid interface. Davidovits and co-workers' model is based on nucleation theory. It treats the interfacial region as if it were a continuous transition from the bulk liquid phase to the gas phase without a distinct interface. We do not believe that this is the 'true' nature of the gas-liquid interface, in fact, it does have a distinct discontinuous transition from the gas to the liquid, but due to thermal excitation the surface is always mobile.

6.2 Davidovits and Co-workers' Model

6.2.1 Experimental approach

Davidovits and co-workers have done a huge amount of work on the uptake of gases by water droplets. Their interest in this is primarily directed towards understanding atmospheric processes. They measure the uptake of gases using a droplet train apparatus, (for example (Worsnop, Zahniser, Kolb, Gardner, Watson, Van Doren, Jayne and Davidovits 1989). To measure the uptake coefficients of a gas, the gas is exposed to the water droplet train where n_g, the number density of the trace gas, is known. This is done before contact with the droplets and the change in number density of the trace gas is measured as a function of droplet surface area and time. The parameter that is ultimately wanted from this data is the mass accommodation coefficient α, defined as

$$\alpha = \frac{\text{no. of molecules entering the liquid phase}}{\text{no.of molecular collisions with the surface}} \tag{33}$$

The mass accommodation coefficient provides a great deal of information about the process of gas uptake into a liquid. Davidovits et al. have measured the mass accommodation coefficient into water, and its temperature dependence, for a large number of atmospherically relevant species; they observe a negative temperature dependence. The mass accommodation coefficient alone gives useful information about the nature of gas-liquid uptake processes, but the temperature dependence of the mass accommodation coefficient gives a lot more information because thermodynamic data about the process of gas uptake can be extracted.

6.2.2 Thermodynamic Information about Gas Uptake into Liquids

Before looking at how thermodynamic information can be obtained from the temperature dependence of the mass accommodation coefficient, it is worthwhile to consider the processes that the thermodynamic information describes.

The process of gas uptake by a liquid can be thought of in terms of a number of sub-processes. A gas molecule must first strike the liquid surface where it can either stick or bounce off back into the gas phase. A molecule adsorbed on the surface can either be accommodated into the bulk liquid or desorb from the surface without entering the liquid. If liquid phase saturation and evaporation is also being considered, then a solute molecule dissolved in the liquid can diffuse to the surface and enter the adsorbed state. An adsorbed molecule has the same reaction pathways open to it regardless of whether it originated on the gas or the liquid; it can accommodate/solvate into the liquid or desorb into the gas. Remembering that the probability of a gas phase molecule at thermal velocity sticking on the liquid surface is unity, and disregarding evaporation processes, the process of a gas molecule entering a liquid can be represented as

$$n_g \underset{k_{desorb}}{\overset{k_{ads}}{\rightleftharpoons}} n_s \xrightarrow{k_{sol}} n_l \tag{34}$$

In equation (34) the subscripts g, s and l represent the gas, surface and liquid states of the species, and the k's are the rate constants for the indicated processes. The rate constant for adsorption, k_{ads}, is derived form the kinetic theory of gases and is proportional to the average thermal velocity in the gas phase, $k_{ads} = \frac{1}{4}\bar{c}$. The flux to the surface is the number of molecules in the gas phase, multiplied by the rate of adsorption, $J_{ads} = n_g k_{ads} = \frac{1}{4} n_g \bar{c}$. The flux of molecules from the gas into the liquid is the mass accommodation coefficient, multiplied by the flux from the gas to the surface.

$$J_{g \to l} = \alpha J_{ads} = \frac{\alpha n_g \bar{c}}{4} \tag{35}$$

Using equation (34), equation (35) can be expressed as

$$\frac{\alpha n_g \bar{c}}{4} = \frac{n_g \bar{c}}{4} - n_s k_{desorb} = n_s k_{sol} \tag{36}$$

From equation (36), it is clear that the mass accommodation can be expressed in terms of the rate constants for solvation and desorption.

$$\alpha = \frac{k_{sol}}{k_{sol} + k_{desorb}} \tag{37}$$

A surface state is defined as a state to which molecules can diffuse from the gas and liquid phases, and from which molecules can desorb into the gas phase and solvate into the liquid phase. Molecular dynamics simulation of gas uptake into liquids fail to corroborate the existence of such a state (Taylor, Tay and Garrett 1997). However, this surface state is required by the experimentally measured values of the mass accommodation coefficient combined with measured values of the sticking coefficient. At thermal velocities all of the sticking coefficients are almost always one; every molecule that strikes the surface of water is adsorbed (Saecker and Nathanson 1993). Table 6.1 contains a selection of typical mass accommodation coefficients for molecules that are soluble in water (Jayne, Duan, Davidovits, Worsnop, Zahniser and Kolb 1991).

Table 6.1 Selected mass accommodation coefficients and thermodynamic data

Molecule	A(273 K)	ΔH_{obs} kcal mol^{-1}	ΔS_{obs} cal mol^{-1} K^{-1}
Methanol	0.056	-8.0	-34.9
Ethanol	0.048	-9.2	-46.2
1-propanol	0.026	-7.9	-40.9
2-propanol	0.032	-6.6	-43.0
Formic acid	0.047	-11.0	-34.9
Acetic acid	0.067	-9.9	-34.9
HNO_3	0.157	-8.1	-27.6
H_2O_2	0.234	-5.5	-22.5

Hydrogen peroxide, a very soluble and reactive molecule, has the largest value with $\alpha =$ 0.234; approximately four out of five hydrogen peroxide molecules are adsorbed on the surface of water, but do not penetrate it. The mass accommodation coefficients of organic alcohols are an order of magnitude smaller. These small values of α imply that at any given time a large number of molecules will be adsorbed on the surface but, rather than being solvated, will ultimately return to the gas.

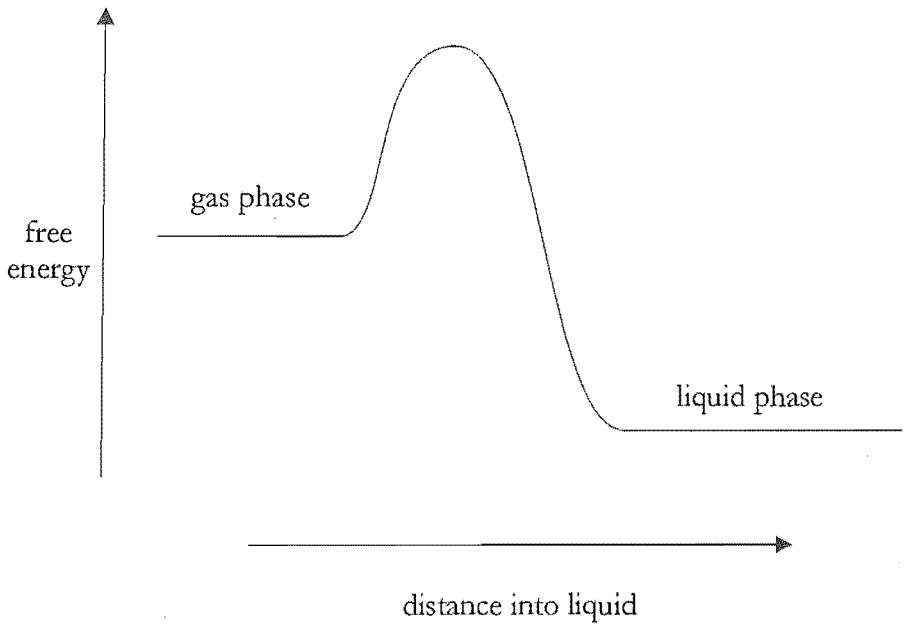

Figure 6.1 The free energy diagram for solvation without a surface state

Figure 6.1 shows the free energy diagram for solvation without a minimum at the surface, in other words, with no surface state. The fact that the mass accommodation coefficients are not unity implies that there is a barrier. However, Figure 6.1 does not represent the experimental information available on sticking and mass accommodation coefficients. In fact, it suggests that any molecule with sufficient energy will overcome the barrier and penetrate the surface and be solvated. This model of solvation is inconsistent with the experimental observation that every molecule striking the liquid surface are adsorbed, while only a fraction of those molecules are solvated.

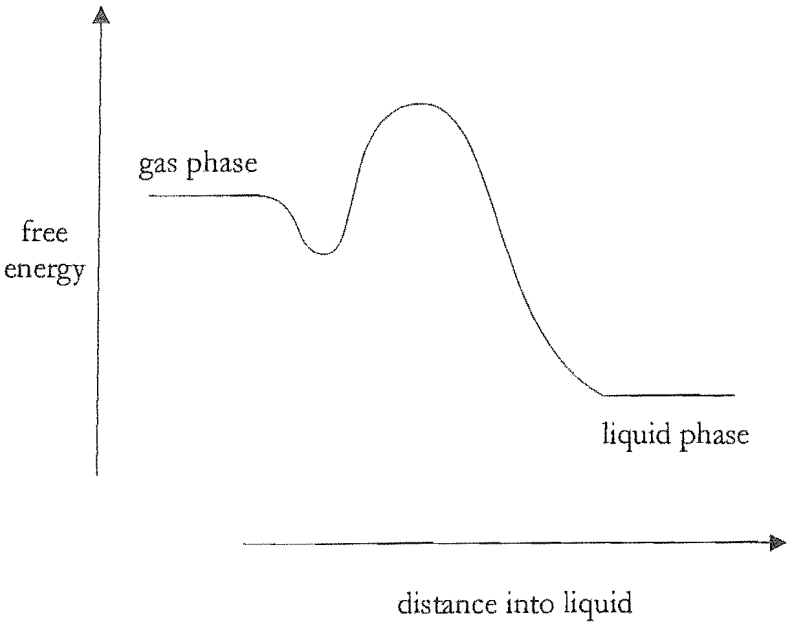

Figure 6.2 The free energy diagram for solvation with a surface state

Figure 6.2 is the free energy diagram for solvation where there is a minimum at the surface. This is much more consistent with the experimental observations. No gas-phase molecules at thermal velocities have enough energy to escape from the attractive potential of the surface, but the majority of them get enough energy to escape from the surface state back into the gas phase before having enough energy to overcome the barrier to solvation. One consequence of this model is that if the solute molecules do not have enough energy to escape the attractive potential of the surface state, then neither do they bring enough energy from their gas phase state to penetrate the surface. However, a molecule adsorbed on the surface is coupled to a very large bath, the liquid itself, and this coupling could provide enough energy to facilitate solvation, although it is hard to imagine how this could lead to solvation before it led to desorption. It might also be necessary for the liquid itself to change configuration in such a way that the barrier height is reduced, or for the molecule to change orientation with respect to the barrier.

Thus, it is physically quite reasonable to describe these molecules as being in an explicit adsorbed surface state. This can be expressed in four ways: Solute molecules that are located at the surface are actually resident on the surface (the surface is not just another point they pass through between the gas and the liquid); the surface represents a minimum in the reaction coordinate; molecules adsorbed on the surface are in an energy minimum;

there is a barrier between the surface state and the state the represents complete solvation in the liquid.

The temperature dependence of the mass accommodation coefficient allows the nature of the surface state energy minimum to be probed. The height of the barrier to solvation, measured relative to the gas phase free energy, can be expressed in terms of the rate of solvation and the rate of desorption. Using equation (37) this barrier height is $\Delta G^{\ddagger}_{obs}$ by

$$\frac{\alpha}{1-\alpha} = \frac{k_{sol}}{k_{desorb}} = \exp\left(\frac{-\Delta G^{\ddagger}_{obs}}{RT}\right) \tag{38}$$

From equation (38) it can be seen that a semilogarithmic plot of $\alpha/(1-\alpha)$ against $1/T$ will be a straight line with a slope of $\Delta H_{obs}/R$ and an intercept of $\Delta S_{obs}/R$. Table 6.1 also shows the values of ΔH_{obs} and ΔS_{obs} that Davidovits et al. have calculated (Jayne et al. 1991). From this data it can be seen that all of the enthalpy and entropy changes associated with going from the surface into the bulk liquid are negative; the barrier is entropic.

This is not particularly surprising, and it is physically reasonable that the major thermodynamic barrier to solvation would be entropic in origin. The molecules being considered here are all soluble in water; the overall Gibb's free energy change from the gas to the liquid is negative. The enthalpic part of the Gibb's free energy change comes from electrostatic interactions between the solute molecule and the water molecule. For the sake of convenience, I will often refer to these electrostatic interactions as bonds. The range of motion, and hence the number of microscopic states (in the statistical mechanical sense), available to a molecule in the gas phase is much greater than in the liquid phase. A gas phase molecule cannot form any bonds to other molecules, but when it is dissolved in water (assuming it is not hydrophobic), it can form many bonds and lower its enthalpy. In fact, the energy minimum associated with the surface state can be rationalised in terms of the relative rates of these changes as the molecule approaches and penetrates the liquid surface.

It is useful to consider how these thermodynamic properties change along the reaction coordinate of solvation because this sheds light on the thermodynamic origin of the surface minimum and the barrier to solvation. Here, I treat the reaction coordinate of solvation as a

line normal to the surface that a gas phase molecule moves along, becoming progressively more 'solvated' until it is a liquid phase solute.

Assuming that, with increasing solvation, the enthalpy and entropy of solutes entering the liquid phase must decrease monotonically, it is necessary to demonstrate the origin of the non-monotonic curve for the free energy in Figure 6.2. Mathematically speaking, this sort of curve can be obtained subtracting a curve with a point of inflection from another curve, or vice versa. Provided that the initial and final gradients of the curve being subtracted from are less than the initial and final gradients of the other curve, the appropriate curve will be generated in the sense of equation (39).

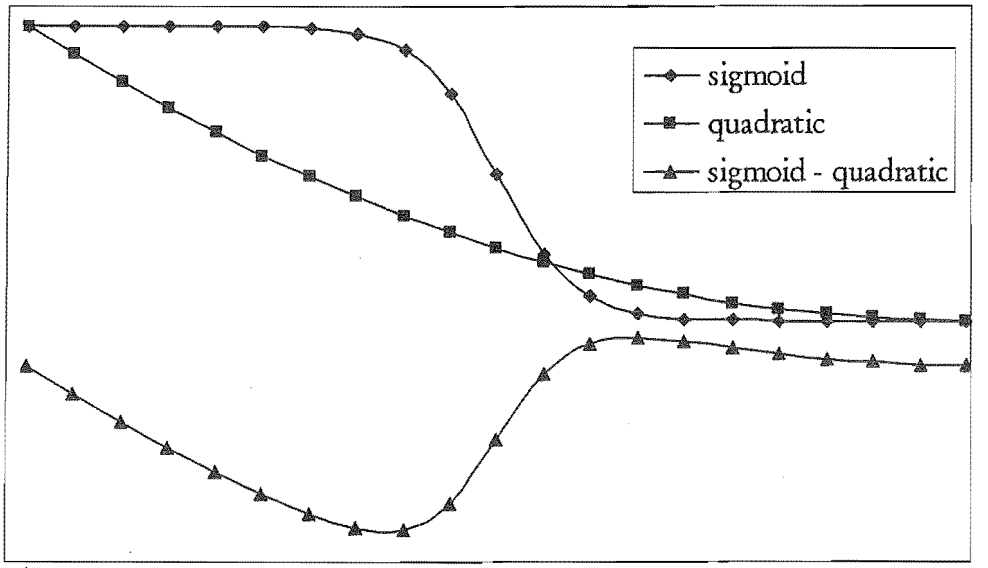

Figure 6.3 A curve with a minimum and a maximum generated from a sigmoid and a quadratic curve

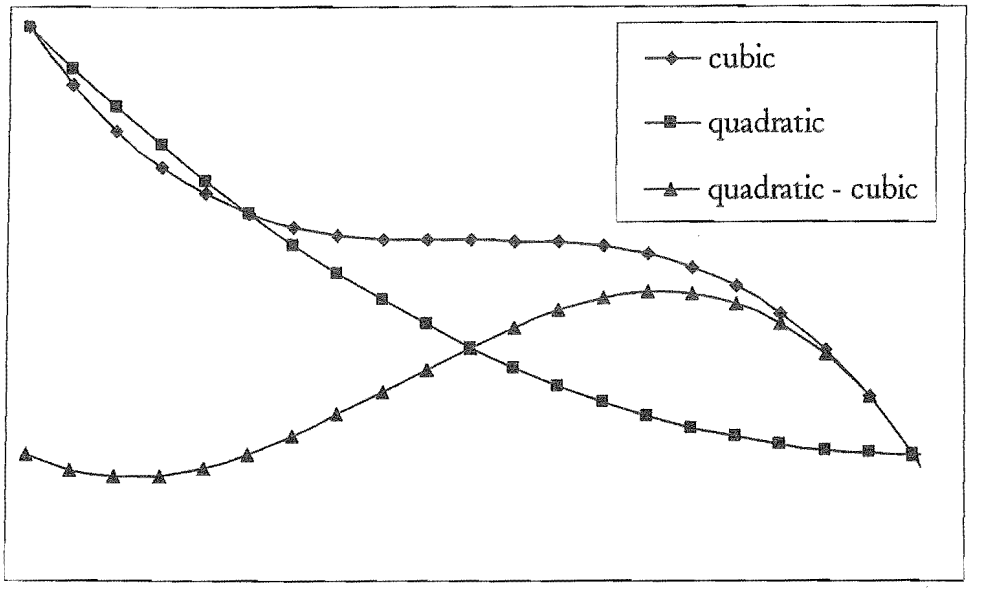

Figure 6.4 A curve with a minimum and a maximum generated from a cubic and a quadratic

Figure 6.3 and figure 6.4 demonstrate how the required curve, one with a minimum representing surface adsorption and a maximum representing the barrier, can be obtained from two monotonic functions. The free energy change at point x on the difference curve is defined as

$$\Delta G_x = (H_x - H_i) - T(S_x - S_i) \tag{39}$$

Physically this means that a free energy curve of the required form is obtained if the initial and final rates of change of the entropy are greater than those of the enthalpy. This model predicts that the greatest entropy changes in the process of solvation will occur at the beginning and end of the process. This seems reasonable, because we would expect the greatest entropy costs to be associated with adsorption onto the surface and solvent rearrangement around the solute when it is finally solvated.

This is a more stringent requirement on the type of entropy and enthalpy change curves required to model the free energy changes associated with solvation than we had in mind when we published our paper on the topic (Knox and Phillips 1998). In that publication we thought all that was required to produce the free energy curve was for the initial rate of change of entropy to be greater than that of enthalpy. However, this requirement, is only sufficient to provide a minimum in the free energy profile of solvation; it does not generate a maximum.

An interesting consequence of this analysis is that it calls into question the statement, 'the barrier is entropic in origin due to the fact the both ΔH_{obs} and ΔS_{obs} are both negative'. This is a conclusion that Davidovits et al. have drawn from their results, (Nathanson, Davidovits, Worsnop and Kolb 1996). Indeed, it seems quite counter-intuitive to say that, because the enthalpy change to the barrier is in the direction spontaneous for enthalpy and the entropy change to the barrier is in the non-spontaneous direction for entropy, the barrier is not actually entropic in origin. However, this is a consequence of considering how the free energy diagram can arise from monotonic functions. At any point on the free energy curve, both the enthalpy and entropy changes relative to the gas phase are going to be negative; this is a consequence of the requirement that the functions are monotonic. However, it would be invalid to say that the whole curve is entropic in origin. Mathematically, the shape of the free energy curve is determined by the relative gradients of the enthalpy and entropy curves. Each feature on the free energy curve is the result of the relative changes in entropy and enthalpy before and after that point. In fact, the free energy minimum is generated when the entropy is decreasing faster than the enthalpy and the maximum occurs when the enthalpy is changing faster than the entropy. If 'the origin of the barrier is entropic' means that the barrier occurs because the entropy changes are not keeping up with the enthalpy changes, then it is true, but I suspect that is not what most people mean when employing this statement. The problem is that a single reaction coordinate is not sufficient to describe accommodation; the orientation of a solute molecule with respect to the barrier is important.

The assumption that the enthalpy and entropy must decrease monotonically is almost certainly valid for hard sphere type solutes dissolving in hard sphere liquids. However, it is less certainly valid when considering hydrogen bonding between the solute and solvent and within the solvent. It is possible that hydrogen bonds formed by the solute molecule in the surface state have to be broken in order to be accommodated into the liquid. It is also possible that as the solvent relaxes around the newly accommodated solute, particularly if it has a significant hydrophobic region, the enthalpy and entropy could change non-monotonically. However, in the absence of direct contradiction I think that the monotonic treatment is still very useful.

6.2.3 The Nucleation Theory Model of Gas Uptake by Liquids

Davidovits et al. point out a number of features in their results and use them to develop their model (Davidovits et al. 1991, Nathanson et al. 1996). Firstly, the temperature dependence of all the mass accommodation coefficients is negative; the ΔH_{obs} is negative in all cases. Secondly, the magnitudes of ΔH_{obs} are roughly inversely proportional to the expected hydrogen bonding ability of the species: diols and DMSO < acids < haloethanols < alkyl alcohols < acetone. Thirdly, the magnitudes of ΔH_{obs} and ΔS_{obs} do not depend on the size or shape of the solute molecules. The classic example of this is methanol (ΔH_{obs} = -8.0 kcal·mol^{-1}, ΔS_{obs} = -34.9 cal·mol^{-1}·K^{-1}) and 2-methyl-2-propanol (ΔH_{obs} = -8.2 kcal·mol^{-1}, ΔS_{obs} = -35.8 cal·mol^{-1}·K^{-1}). Within experimental error, these values are the same, but 2-methyl-2-propanol has a much larger hydrophobic component than methanol, and its molar volume is 2.3 times larger. Finally, and perhaps most significantly for Davidovits and co-workers' model, there is a direct correlation between ΔH_{obs} and ΔS_{obs}, and there is no such correlation in the total solvation parameters.

The nucleation theory model is based around the formation of more liquid-like aggregates or clusters from more loosely bound gas-like species in the interfacial region. The change in free energy associated with cluster formation ΔG_N is defined as the molar free energy for the formation of a cluster containing N molecules. Classical nucleation theory shows that as N increases so does ΔG_N, initially, until critical cluster size is reached, and then ΔG_N decreases as N increases. The initial increase in free energy comes from the surface free energy requirement associated with the formation of a new phase. When this process takes place in close proximity to a liquid bulk, any clusters that reach a critical size N^* will continue to grow until they merge with the adjacent liquid. This is the nucleation theory model's mechanism for gas uptake. Solute molecules enter the interfacial region by the usual diffusive processes and can then act as centres for cluster formation. If the cluster reaches the critical size N^* then the cluster is incorporated back into the bulk liquid and carries the solute molecule with it.

This model makes a number of predictions that are in accord with experimental observations. In particular, it enables the relative unimportance of the hydrophobic portion of solute molecules to be understood. The cluster can form around the hydrogen bonding

hydrophilic portion of the molecule, and once the critical cluster size is reached then the molecule is engulfed regardless of the nature of the rest of the molecule.

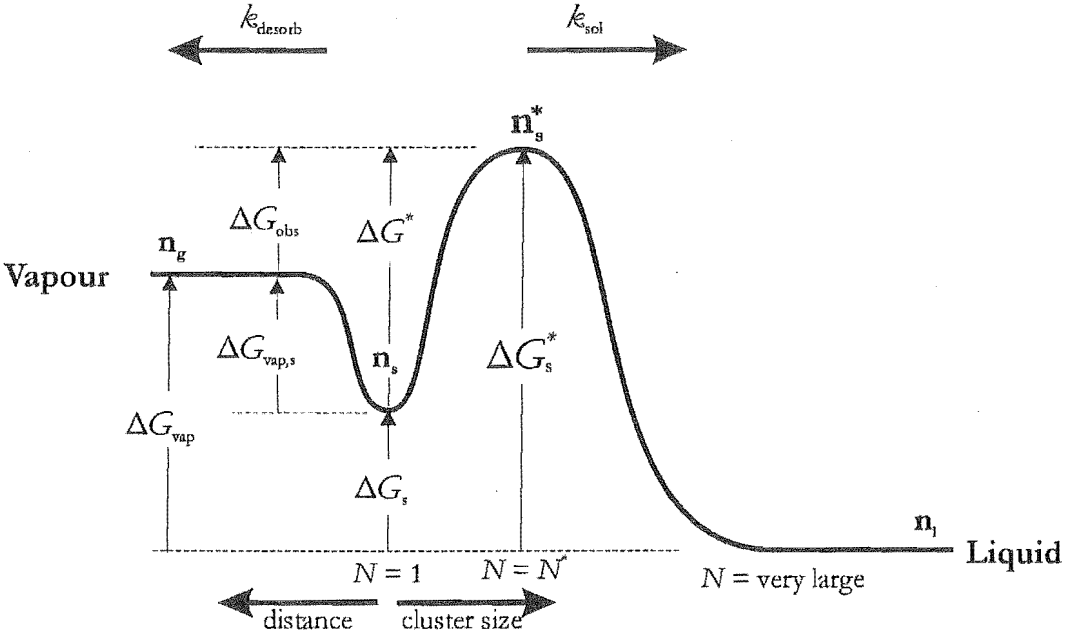

Figure 6.5 The free energy diagram for the nucleation theory model

Figure 6.5 shows the free energy diagram for the nucleation theory model. The reaction coordinate is not trivial. When the molecule is in the gas phase it is the distance between the molecule and the interface. However, once the molecule has been adsorbed at the interface, the distance to the interface loses meaning; the reaction coordinate is then described by increasing cluster size.

Using the nucleation theory model (34) can be rewritten to include the critical cluster n_s^*

$$n_g \underset{k_{desorb}}{\overset{k_{ads}}{\rightleftharpoons}} n_s \xrightarrow{k_s} n_s^* \xrightarrow{k_{sol}} n_l \qquad (40)$$

Once a molecule reaches the critical cluster size n_s^* it is considered to be irreversibly solvated.

6.3 Objections to the Nucleation Theory Model

The primary objection to the nucleation theory of gas uptake by liquids is that the theory uses a model of the interface that is unphysical. Experimental (Doerr, Tolan, Prange, Schlomka, Seydel, Press, Smilgies and Struth 1999) and computational (Sides, Grest and Lacasse 1999) studies indicate that the interface is best represented by a discrete, one molecular diameter transition, rather than a continuous transition over several molecular diameters.

In a recent experimental study of the gas-liquid interface at short length scales, the continuous model of the interface is described as an old model, while the capillary wave model is the new model supported by experimental observations (Fradin, Braslau, Luzet, Smilgies, Alba, Boudet, Mecke and Daillant 2000). The results of this paper support the basic assumptions of the capillary wave model of the liquid interface. However, they indicate that capillary waves themselves are not a good description of the interface at nanometre-scale resolution. Indeed, it would be surprising if a macroscopic model like capillary waves worked at this length scale.

Second Harmonic Generation Spectroscopy (Eisenthal 1996a) is in itself implicit evidence for the existence of a discrete interface. Second harmonic generation requires an asymmetric environment and this is not provided by a continuous interface, yet second harmonic generation occurs at the liquid surface.

It is important for theories to be continuous with other related problems and the nucleation theory model does not have this quality. Assuming that its basis is validated experimentally, it is difficult to see how it could be extended to cover a wider range of the phenomena occurring at the liquid interface. Qualitatively it is hard to visualise how the nucleation theory model could be used to describe the uptake of hydrophobic solutes like ethane, which, while they are not readily absorbed by water, still dissolve to some extent. However, it is very difficult to imagine dense gas-like water molecules forming a cluster around an ethane molecule. More importantly, a desirable feature of a gas uptake model is that it should be extendible to other liquids. Low vapour pressure liquids such as glycerol and squalane certainly have a discrete interface. Despite the fact that the nucleation theory model is clearly inapplicable to low vapour pressure liquids, the uptake of gases into these

liquids is still observable. Another model of gas uptake must be used to describe these situations. A model of gas uptake that was applicable to all liquid surfaces would be more intellectually satisfying. Furthermore, it is difficult to see how the nucleation theory model could be used to provide quantitative information about evaporation, beyond diffusion into the interfacial region and then diffusion out of the interfacial region in a manner similar to that required for molecules that are adsorbed but not absorbed.

Many of these difficulties can be overcome by using a model of gas-liquid uptake, based on a discrete interface. This model is called the 'Capillary Wave Model of Gas-Liquid Exchange' (Knox and Phillips 1998). While this theory is a critique of the Nucleation Theory Model, it has also been inspired by it and includes many ideas from the Nucleation Theory Model.

6.4 Capillary Wave Model of Gas-Liquid Exchange

The central assumption of the capillary wave model is the belief that the transfer of molecules in and out of a liquid is facilitated by the thermal fluctuations of the surface. Capillary waves serve as an initial basis set for describing the motion of the surface, and its affect on accommodation and evaporation. Capillary waves are waves for which surface tension is the sole restoring force. They have been used to describe the interfacial density profile (Buff, Lovett and Stillinger 1965). However, this view of interfacial transport is not dependent upon the capillary wave theory of the interface. Thus, an experimentally measured decrease in surface energy at short length scales (Fradin et al. 2000) that cannot be explained by classical capillary wave theory, does not imply the failure of the capillary wave model of gas uptake. Rather, the model will be recast in terms of a basis set that is a better description of the fluctuations and structure of the gas-liquid interface.

In the following sections, I describe the use of the capillary wave model to derive an expression for the rate of accommodation. Subsequent theoretical work has shown that capillary waves, in the classical sense, are not a sufficient basis set for the description of the liquid surface at the molecular length scale (Phillips 2001a, 2001b, Phillips 2000b, 2000a, Phillips 2000c). However, the approach discussed below remains valid and when a

full description of the surface is developed at molecule length scales, the capillary wave model will be reformulated accordingly.

6.4.1 Interfacial Exchange

Consider a gas-phase solute molecule adsorbed on the surface of a liquid: it has two possible fates, accommodation into the bulk liquid or desorption back into the gas. Likewise, a liquid-phase solute molecule that has diffused to the surface of the liquid has two possible fates: reincorporation back into the liquid, or evaporation into the gas. 'Solute' is used here to designate the molecules being transferred; it includes evaporating or accommodating molecules of the same species as the bulk liquid. Because of the fluctuations of the liquid surface, the coordination state of surface adsorbed molecules will always be changing.

The principal hypothesis of the capillary wave model is that there are two critical coordination states described by the coordination numbers n_a and n_e. When the coordination number of a solute molecule exceeds n_a the molecule is irreversibly accommodated, and, conversely, a coordination number less than n_e results in evaporation. This is illustrated by equation (41).

$$n_g \leftarrow n_e \leftrightarrow [n_e + ...] \leftrightarrow [n_s - ...] \leftrightarrow n_s \rightarrow n_l \tag{41}$$

Alternatively, coordination numbers between n_e and n_a represent molecules that are adsorbed at the surface and any molecules that exceed these parameters are no longer surface species.

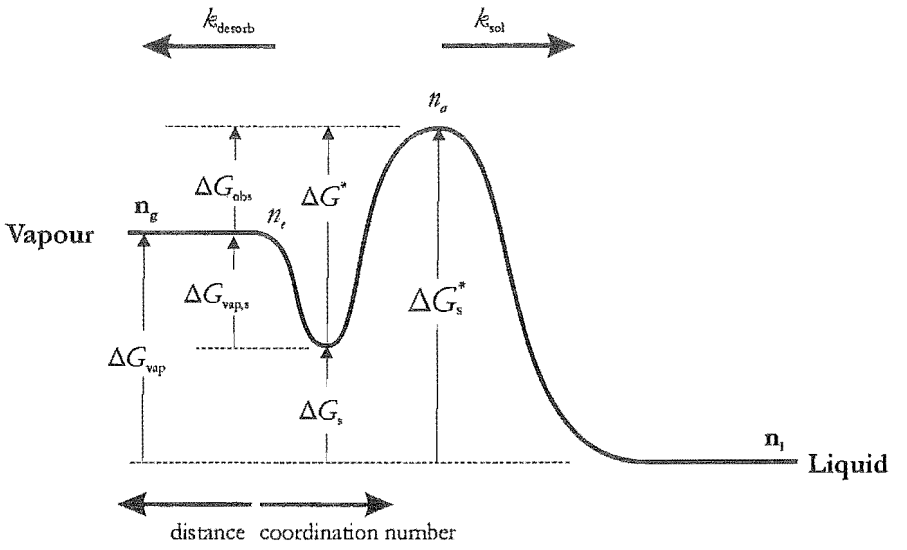

Figure 6.6 Free energy diagram for the capillary wave model of interfacial transport

Figure 6.5 can be recast in terms of increasing coordination number (Figure 6.6). Another alternative way of stating the capillary wave model of gas-liquid exchange is: the coordination number n_a represents the coordination state of species at the top of the barrier to accommodation, and the coordination number n_e represents the coordinate number state at the top of the barrier to evaporation. Its coupling to the bulk liquid provides the energy required for an adsorbed molecule to move about on this free energy surface, in other words, the fluctuations of the liquid surface.

6.4.2 Accommodation

Capillary wave theory provides an estimate of the rate of accommodation into a liquid. There is some analogy between the capillary wave theory of accommodation and the diffusion theory of chemical reactions (Chapter 6 Nikitin 1974). In this formulation of transition state theory, the rate constant of a reaction can be expressed in terms of the rate of motion along the critical coordinate $k^\dagger$, as

$$k = k^\dagger \exp\left(\frac{\Delta S^\dagger}{R}\right)\exp\left(\frac{-\Delta H^\dagger}{RT}\right) \tag{42}$$

$k^\dagger$ is usually equal to k_BT/h. If we equate the critical coordinate of accommodation with the motion of an adsorbed species normal to the surface then $k^\dagger$ is the velocity of the surface

fluctuations that govern the motion of the adsorbed species. The velocity can be derived from the properties of capillary waves.

The vertical displacement of a single capillary wave mode is given by

$$\varsigma_x = a_x \cos(\omega t - kx) \tag{43}$$

In equation (43), a_x is the amplitude of a capillary wave mode characterised by the circular frequency ω and the wave vector k. The rate of penetration of a molecule into the bulk liquid is given by $v^\dagger$, which is its average velocity relative to the adjacent molecules.

$$\begin{aligned} v^\dagger &= \Delta\left(\frac{d\varsigma_x}{dt}\right) \\ &= -a_x\omega\left\{\sin\omega t - \tfrac{1}{2}\left(\sin[\omega t - k\sigma] + \sin[\omega t + k\sigma]\right)\right\} \\ &= -a_x\omega \sin\omega t\left[1 - \cos k\sigma\right] \end{aligned} \tag{44}$$

In equation (44), σ is the molecular diameter. A similar expression can be written for molecules that are displaced along the y-axis, therefore, the x subscript can be dropped and all subsequent expressions are valid independent of direction.

Equation (44) is the average velocity of a surface adsorbed molecule relative to its nearest neighbours. However, the motion of the surface is never going to be described by a single mode. In order to relate (44) to the rate of accommodation it is necessary to determine the average value of $v^\dagger$.

The energy per unit area in one mode, E_i, is

$$E_i = \frac{a^2 k^2 \gamma}{2} \tag{45}$$

In equation (45), γ is the surface tension and the expression applies to a region with a total area of $\pi L^2/4$, where

$$L = \pi\sqrt{\frac{\gamma}{\rho g}} \tag{46}$$

In equation (46), g is the gravitational acceleration and ρ is the density (Phillips 1997). The total number of vertical modes in this region is

$$n = \frac{\pi L^2}{4\sigma^2} \tag{47}$$

and the degeneracy of mode number m is $\pi m/2$, where m = πm/L. The surface modes are thermally excited, therefore the average energy per mode is $k_B T/h$. Using this value and equations (45), (46) and (47), the mean value of a^2 can be determined.

$$a^2 = \frac{8k_B T}{\pi^3 m^2 \gamma} \tag{48}$$

The surface is stable and therefore the average value of $v_i^\dagger$ for any mode, i, must be zero, so the variance of $v_i^\dagger$ is equal to its mean square value. Using $\langle \sin^2 \omega t \rangle = 1$

$$\left\langle \left(v_i^\dagger\right)^2 \right\rangle = \frac{4\omega^2 k_B T \left(1-\cos k\sigma\right)^2}{\pi L^2 \gamma k^2} \tag{49}$$

The number of surface modes in the region under consideration is of the order of 10^7. Thus, the central limit theorem will apply and the variance of the superposition of the modes will be equal the variance of a single mode multiplied by the number of modes. The total variance for all modes with mode number m is

$$\left\langle \left(v_m^\dagger\right)^2 \right\rangle = \frac{2m^2 k_B T \left[1-\cos\left(\frac{\sigma}{L}\right)\right]^2}{L^3 \rho} \tag{50}$$

In (50), ω^2/k^2 has been replaced by $\gamma k/\rho$ and $k = \pi m/L$, and the degeneracy of mode m is $\pi m/2$. To obtain variance of all modes (50) must be integrated from $m = 1$ to $m = L/\sigma$. The integral is not greatly affected and is simplified by taking the lower limit as zero. The final result is

$$\left\langle \left(v^\dagger\right)^2 \right\rangle = \frac{k_B T \left(8.5+\pi^2\right)}{\pi \rho \sigma^3} \tag{51}$$

A Gaussian distribution with this variance implies that the absolute average value is

$$\left|v^{\dagger}\right| = \sqrt{\frac{2k_B T\left(8.5+\pi^2\right)}{\pi^2 \rho \sigma^3}} \tag{52}$$

Now that the average velocity of the surface has been determined, the rate constant for motion along the critical coordinate can be defined as

$$k^{\dagger} = \frac{\left|v^{\dagger}\right|}{\sigma} \tag{53}$$

When ρ = 1, σ = 3 × 10^{-8} cm, and T = 300 K, and allowing for the fact that half of the motions of the surface are directed out of the bulk liquid, and requiring both ζ_y and ζ_x to be changing in the same direction, $k^{\dagger}$ = 1.3 × 10^{12} s^{-1}. This is only about four-fold smaller than $k_B T/h$.

The derivation of a rate constant for accommodation into a liquid from the basis of capillary wave produces a sensible result. This result is only an approximation because the model has not yet been extended to include the nature of the solute and its interaction with the solvent. In addition, as stated previously, it has been shown subsequently that capillary waves are not a sufficient description of the surface at molecular length scales. The derivation above was not made in anticipation that a macroscopic description like capillary waves would be suitable at molecular length scales. Rather, it seeks to demonstrate the plausibility of the hypothesis that the exchange of material across the gas-liquid interface is mediated by the fluctuations of the interface itself. The plausibility of the rate constant derived above testifies that this is indeed the case, and the derivation itself serves as a template for the reformulation of the model in terms of a more elaborate description of the structure of the gas-liquid interface.

7 Conclusion

This thesis has been a preliminary investigation of process liquid aerosol photochemistry. Process liquid aerosol photochemistry is the use of the morphological properties of aerosols to enhance the reactivity of a system without any particular structural requirements for the products. The morphological properties of aerosols ensure that liquid aerosol photochemistry and photocatalysis exhibit enhanced rates of gas-liquid transport, enhanced reactivity due to the importance of interfacial reactivity, and unique interactions with incident radiation, all of which allow both enhanced reactivity and greater reaction control.

7.1 Experimental Systems

A significant part of this work was devoted to the development of systems for the photochemistry of liquid aerosols. I initially used transparent systems with monodisperse aerosol and monochromatic radiation. These systems evolved into optically sealed systems with polydisperse aerosol and broadband radiation. Given that I had considerable difficulty with lack of reproducibility, which seems to be a prevalent problem in liquid aerosol systems, I am still unsure whether this evolution was fruitful. However, I am certain that any liquid aerosol photochemical system that utilises monodisperse aerosol will require an on-line aerosol characterisation system in order for the state of the aerosol to be always known. Although aerosol characterisation is more difficult, high volume polydisperse aerosol systems should also attempt characterisation of the aerosol in real time.

In my work, I have not attempted to utilise any of the advanced techniques that are available for the study of aerosol reactions: for example, single droplet resonance Raman spectroscopy (Davis et al. 1998) or optical resonance spectroscopy (Taflin and Davis 1990). I hoped to find a functional liquid aerosol photocatalytic system and then carry out mechanistic studies of the system using single droplet aerosol techniques. Unfortunately, this approach did not work and I now believe that a more productive approach to the development of liquid aerosol photocatalytic systems would be to combine single droplet studies with the type of investigations that I have conducted.

Although I have developed some useful systems for liquid aerosol photochemistry, there is still considerably more opportunity for system development. This is particularly true for the monitoring components of the systems; I was unable to develop a satisfactory online technique for monitoring aerosol chemical reactions.

7.1.1 The Photolysis of Molybdenum Hexacarbonyl

Despite being unable to develop a functional liquid aerosol photocatalytic system, I was able to demonstrate the principal hypothesis of my thesis; that the use of liquid aerosol systems provides significant enhancements in reactivity over the equivalent liquid phase systems. Although further characterisation of the reaction is still required, the photolysis of molybdenum hexacarbonyl is a dramatic demonstration of superior reactivity in the aerosol phase. Because of the importance of transition metal carbonyls in photocatalysis, this represents a significant step in the development of a working liquid aerosol photocatalytic system.

The increased rate of photolysis of molybdenum hexacarbonyl in liquid aerosols is due to a combination of the features of aerosols discussed in Chapter 2. The unique nature of the interaction of micron-sized droplets with light ensures that the rate of photolysis near the droplet is significantly enhanced. If an equivalent enhancement of photolysis near the surface occurred in a liquid system, it would be insignificant because the surface region is only a minor part of the system. However, in an aerosol system, the surface region is very important, and not only is the rate of photolysis increased, but the rate of recombination is also decreased.

The observation of an enhanced rate of photolysis of molybdenum hexacarbonyl, without the accompanying hydrogenation of decene or ethylene, forced the re-evaluation of some of my previous suppositions about the rate of gas-transfer in and out of liquid aerosols. Either molybdenum hexacarbonyl was being photolysed, but not to a catalytic species, or the catalytic species was being produced, but there was insufficient hydrogen and/or ethylene in the system for the hydrogenation reaction to take place. Clearly, further work is required to understand the processes taking place in this system. Once the nature of the photolysis is understood, then it can be used to develop a photocatalytic system.

7.2 Mie Calculations

The recognition that many photochemically and photocatalytically active solutions can be approximated as transparent solutions in Mie absorbance calculations is an important result in my work. It is not a feature that I have seen discussed anywhere. Consequently, the behaviour of the internal electric field inside the droplets of liquid aerosol photochemical systems is considerably more interesting than one might initially think, considering the usual presentation of the internal field distribution of absorbing droplets.

The calculated internal field intensity distributions demonstrate the plausibility of two interesting applications of liquid aerosol photochemistry. Firstly, the concentration of the internal field in a small part of the droplet will be useful in photogenerated catalysis. Catalyst generation will take place in the high intensity region, while the actual catalytic reactions take place in the 'dark' regions. This could improve the efficiency of the system's utilisation of light. Secondly, the large enhancement in the intensity of certain wavelengths of light due to optical resonances raises the possibility of reaction pathway selectivity. Essentially, monodisperse aerosol droplets can act as both a lens and a monochromator.

7.3 Process Liquid Aerosol Photochemistry

In this thesis, I have discussed the reasons for, and the promise of, process liquid aerosol chemistry. The implementation of process liquid aerosol systems has been considerably more difficult than was anticipated. Although I was unable to develop a functional process liquid aerosol photochemical system, I have demonstrated the ability of liquid aerosol systems to enhance reactivity. Considerable work remains to be done in this area, and as our understanding of aerosol systems and the liquid surface increases, so will our ability to exploit the reactivity of aerosol systems.

7.4 Directions for Future Research

In order to exploit the enhanced photolysis of molybdenum hexacarbonyl that occurs in liquid aerosols it will be necessary to identify the photolysis products. This could be done

with the help of a quantum chemistry computational package. The structures and vibrational frequencies of possible products (for example, $Mo(CO)_5$(decene) or $Mo_2(CO)_{10}$) could be determined. The calculated vibrational frequencies would help identify the unknown peaks in the product FTIR spectra.

It is also important to obtain a rate constant for the photolysis of molybdenum hexacarbonyl in liquid aerosols. Once a technique has been developed to do this it would be very interesting to find out in the rate constant is dependant on the size distribution of the aerosol droplets.

Before much more progress can be made it will be necessary to develop an online technique that monitors the reaction inside the cell. It may be possible to use an infrared laser to do this.

There is a considerable amount of possible theoretical work on liquid aerosol photochemistry. One area that would be particularly useful is the development of a kinetic model of photocatalytic processes in liquid aerosols that takes into account the internal intensity distribution within a droplet.

Appendix

A.1 Discussion of Approaches to Computational Research

The range of resources available for the numerical computations is huge. There is the time-honoured language Fortran; there are languages like Basic or C/C++, for which a huge number of different numerical libraries can be downloaded; there are modern languages like Python; advanced symbolic mathematics packages like Maple and Mathematica; specialised numerical computation packages like Matlab and O-Matrix; and free variants of these, such as Octave and SciLab, to name a few. Some languages are compiled while some are interpreted; both methods have their advantages and disadvantages. Some languages and packages are proprietary and some are open source, and again there are advantages and disadvantages in these options. I believe that the nature and philosophies of open source and proprietary software raise important questions about the practice of science.

Code can be written as a simple command line application or it can be made more like windows, with tools such as Borland C++ Builder or Microsoft Visual Studio. Programmes can be written and executed on a powerful central UNIX workstation or on a PC that runs either Windows or Linux. Furthermore, there is a range of techniques available for the actual design of computer code, such as object-orientation and generic programming.

Faced with this range of possibilities and approaches to numerical computing I did not want to use Fortran. On the other hand, I did not want to spend an entire PhD attempting to come to grips with the huge range of techniques and tools available. With this in mind, I investigated a small number of the available techniques and settled on an approach using C++ and Python, which I think is elegant, simple, powerful, and philosophically pleasing. In the following sections, I shall briefly outline my investigations, the solution I used, and the reasons for that. Ultimately, I would like to publish this section on a webpage, as a guide for people in the same situation as I was, wanting to do some numerical work and having no historical inertia in their

research group to guide them to a particular technique. I also plan to publish the calculated internal intensity distributions on the web as they are much easier to visualise in electronic form.

A.1.1 Investigation of Numerical Techniques

During the course of the computational investigation of optical effects in microdroplets, I experimented with a number of different languages and programming techniques. This section contains an outline of the languages and approaches I looked at, and a more detailed discussion of the solution I chose.

I decided that I wanted to work on a Windows platform for the computational work. The main reason for this was that the chemistry department is set up with a Windows network and all the programmes that I used for instrument control were Windows-based. There are some disadvantages in the use of Windows platforms for numerical work: many of the numerical tools only work on UNIX/Linux platforms and the Windows operating system does not utilise the processing power of the computer as well as a Linux system. However, I did not think that the calculations I was going to do were computationally intense enough for that to be a problem. I also tried to write my code so that if I ran out of processing power, the important parts of the code would be sufficiently portable so that they could be compiled and run on the university's UNIX or VAX workstations. The Windows languages that I had access to through the University's licensing agreements were Microsoft Visual C++, Microsoft Visual Basic, and Borland C++ Builder. The commonly used free compilers that I could use were the mingw compilers (C++, C, and Fortran77)[i] and the Borland free command-line tools. I could also use Python, which is an open source interpreted language. The university runs a copy of Matlab and an older version of Mathematica on a Sun workstation that was accessible from my PC and I also had access to a copy of Maple that I could put on my PC.

---

[i] Unfortunately, I was unable to try out any of the newer version of Fortran because there are no free versions of Fortran90 or Fortran95. Therefore, the criticisms I make of Fortran are really only criticisms of Fortran77 and may not be at all relevant to the later versions.

Programmers always build with a design philosophy, even if that design philosophy is "I'll write the code and hope it works". The most prominent design technique in the software industry is object-oriented design or object-oriented programming. I was attracted to this idea and was interested in its application to scientific software. The major advantage of object-oriented programming is that it facilitates the reuse of code. In many ways, this has been driven by very large projects, with many programmers, where no one person can possibly understand all the code. In this situation an individual programmer needs to be able to interface the code with someone else's code without actually understanding how the code works. Of course, object-oriented techniques have advantages even in the single programmer projects that dominate scientific computing. There are innumerable books written on object-oriented programming, but I found a book called *Object Technology for Scientific Computing: Object-Oriented Numerical Software in Eiffel and C* (Dubois 1997) particularly helpful and influential[i]. Dubois opens his book with a statement that neatly summarises what I think about object-oriented programming and scientific software.

> Object-oriented programming languages have revolutionised the production of software in most of computing. Business and industry driven by the need for instant response to changing conditions, correctness, safety, and reliability have embraced object technology and realised its benefits. Scientific programmers have been bystanders, continuing to produce software by methods that have been supplanted in every other area of computing. Most scientists cite their special software needs and wait, though the conditions that have kept scientists sitting on the sidelines have nearly disappeared.

Some languages are more object-oriented than others are. Eiffel forces programmers to use object-oriented methods, C++ facilitates it but does not require it, and C and Fortran have existed for longer than object-oriented programming. However, it is still possible to apply the

---

[i] Other books that I found useful were Stroustrup, B. 1997, *The C++ programming language*, 3rd edn, Addison-Wesley, Reading, Mass, Flowers, B. H. 1995, *An introduction to numerical methods in C++*, Clarendon Press, Oxford ; New York..

principles of object-oriented programming, if not the specific methods, to programmes written in Fortran.

Dubois defines object-oriented programming as "... the construction of a program as a structured collection of instances and implementations of abstract data types," and adds that there are three concepts central to, and that provide the power of, object-oriented programming: encapsulation, inheritance, and dynamic binding (Dubois 1997 pp. 10-11).

This is not an appropriate place for a detailed discussion of object-oriented programming, but some discussion is necessary. I shall briefly expand on the above paragraph in the context of Mie theory.

Central to any light-absorption-by-microdroplets calculation are the size parameter $x = ka$, complex refractive index: m, spherical Bessel functions: j_n & y_n, and the internal field coefficients: c_{oln} & d_{eln}. The internal field coefficients are defined in terms of spherical Bessel functions of the size parameter and the refractive index.

$$c_{oln} = i^n \frac{2n+1}{n(n+1)} \left[\frac{i/x}{\left[j_n(\mathrm{m}x) h_{n-1}^{(1)}(x) - \mathrm{m} h_n^{(1)}(x) j_{n-1}(\mathrm{m}x) \right] x} \right] \tag{54}$$

In (54) the spherical Hankel function, $h_n^{(1)}$, is the complex sum, $j_n + iy_n$, of the spherical Bessel functions. In the actual calculation it is also necessary to define a cut-off value of n, which is a function of the size parameter. In many ways, the internal field coefficients are almost customised for an object-oriented approach.

Assuming that the programme inputs are the size parameter x, and the refractive index m, I would define functions to calculate the Bessel functions, and the internal field coefficients, using procedural programming techniques. Each function would return a value that would become the argument for the next function. It would also be necessary to pass the cut-off value to each function.

Using object-oriented methods, I would define a size parameter class. Size parameter objects are instances of the size parameter class, classes are user-defined types, and types are objects like **int**, an integer. The programming language creates, accesses, stores and uses integers in a certain way. In the same sense, a size parameter class can be defined to create size parameter objects that the programme creates, accesses, stores and uses in certain ways. Often the methods for creating, accessing, storing and using mathematical objects are messy and can obscure the mathematical purpose of the code, but in an object-oriented programme this messy code is moved away from the mathematical code and a size parameter object can be used almost as it would be used mathematically. Even on its own, the separation of the methods that a mathematical object uses, from its use as a mathematical object, would represent a big improvement in a lot of scientific code. Code that transparently demonstrates its mathematical purpose is invaluable, especially in a situation where the code was written by someone no longer in your research group.

Obviously, classes can be used to define more complicated objects than those representing size parameters: spherical Bessel functions and internal field parameters, for instance. This is where the power of object orientation starts to become evident. It is not necessary to design the spherical Bessel function class so that it can create, access, store and use the information given by a size parameter, but rather we can define the spherical Bessel function class so that it inherits from the size parameter class. Thus, all the properties of the size parameter class become properties of the spherical Bessel function class. The utility of inheritance is more apparent when the spherical Bessel function and the internal field parameter classes are considered. Rather than having the internal field coefficient routine call a function to calculate the spherical Bessel function and pass the results back, the internal field parameter class can inherit the methods for calculating, storing and handling spherical Bessel functions from the spherical Bessel function class.

In isolation, inheritance appears to make a problem already prevalent in scientific software, even worse; the problem of the dependencies that exist throughout a programme. These dependencies mean that when we alter a small bit of code to make it better, it breaks the whole programme. This is where encapsulation, another of the central concepts of object-oriented

programming, comes into play. Every class is defined with an interface; classes have public and private members. A class's interface, its public interface, is what it shows to other classes. The interface must be defined so that other classes can still use the class even if the way it is implemented is completely changed, which is very useful in scientific programming. The most important part of any Mie theory based calculation is the efficiency with which spherical Bessel functions are calculated, because most Mie theory calculations use many spherical Bessel functions. If an object-oriented programme is well written and the author discovers a much better way to calculate spherical Bessel functions, then the spherical Bessel function class can be rewritten without having to change any other code. Whereas, for many scientific programmes the discovery of a more efficient implementation would require a virtual rewrite of the whole programme, especially if the way that the data was handled and stored was changed.

Encapsulation also has advantages during the development stage of programming. The use of pointers and references increases the speed of code by making it possible to point a function to the place where a large array is stored, rather than having to make a copy of the array and pass it to the function. Unfortunately, I could not get them to work properly, but I was able to write the spherical Bessel function class using the easier and less efficient array handling techniques. The advantage of this was that I could finish the programme despite the difficulty I was having with one part of it. As soon as I had the programme working, I was able to go back and rewrite the class, confident (in theory) that making the implementation of class more efficient would not affect the rest of the programme.

The third and final of Dubois' three core concepts of object-oriented programming is dynamic binding and intimately related to dynamic binding is polymorphism. Together these concepts make it possible to define a general way of calculating spherical Bessel functions and have special cases where, for certain spherical Bessel functions, a different method of calculation is used. For example, I defined the general spherical Bessel function calculation method to be downward recursion because it is more stable, but in Mie calculations it is not necessary to calculate spherical Bessel functions of the second type, y_n, by downward recursion because they are stable for upward recursion, which is faster. Dynamic binding means that the correct

method is used for the y_n entity at run time, rather than compile time, by examining the actual type of object the y_n entity is bound to. Mie type calculations do not demonstrate the real utility of polymorphism and dynamic binding in scientific computing, because anyone doing the calculation will already know that j_n functions require downwards recursion while y_n functions only need upwards recursion. However, in a situation where it is not already known what calculation method is most appropriate, the programmer can start with the safest and most stable technique, which generally produces the slowest programme. Once this is working, it is not necessary for the programmer to rewrite code to experiment with faster, less stable, methods. Instead, the programmer can simply define an object that inherits most of its methods from the original class, but that uses a different calculation technique; this is polymorphism. Dynamic binding means that the run-time system works out which calculation method to use, depending on the type of object that the entity is.

There are a number of other features that are part of, or closely related to, object-oriented languages (Dubois 1997 pp. 18-39). While most of these features are not sufficiently important in scientific programming to discuss here, two of these features can be used very elegantly and are worth discussing.

Overloading is just what it sounds like; in a language that permits function overloading two different functions can have the same name. This is not an exclusive feature of object-oriented languages, but it is very easy to implement in an objected-oriented environment. Mie calculations are essentially a number of different infinite summations, and it is necessary to determine and use a maximum value of the summation index n. Mie calculations also involve the calculation of many Bessel functions; some of the Bessel functions need to have the maximum number of terms and others do not. Using operator overloading it is possible to define two functions, both with the same name *bessel*, for the calculation of Bessel functions: one which takes only the mathematical argument of the Bessel function as an argument and calculates the maximum number of terms, and one which takes the mathematical argument and the number of terms required as arguments. When the function *bessel* is called, the programme selects the appropriate method based on the number of arguments of the calling function.

Operators can be overloaded in a similar way. Mie calculations require the calculation of Hankel functions of the first kind, which are defined as $j_n + iy_n$. The classes that represent j_n and y_n can be defined with an overloaded operator '+' so that when a j_n object is added to a y_n object the result is a spherical Hankel function.

One of the aims of mathematical programming is to avoid obscuring the mathematical purpose of the code. Overloading is a technique that removes the necessity to define a range of functions or operators that, although they have different names, are actually just the same function or operator in a different context.

Generic classes, or templates, are an extension of the ideas of classes and overloading. Generic programming is a programming technique that takes advantage of templates. It has been used very elegantly in the production of the Standard Template Library (STL) and the Matrix Template Library (MTL). The simple applications of generic programming are perhaps the most revolutionary aspect of the new programming techniques for scientific programming.

In a Mie calculation that uses a complex refractive index, some of the j_n functions that are calculated have complex arguments and some have real arguments. It is inefficient to make every variable that might be passed to a Bessel function complex. It is also undesirable to write two Bessel function routines, one for complex arguments and one for real argument. Templates make this an easy problem to solve. Rather than defining a separate function for calculating Bessel functions of complex values, the Bessel function can be defined in terms of a template parameter. When the class is instantiated, the parameter can be set to either a real or a complex value. This way, only one function needs to be written, and the programme decides whether it is necessary to use complex variables or real variables for the calculation.

Generic programming moves beyond function overloading because function overloading still requires the programmer to write a routine for real numbers and a routine for complex numbers. Templates allow the programmer to avoid writing large amounts of virtually identical code. It also makes it very easy to switch between double and single precision floating numbers.

One of the most important movements in computing at present is open source software. Open source software is software that is free of cost and available with the source code (www.opensource.org). This software is not unlicensed, it is usually distributed under a copyleft licence, which is more or less the opposite of copyright licence (Lawton 2002).

While there are philosophical and economic reasons for preferring open source software to proprietary software, the practical reasons are probably the most important. If a product is open source and a user discovers a bug they can modify the source to remove the bug and make the improved version of the software available to other users.

In the course of my work, I have used a number of different computer interfaced commercial instruments including a Varian and GBC UV-Visible, Shimadzu FTIR, and MKS mass spectrometers, and a TSI aerodynamic particle sizer. I do not consider any of the software that came with these instruments to be adequate for scientific research. The mass spectrometer and particle sizer software were particularly useless. The problem with these programmes is not in their instability, but their limitation. The software is designed for the typical user of these instruments and was unable to do the things that I wanted it to do. This is the way that instrumental software should be designed as there is no way that a software designer at MKS, TSI, GBC, Shimadzu or Varian could anticipate how every researcher may want to use their instrument. The Varian software was by far the best because it included a macro language, called ADL, which allows users to customise the instrumental control. However, the ADL macro language is not extensible, so while the user has considerably more control than other software packages, he or she is still essentially limited to uses anticipated by the Varian software engineers.

I did not want to write a new programme from scratch to control the instruments, so somewhat naively, and before I had even heard of open source software, I wrote to both MKS and TSI asking for the source code of the programmes so that I could tailor them to my own needs. Both the programmes were proprietary and the companies would not give me the source code. In the end, I persevered with the commercial software.

Open source software provides an attractive alternative to the problems outlined above. The majority of researchers who will be frustrated by the instrument software they are using, will also be capable programmers. In a hypothetical scenario, releasing the control software under an open source agreement effectively provides the companies with a free software development team. Under the terms of the licence agreement, modifications to the software are made available to other users of the instrument. The company that made the instrument code coordinates a website to which people upload customised code. The good packages are eventually incorporated into the main software, while the bad packages die a natural death. If someone wants to use the instrument in a way that the core software does not allow, they first check the website to see if anyone has made an appropriate package, and if not they can write their own.

An open source approach to instrumental software seems to be much more in the spirit of scientific openness and collaboration than the current, largely proprietary, approach. Furthermore, I am unable to see how the companies would lose money by using open source control software. The five instruments that I mentioned above are all so expensive that the cost of a computer to run them, let alone software, is virtually irrelevant. There are not many people in the world wanting to buy TSI Aerosol Instrument Manager Software without an aerodynamic particle sizer. It is possible that companies will not want to release the source code if people could use the source code to figure out how a commercially sensitive part of their instrument worked. However, this is not a part of the source code that most people would want to monitor and there is no reason why the company could not release the sensitive elements of the software in binary form.

Another advantage of open source software is that source code is easier to transfer between platforms. It would enable users to control their instruments from a PC running Linux, with minimum work, especially if the source code was well designed (www.wxwindows.org), and even if the original software was developed on a different platform.

The principles behind open source software are very similar to the principles of science: cooperation, collaboration, openness, and peer review. For this reason there are calls for all

scientific software to be released as open source software (Kiernan 1999, www.openscience.org). This would allow greater cooperation between researchers tackling similar sorts of problems. Numerical results would also be open to greater scrutiny if the source code that produced the results was freely available along with the results themselves.

Following the frustrations that I experienced with proprietary instrument control software, and looking at the role of open source software in computing in general and in science, I decided that it is a good principle to use, and to contribute to open source software whenever possible.

I have not tried to use exclusively open source software, partly because it is not practical, and partly because my commitment to open source software was not consistent throughout the course of my work. I chose to continue to work on Windows platforms rather than Linux platforms because the chemistry department is set up with a Windows network and I did not want to be isolated. Additionally, none of the instruments I used had software that would work on Linux machines. I also do not think that it is a good idea to advocate the use of open source software throughout science, but at the same time restrict open source software to Linux operating systems. This would prevent many people from using open source software.

Following my decision to support open source software in science, I have always looked at what open source tools are available when searching for a new programming tool. This influenced the final choice of software tools I used for my numerical work.

The first calculations I did were in C++ and I used both Borland C++ Builder and Microsoft Visual C++. Both of these programmes provide a very advanced C++ development environment for Windows and, in many ways, they are too specialised for numerical programming. In general, numerical programming does not require a windows-type interface and is actually run more efficiently as console applications.

I then discovered that I had access to Matlab and Mathematica running on a Sun workstation. I met several people who were very enthusiastic about doing numerical computing on Matlab, so I spent some time writing Mie code in Matlab. However, I decided that Matlab was too specialised for Mie calculations; I did not find the built-in Bessel and Legendre functions

useful and I was not using any of the matrix techniques that Matlab is built around. There is some scope for object-orientation in Matlab, but it is not a natural part of the language. I therefore decided to return to working with C++.

When I returned to using C++, rather than using C++ Builder or Visual C++, I used the Borland C++ free command lines tools, which are the command line tools for Visual C++. I wrote the code in an open source editor, SciTE, which uses the open source editing environment, Scintilla, (www.scintilla.org). I would rather not have used Visual C++ at all, but it is the standard for Windows systems and many of the open source tools I used require it to compile them. One thing I noticed when I started coding in C++ again is the difference between developing software using compiled language and an interpreted language; C++ is compiled, while Matlab is interpreted. I found it a lot easier to write code in an interpreted language because I could keep running small pieces of code to see if they gave the answers I expected, but in C++ I had to get the whole programme to work before knowing that the numerical parts were working. On the other hand, the advantage of compiled languages was speed; code generally executes much more quickly in a compiled language than in an interpreted language. This is one of the reasons why Fortran and C/C++, which are both compiled languages, dominate numerical computing.

I had done some simple scripting work in Python: a well-designed, extensible, open source, object-oriented, easy to use, interpreted language in which code is typically between two and three times shorter than the C++ or Fortran code for the same job. It even has a mature additional numerical package called NumPy (www.numpy.org), which was actually developed by Paul Dubois[i]. Development of a scientific package for Python, called SciPy (www.scipy.org), is also underway. I did not consider Python for Mie calculations because it is an interpreted, and therefore slower, language. I then read a paper entitled 'Feeding a Large-scale Physics Application to Python' (Beazley and Lomdahl 1997) and I was interested by the idea even though my Mie calculation is not a Large-scale Physics Application,. Python is

[i] Paul Dubois was the author of *Object Technology for Scientific Computing*

written so that it can be extended using C/C++; Beazley and Lomdahl describe how they took the C code from their project and turned it into a series of C libraries. The C code is then compiled as a shared library and the commands can be loaded into Python. The overall aim of this is to keep the numerically intensive parts of the code written in C, while the rest of the programme, which is not computationally expensive, can be written in Python. This is becoming quite a common technique and it is how large parts of the SciPy and NumPy modules have been built.

The combination of C++ and Python promised to provide the best of both worlds; where necessary the power of C++ could be used, while everything else could be written in Python, which is an easier environment to work in because it is interpreted. If I discovered that a part of the Python code was becoming too computationally intensive, it could be moved into C++ code. It is actually possible to do something similar in Matlab if you purchase the right software to do it, but Python is free and far more customisable and flexible. Python can also be wrapped around Fortran code, so this programming technique for numerical work is not restricted to C/C++. Enthought, the company that is supporting the development of the SciPy package, is also developing electromagnetic radio wave scattering code using Python and Fortran90.

The process of writing extensions for Python in C++ is not overly complicated; nevertheless, there are various tools available to make the process simpler. I chose to use Weave. Weave is part of the SciPy package (www.scipy.org), although it can be used as a stand-alone package. One of the Weave tools, 'inline_tools', facilitates the insertion of C++ code directly into Python. The first time that the code is executed, the C++ portion of the code is compiled into a library which is then available for use by Python. Code listing A.1 is a portion of the programmes I used to calculate Mie absorption distributions. It is the code of a function that calculates spherical Bessel functions of the second kind. It illustrates the use of C++ code, via Weave, to do all the heavy numerical work.

```
def calc_bessely(x):
    'calculates yn (spherical bessel function), uses weave.inline'
    # hash marks signify comments, python uses indentation to distinguish code blocks
    # the interpreter uses the string immediately after the function declaration to
    # provide help for users
    n_max = calc_max(x)
    bessely = zeros([n_max + 1], Float)
    # an array of zeros is defined and passed to the C++ library
    code = """
        bessely(0) = -cos(x)/x;
        bessely(1) = bessely(0)/x - sin(x)/x;
        int i = 2;
        do {
            bessely(i) = (2 * (i - 1) + 1) * bessely(i - 1)/x - bessely(i - 2);
            i = i++;
        } while (i <= n_max);

    """
    # the string code is used by the blitz compiler to generate a library
    inline_tools.inline(code,['bessely', 'x' , 'n_max'],
                type_converters = blitz_type_converters,
                compiler='gcc', verbose = 1)
    # when the bessely functionis called an array of the values is returned
    return bessely
```

Code listing A.1 Python/C++ code for spherical Bessel function using weave

Somewhat ironically, although I used blitz.inline in the development of my Mie absorption code, the majority of the actual calculations were carried out using a modified version of the programme written purely in python. This programme is included in the appendix. The SciPy package is still being developed and in a later release it included python wrappers for the cephes library (www.netlib.org/cephes). The cephes library contains routines for the calculation of many standard mathematical functions, including Bessel functions. The SciPy special functions module is written with the same principles as my code; the actual calculation of the functions is done in C++ or Fortran. However, the SciPy special functions module is a much better example of this than my code. My Mie calculation code executed in about half the time that it took using my Bessel functions.

The use of Python, rather than Fortran or C++, meant that my calculations ran more slowly. However, they were not so slow that it caused frustration, and the ease of use of the Python environment, particularly for graphing results, more than compensated for the slowness of the calculation. If the slowness of the programme were to become a problem, then tools such as Pyfort (http://pyfortran.sourceforge.net/) and F2PY (http://cens.ioc.ee/projects/f2py2e/) could be used to generate a python wrapper for the Barber and Hill Fortran code on which my

Python code was based. As this solution provides both the ease of use of Python and the speed of Fortran, it is probably the best approach to Mie calculations. Unfortunately, I was unable to explore this possibility.

A.2 Mathematical Definitions

A.2.1 Vector Spherical Harmonics

In component form the vector spherical harmonics are (Bohren and Huffman 1983 p. 89)

$$\begin{aligned}\mathbf{M}_{emn} = &\frac{-m}{\sin\theta}\sin m\varphi P_n^m(\cos\theta)\, z_n(\rho)\hat{\mathbf{e}}_\theta \\ &-\cos m\varphi \frac{dP_n^m(\cos\theta)}{d\theta} z_n(\rho)\hat{\mathbf{e}}_\varphi\end{aligned} \tag{55}$$

$$\begin{aligned}\mathbf{M}_{omn} = &\frac{m}{\sin\theta}\cos m\varphi P_n^m(\cos\theta)\, z_n(\rho)\hat{\mathbf{e}}_\theta \\ &-\sin m\varphi \frac{dP_n^m(\cos\theta)}{d\theta} z_n(\rho)\hat{\mathbf{e}}_\varphi\end{aligned} \tag{56}$$

$$\begin{aligned}\mathbf{N}_{emn} = &\frac{z_n(\rho)}{\rho}\cos m\varphi n(n+1) P_n^m(\cos\theta)\hat{\mathbf{e}}_r \\ &+\cos m\varphi \frac{dP_n^m(\cos\theta)}{d\theta}\frac{1}{\rho}\frac{d}{d\rho}\left[\rho z_n(\rho)\right]\hat{\mathbf{e}}_\theta \\ &-m\sin m\varphi \frac{p_n^m(\cos\theta)}{\sin\theta}\frac{1}{\rho}\frac{d}{d\rho}\left[\rho z_n(\rho)\right]\hat{\mathbf{e}}_\varphi\end{aligned} \tag{57}$$

$$\begin{aligned}\mathbf{N}_{omn} = &\frac{z_n(\rho)}{\rho}\sin m\varphi n(n+1)P_n^m(\cos\theta)\hat{\mathbf{e}}_r \\ &+\sin m\varphi\frac{dP_n^m(\cos\theta)}{d\theta}\frac{1}{\rho}\frac{d}{d\rho}\left[\rho z_n(\rho)\right]\hat{\mathbf{e}}_\theta \\ &+m\cos m\varphi\frac{p_n^m(\cos\theta)}{\sin\theta}\frac{1}{\rho}\frac{d}{d\rho}\left[\rho z_n(\rho)\right]\hat{\mathbf{e}}_\varphi\end{aligned} \tag{58}$$

A.2.2 Spherical Bessel Functions

The spherical Bessel functions of the first and second kind are defined in terms of the Bessel functions of the first and second kind (Bohren and Huffman 1983).

$$j_n(\rho) = \sqrt{\frac{\pi}{2\rho}}J_{n+\frac{1}{2}}(\rho) \tag{59}$$

$$y_n(\rho) = \sqrt{\frac{\pi}{2\rho}}Y_{n+\frac{1}{2}}(\rho) \tag{60}$$

The spherical Hankel function of the first kind, sometime called the spherical Bessel function of the third kind is

$$h_n^{(1)}(\rho) = j_n(\rho) + iy_n(\rho) \tag{61}$$

A.3 List of Principle Symbols

A.3.1 Roman Symbols

A	area

a	droplet radius
a_x	amplitude of capillary wave
C	concentration
c_{oln}	odd internal field expansion coefficient
D	diffusion coefficient
d_d	droplet diameter
d_{eln}	even internal field expansion coefficient
d_eS	external entropy change
d_iS	irreversible entropy change
d_p	penetration depth
E_0	incident electric field amplitude
$\mathbf{E}^i$	incident electric field
$\mathbf{E}^{\text{int}}$	internal electric field
$\mathbf{E}^s$	scattered electric field
f	frequency
F	Helmholtz free energy
f_{oln}	odd external field expansion coefficient
G	free energy
g	gravitation acceleration
g_{eln}	even external field expansion coefficient
H	enthalpy
h	Plank's constant
$h_n^{(1)}$	spherical Hankel function of the first kind
j_n	spherical Bessel function of the first kind
k	wavenumber/wavevector
k	rate constant
$k^{\dagger}$	rate along critical coordinate
k_B	Boltzmann's constant
L	length scale
m	complex refractive index
m	mode number
$\mathbf{M},\mathbf{N}$	vector spherical harmonics
n'',n'	number of moles
p	pressure
p	pressure
Q	heat
Q_L	flow rate of liquid
r	radius
$\mathbf{r}$	radial vector
R	gas constant
R_1	1st principal radii of curvature
R_2	2nd principal radii of curvature
S	entropy

T	temperature
t	time
T	temperature
U	internal energy
V	volume
v'',v'	specific molar volume
$v^{\dagger}$	surface velocity
x	size parameter
y_n	spherical Bessel function of the second kind
z_n	generic Bessel function

A.3.2 Greek Symbols

α	mass accommodation coefficients
γ	surface free energy or surface tension
ζ	vertical displacement
θ	zenith angle
κ	general diffusion coefficient
λ	wavelength
ν	frequency
Ξ_{CM}	count median diameter
ρ	density
σ	molecular diamater
ϕ	azimuthal angle
Ψ	general diffusion quantity
ω	circular frequency

A.4 Code Listing

```
from Numeric import *
from types import *
from scipy import special
#scipy module provides bessel functions
import pickle
#pickle module handles i/o
import pyvtk
#this module formats data for use by vtk
import mayavi
#mayavi generates all the 3-d graphs


class Droplet:
    'class containing macroscopic properties of the droplet'
    # the program is designed with Droplet as the base class from which
    # the classes InternalFieldParam and and the various slice classes are derived.
    # Droplet handles grid sixes, i/o, series truncation etc
    # the class requires five variables for initalisation
    # size_parameter - unsurpisingly the size parameter x
    # refractive_index - complex refractive index m
    # slices - the number of slices through the sphere to be calculated
    ##    the vast majority of calculation were done for a single XZ slice
    # points - defines the resolution - always 50
    ##     this corresponds to 50 points in the x direction and 200 in the Z
    ##    the internal field changes more rapidly in the Z direction
    # xyz - buggy parameter used to define orienation of slices
    # this class in only ever instantiated as a base class via the InternalFieldCoeff class
    # for one of the slice classes
    # the slice classes are were the actual computation is done
    def __init__(self, size_paramater, refractive_index, slices, points, xyz):
        'initialisation function for class droplet'
        self.x = size_paramater
        self.m = refractive_index
        self.set_max_values() # truncation
        self.set_increment(points, slices, xyz) # controls the loops used in the calculation
        self.set_pickling() #i/o


    def set_max_values(self):
        'nMax is the truncation value for the Mie summation'
        self.nMax = int(self.x + 4.05 * self.x ** (1.0/3.0) + 2)
        #this is the standard formula for Mie calculations

    def set_pickling(self):
        self.dir = 'C:\\Documents and Settings\\chem246.LFPC466\\My Documents\\My PhD\\My Code\\pyth
on\\'
        self.file = 'x_' + str(int(self.x)) + '_m_' + str(self.m) + '_res_' + str(int(self.x_pnts))
+ '_' + str(int(self.z_pnts))

    def set_increment(self, points, slices, xyz):
        if xyz == 'psi':
            self.x_pnts = points / 2.0
            self.z_pnts = 2 * points
            self.y_pnts = slices + 1
            # x_pnts is the number of points in the x direction between 0 and 1 etc
            self.dlt_x = 1.0/self.x_pnts
            self.dlt_z = 1.0/self.z_pnts
            self.dlt_y = 1.0/ (slices + 1)
            # dlt_x is the increment along the x axis etc
```

```
class InternalFieldCoeff(Droplet):
    'class for coln and deln'
    # this class is derived from Droplet and it calculated the internal field parameters
    # these parameters depend only on the size parameter 'x' and the complex
    # refractive index 'm'
    def __init__(self, size_paramater, refractive_index, slices, points, xyz):
        Droplet.__init__(self, size_paramater, refractive_index, slices, points, xyz)
        self.calc_Coeff()

    def calc_Coeff(self):
        #should move all this into another class so this one isn't so ugly
        def c_nFact(n): return((0 + 1j) ** n * (2 * n + 1 ) / (n * (n + 1)))
        def d_nFact(n): return(-(0 + 1j) ** (n + 1) * (2 * n + 1) /(n * (n + 1)))
        n = arange(self.nMax + 1)
        h1x_1 = myhl(n, self.x)
        # h1x is a spherical hankel function with argument x
        # h1x_1 is and array used to add the x-1 hankel function value to the x
        # hankel function value
        jmx_1 = myjv(n, self.m * self.x)
        # jmx is a spherical bessel function with argument m*x
        # jmx_1 ditto h1x_1
        h1x = h1x_1[1: self.nMax + 1]
        jmx = jmx_1[1: self.nMax + 1]
        h1x_1 = h1x_1[0:self.nMax]
        jmx_1 = jmx_1[0:self.nMax]
        n = n[1:self.nMax + 1]
        c_nFactor = array(map(c_nFact, n))
        d_nFactor = array(map(d_nFact, n))
        c_denom = (jmx * h1x_1 - self.m * h1x * jmx_1) * self.x
        self.coln = c_nFactor * ((0 + 1j) / self.x)/c_denom
        self.celn = -self.coln
        d_denom = self.x * (self.m ** 2 * jmx * h1x_1 - self.m * h1x * jmx_1) - n * (self.m ** 2 -
1) * h1x * jmx
        self.deln = d_nFactor * (self.m * (0 + 1j) / self.x) / d_denom
        self.doln = self.deln

    # ideally the remaining member function of class should be in the Droplet class
    # but they are not

    def mayavi_set(self, E2, slice):
        q = E2
        q1 = reshape(transpose(q), (-1,))
        point_data = pyvtk.PointData(pyvtk.Scalars(q1))
        grid = pyvtk.StructuredPoints((len(E2[:,0]), len(E2[0,:]), 1), (-1.0, -1.0 - self.dlt_z/2.0,
0), (self.dlt_x, self.dlt_z, 100))
        data = pyvtk.VtkData(grid, point_data)
        data.tofile(self.dir + 'vtk\\' + self.file + '_slice_' + str(int(slice)) + '.vtk')

    def calc_legendre(self):
        'calculates legendre function in the form required for Mie calcs'
        nr = arange(len(self.theta[:,0]))
        nc = arange(len(self.theta[0,:]))
        self.P_1 = zeros([len(nr),len(nc),self.nMax+1],Float)
        for u in nr:
            for v in nc:
                self.P_1[u,v,:] = bhlp(self.theta[u,v],self.nMax)

    def pickle_intensity(self, E2, slice):
        pickle.dump(E2, open(self.dir + 'pickle\\' + self.file + '_slice_' + str(int(slice)) + '.pic
kle', 'w'))

    def pickle_intensity_no_slice(self, E2):
        pickle.dump(E2, open(self.dir + 'pickle\\' + self.file + '.pickle', 'w'))

class XZslice(InternalFieldCoeff):
    # slice classes are where all the compution is done
    # this class calculates multiple XZ slices - defaults to a single slice
    # all the slice classes are essientially the same - could have been written much better
    # there was a buggy class for XY slices which left the remant 'xyz' parameter in the
```

```
    # Droplet class - it is now gone
    def __init__(self, size_paramater, refractive_index, slices = 1, points = 50):
        xyz = 'psi'
        InternalFieldCoeff.__init__(self, size_paramater, refractive_index, slices, points, xyz)
        self.set_grid()
        self.loop_intensity()

    def set_grid(self):
        'defines a 3-d grid of values for the compuation'
        x_ax = arange(-1.0, 1.0+ self.dlt_x/4.0, self.dlt_x)
        z_ax = arange(-1.0 - self.dlt_z/2.0, 1.0 + self.dlt_z/2.0 + self.dlt_z/4.0, self.dlt_z)
        y_ax = arange(0.0, 1.0 - self.dlt_y/2.0 , self.dlt_y)
        r0 = sqrt(x_ax[:,NewAxis]**2 + z_ax**2)
        self.r = sqrt(r0[:,:,NewAxis]**2 + y_ax**2)
        self.theta = arctan(x_ax[:,NewAxis]/z_ax)
        self.psi = zeros([len(r0[:,0]), len(r0[0,:]), len(y_ax)],Float)
        n1 = arange(len(r0[:,0]))
        n2 = arange(len(r0[0,:]))
        n3 = arange(len(y_ax))
        for i1 in n1:
            for i2 in n2:
                for i3 in n3:
                    self.psi[i1,i2,i3] = arccos(r0[i1,i2]/sqrt(r0[i1,i2]**2 + y_ax[i3]**2))

    def loop_intensity(self):
        'calculates the actual intensity'
        lr = len(self.r[:,0,0])
        lc = len(self.r[0,:,0])
        ls = len(self.r[0,0,:])
        nr = arange(lr)
        nc = arange(lc)
        ns = arange(ls)
        nn = arange(1,self.nMax)
        E2 = zeros([lr,lc],Float)
        for t in ns:
            for u in nr:
                for v in nc:
                    #probably move into signle function
                    if self.r[u,v,t] <= 1.00001:
                        Er_para = 0
                        Etheta_para = 0
                        Epsi_para = 0
                        n = arange(self.nMax + 1)
                        mkr = (self.m * self.x * self.r[u,v,t])
                        jmkr = myjv(n, mkr)
                        if v > lc/2:
                            tht = self.theta[u,v]
                        else:
                            tht = pi - self.theta[u,v]
                            P = bhlp(tht, self.nMax)
                            sinth = sin(tht)
                            costh = cos(tht)
                            cospsi = cos(self.psi[u,v,t])
                            sinpsi = cos(self.psi[u,v,t])
                            #cospsi = cos(pi/4)
                            #sinpsi = sin(pi/4)
                        for w in nn:
                            Er_para = Er_para + (w * (w + 1)  / mkr * jmkr[w] * cospsi * P[w] * s
* self.deln[w - 1])
                            Etheta_para = Etheta_para + (jmkr[w] * cospsi * P[w] * self.coln[w -
(jmkr[w - 1] - w / mkr * jmkr[w]) * cospsi * (w * costh * P[w] - (w + 1) * P[w-1]) * self.deln
)
                            Epsi_para = Epsi_para +(-jmkr[w] * sinpsi * (w * costh * P[w] - (w +
P[w - 1]) * self.coln[w-1] + (jmkr[w-1] - w * jmkr[w] / mkr) * sinpsi * P[w] * self.deln[w-1])
                        E2[u,v] = abs(Er_para) ** 2 + abs(Etheta_para) ** 2 + abs(Epsi_para) ** 2
            self.pickle_intensity(E2, t)

class SingleXZslice(InternalFieldCoeff):
    # principle difference to XZslice is it allows external control of i/o
    def __init__(self, size_paramater, refractive_index, points = 50):
```

```
        xyz = 'psi'
        slices = 0
        InternalFieldCoeff.__init__(self, size_paramater, refractive_index, slices, points, xyz)
        self.set_grid()
        self.loop_intensity()

    def set_grid(self):
        x_ax = arange(-1.0, 1.0+ self.dlt_x/4.0, self.dlt_x)
        z_ax = arange(-1.0 - self.dlt_z/2.0, 1.0 + self.dlt_z/2.0 + self.dlt_z/4.0, self.dlt_z)
        self.r = sqrt(x_ax[:,NewAxis]**2 + z_ax**2)
        self.theta = arctan(x_ax[:,NewAxis]/z_ax)

    def loop_intensity(self):
        lr = len(self.r[:,0])
        lc = len(self.r[0,:])
        nr = arange(lr)
        nc = arange(lc)
        E2 = zeros([lr,lc],Float)
        for u in nr:
            for v in nc:
                if self.r[u,v] <= 1.00001:
                    Er_para = 0
                    Etheta_para = 0
                    Er = 0
                    Etheta = 0
                    Epsi = 0
                    mkr = (self.m * self.x * self.r[u,v])
                    nMaxLocal = min(self.nMax, int((abs(mkr) + 4.05 * (abs(mkr)) ** (1.0/3.0) + 2)))
                    n = arange(nMaxLocal + 1)
                    nn = arange(1,nMaxLocal)
                    jmkr = myjv(n, mkr)
                    if v > lc/2:
                        tht = self.theta[u,v]
                    else:
                        tht = pi - self.theta[u,v]
                    P = bhlp(tht, nMaxLocal)
                    sinth = sin(tht)
                    costh = cos(tht)
                    for w in nn:
                        Er_para = Er_para + (w * (w + 1)  / mkr * jmkr[w] * P[w] * sinth * self.deln
[w - 1])

                        Etheta_para = Etheta_para + (jmkr[w] * P[w] * self.coln[w - 1] + (jmkr[w - 1
] - w / mkr * jmkr[w]) *  (w * costh * P[w] - (w + 1) * P[w-1]) * self.deln[w - 1])
                    E2[u,v] = abs(Er_para) ** 2 + abs(Etheta_para) ** 2
        self.E2 = E2


class Point(InternalFieldCoeff):
    'used to calculate the intensity at a single point'
    def __init__(self, size_paramater, refractive_index, r, theta):
        xyz = 'psi'
        slices = 0
        points = 50
        InternalFieldCoeff.__init__(self, size_paramater, refractive_index, slices, points, xyz)
        self.r = r
        self.theta = theta
        self.intensity()


    def intensity(self):
        Er_para = 0
        Etheta_para = 0
        E2 = 0
        mkr = (self.m * self.x * self.r)
        nMaxLocal = min(self.nMax, int((abs(mkr) + 4.05 * (abs(mkr)) ** (1.0/3.0) + 2)))
        n = arange(nMaxLocal + 1)
        nn = arange(1,nMaxLocal)
        jmkr = myjv(n, mkr)
        tht = self.theta
        P = bhlp(tht, nMaxLocal)
```

```
        sinth = sin(tht)
        costh = cos(tht)
        for w in nn:
            Er_para = Er_para + (w * (w + 1)  / mkr * jmkr[w] * P[w] * sinth * self.deln[w - 1])
            Etheta_para = Etheta_para + (jmkr[w] * P[w] * self.coln[w - 1] + (jmkr[w - 1] - w / mkr
* jmkr[w]) *  (w * costh * P[w] - (w + 1) * P[w-1]) * self.deln[w - 1])
        E2 = abs(Er_para) ** 2 + abs(Etheta_para) ** 2
        self.E2 = E2


def bhlp(theta, nMax):
    legendre = zeros([nMax + 1], Float)
    legendre[1] = 1
    costh = cos(theta)
    n = 2
    while n <= nMax:
        legendre[n] = ((2 * n - 1) * costh * legendre[n - 1] - n * legendre[n - 2]) / (n - 1)
        n = n + 1
    return legendre

def myjv(v, z):
    'calclates spherical bessel j function'
    return sqrt(pi/(2 * z)) * special.jv(v + 1.0/2.0,z)

def myyv(v, z):
    'calclates spherical bessel y function'
    return sqrt(pi/(2 * z)) * special.yv(v + 1.0/2.0,z)

def myh1(v, z):
    'calclates spherical hankel function of the first kind'
    return sqrt(pi/(2 * z)) * special.hankel1(v + 1.0/2.0,z)
```

References

Anastas, P. T. & Warner, J. C. 1998, *Green chemistry : theory and practice*, Oxford University Press, Oxford [England] ; New York.

Andrews, D. L., Craig, D. P. & Thirunamachandran, T. 1989, 'Molecular Quantum Electrodynamics in Chemical Physics', *International Reviews in Physical Chemistry*, vol. 8, no. 4, pp. 339-383.

Armstrong, R. L., Xie, J. G., Ruekgauer, T. E. & Pinnick, R. G. 1992, 'Energy-transfer-assisted lasing from microdroplets seeded with fluorescent sol', *Optics Letters*, vol. 17, no. 13, pp. 943-5.

Arnold, S. & Folan, L. M. 1989, 'Energy transfer and the photon lifetime within an aerosol particle', *Optics Letters*, vol. 14, no. 8, pp. 387-9.

Arnold, S., Holler, S. & Druger, S. D. 1996a, 'Imaging enhanced energy transfer in a levitated aerosol particle', *Journal of Chemical Physics*, vol. 104, no. 19, pp. 7741-7748.

Arnold, S., Holler, S. & Druger, S. D. 1996b, 'The Role of MDRs in Chemical Physics: Intermolecular Energy Transfer in Microdroplets', In *Optical Processes in Microcavities*, (eds) Chang, R. K. & Campillo, A. J., World Scientific, Singapore, pp. 285-314.

Arnold, S., Holler, S. & Goddard, N. L. 1997, 'Fluorescence microscopy and spectroscopy of an isolated micro-droplet', *Materials Science and Engineering B*, vol. B48, no. 1,2, pp. 139-146.

Arnold, S., Holler, S., Li, J. H., Serpenguzel, A. & Auffermann, W. F. 1995, 'Aerosol-particle microphotography and spectroscopy \"in-situ\"', *Book of Abstracts, 210th ACS National Meeting, Chicago, IL, August 20-24*, no. Pt. 1, pp. ENVR-007.

Balboa, A., Partch, R. E. & Matijevic, E. 1987, 'Preparation of uniform colloidal dispersions by chemical reactions in aerosols. IV. Mixed silica/titania particles', *Colloids and Surfaces?*, vol. 27, no. 1-3, pp. 123-31.

Barber, P. W. & Chang, R. K. 1988, *Optical Effects Associated with Small Particles*, World Scientific, Singapore.

Barber, P. W. & Hill, S. C. 1990, *Light Scattering by Particles: Computational Methods*, World Scientific, Singapore.

Baron, P. 2001, *Aerosol Calculator* (computer program), Available at: www.tsi.com/particle/downloads/software/software/htm#Aerosol_Calculator_Program (2001)

Bayvel, L. P. & Orzechowski, Z. 1993, *Liquid atomization*, Taylor & Francis, Washington, DC.

Beazley, D. M. & Lomdahl, P. S. 1997, 'Feeding a Large-Scale Physics Application to Python', In *Proceedings of the Sixth International Python Conference*, http://www.python.org/workshops/1997-10/proceedings/beazley.html.

Biggus, J. 2002, *'Sketches of a History of Classical Electromagnetism'*, Available at: http://history.hyperjeff.net/electromagnetism.html

Bohren, C. F. & Huffman, D. R. 1983, *Absorption and scattering of light by small particles*, Wiley, New York.

Braslavsky, S. E. & Kuhn, H. J. 1987, 'Provisional List of Actinometers', *EPA Newsletter*, vol. 29, no. March, pp. 49-60.

Bronson, S. D. & Skovgaard, P. M. W. 1996, 'Optical Mode Density and Spontaneous Emission in Mircavities', In *Optical Processes in Microcavities*, (eds) Chang, R. K. & Campillo, A. J., World Scientific, Singapore, pp. 77-100.

Buff, F. P., Lovett, R. A. & Stillinger, F. H. 1965, 'Interfacial Density Profile for Fluids in the Critical Region', *Physical Review Letters*, vol. 15, pp. 621-623.

Burkholder, J. B., Mills, M. & Mckeen, S. 2000, 'Upper Limit for the UV Cross Sections of H_2SO_4', *Geophysical Research Letters*, vol. 27, no. 16, pp. 2493-2496.

Calvert, J. G. & Pitts, J. N. 1966, *Photochemistry*, Wiley, New York.

Campillo, A. J., Eversole, J. D. & Lin, H. B. 1992, 'Cavity quantum electrodynamic enhancement of spontaneous and stimulated emission in microdroplets', *Modern Physics Letters B*, vol. 6, no. 8, pp. 447-57.

Campillo, A. J., Eversole, J. D. & Lin, H.-B. 1996, 'Cavity QED Modified Stimulated and Spontaneous Processes in Microdroplets', In *Optical Processes in Microcavities*, (eds) Chang, R. K. & Campillo, A. J., World Scientific, Singapore, pp. 167-208.

Chang, R. K. & Campillo, A. J. 1996, *Optical Processes in Microcavities*, World Scientific, Singapore.

Chanon, M. 1997, *Homogeneous photocatalysis*, Wiley, Chichester ; New York.

Chanon, M. & Schiavello, M. 1997, 'Introduction to Photocatalysis', In *Homogeneous Photocatalysis*, (ed.) Chanon, M., Wiley, Chichester ; New York, pp. 1-13.

Ching, E. S. C., Leung, P. T. & Young, K. 1996, 'Optical Processes in Microcavities - the Role of Quasinormal Modes', In *Optical Processes in Microcavities*, (eds) Chang, R. K. & Campillo, A. J., World Scientific, Singapore, pp. 1-76.

Ching, S. C., Lai, H. M. & Young, K. 1987a, 'Dielectric microsspheres as optical cavities: Einstein A and B coefficients and level shift', *Journal of the Optical Society of America B*, vol. 4, no. 12, pp. 2004-2009.

Ching, S. C., Lai, H. M. & Young, K. 1987b, 'Dielectric Spheres as Optical cavities: thermal spectrum adn density of states', *Journal of the Optical Society of America B*, vol. 4, no. 12, pp. 1995-2003.

Clark, R. J. H. & Crociani, B. 1967, 'Solvent effects on the infrared spectra of chromium, molybdenum, and tungsten hexacarbonyls', *Inorganic Chemistry*, vol. 1, no. 1, pp. 12-16.

Cornils, B. & Hermann, W. A. 1998, *Aqueous-phase organometallic catalysis : concepts and applications*, Wiley-VCH, Weinheim ; New York.

Cornils, B. & Herrmann, W. A. 2000, *Applied homogeneous catalysis with organometallic compounds : a comprehensive handbook*, Special work-bench edn, Wiley-VCH, Weinheim ; New York.

Cornils, B., Herrmann, W. A., Horváth, I. T., Panster, P., Wieland, S., Basset, J.-M., Niccolai, G. P., Schmind, G. & Bahrmann, H. 2000, 'Homogeneous Catalysts and Their Heterogenisation or Immobilisation', In *Applied homogeneous catalysis with organometallic compounds : a comprehensive handbook*, Special work-bench edn, (eds) Cornils, B. & Herrmann, W. A., Wiley-VCH, Weinheim ; New York, pp. 575-654.

Craig, D. P. & Thirunamachandran, T. 1982, 'Radiation-molecule interactions in chemical physics', *Advances in Quantum Chemistry*, vol. 16, pp. 97-160.

Craig, D. P. & Thirunamachandran, T. 1984, *Molecular Quantum Electrodynamics: An Introduction to Radiation-Molecule Interactions*.

Craig, D. P. & Thirunamachandran, T. 1986, 'Radiation-molecule and molecule-molecule interactions. A unified viewpoint from quantum electrodynamics', *Acc. Chem. Res.*, vol. 19, no. 1, pp. 10-16.

Danckwerts, P. V. 1951, 'Absorption by Simultaneous Diffusion and Chemical Reaction into Particles of Various Shpaes and Into Falling Drops', *Transaction of the Faraday Society*, vol. 47, no. 9, pp. 1014-23.

Danckwerts, P. V. 1970, *Gas-liquid reactions*, McGraw-Hill Book Co., New York.

Davidovits, P., Jayne, J. T., Duan, S. X., Worsnop, D. R., Zahniser, M. S. & Kolb, C. E. 1991, 'Uptake of gas molecules by liquids: a model', *Journal of Physical Chemistry*, vol. 95, no. 16, pp. 6337-40.

Davis, E. J., Aardahl, C. L. & Widmann, J. F. 1998, 'Raman studies of aerosol chemical reactions', *Journal of Dispersion Science and Technology*, vol. 19, no. 2 & 3, pp. 293-309.

Defay, R., Prigogine, I. & Bellemans, A. 1966 Surface tension and adsorption trans. Everett, D. H.,

Descartes, R. 1639 Dioptrique trans. as Discourse on Method, Optics, Geometry and Meterology by Olscamp, P. J., Bobbs-Merrill Indianapolis 1965

Doerr, A. K., Tolan, M., Prange, W., Schlomka, J. P., Seydel, T., Press, W., Smilgies, D. & Struth, B. 1999, 'Observation of capillary waves on liquid thin films from mesoscopic to atomic length scales', *Physical Review Letters*, vol. 83, no. 17, pp. 3470-3473.

Donaldson, D. J. 1999, 'Adsorption of atmospheric gases at the air-water interface. I. NH_3', *Journal of Physical Chemistry A*, vol. 103, no. 1, pp. 62-70.

Donaldson, D. J. & Anderson, D. 1999, 'Adsorption of atmospheric gases at the air-water interface. 2. C-1-C-4 alcohols, acids, and acetone', *Journal of Physical Chemistry A*, vol. 103, no. 7, pp. 871-876.

Donaldson, D. J., Guest, J. A. & Goh, M. C. 1995, 'Evidence for Adsorbed SO_2 at the Aqueous Air Interface', *Journal of Physical Chemistry*, vol. 99, no. 23, pp. 9313-9315.

Donohue, T. 1989, 'Applied Laser Photochemistry in the Liquid Phase', In *Laser Applications in Physical Chemistry*, (ed.) Evans, D. K., M. Dekker, New York, pp. 89-172.

Druger, S. D., Arnold, S. & Folan, L. M. 1987, 'Theory of enhanced energy transfer between molecules embedded in spherical dielectric particles', *Journal of Chemical Physics*, vol. 87, no. 5, pp. 2649-59.

Dubois, P. F. 1997, *Object Technology for Scientific Computing: Object-Orientated Numerical Software in Eiffel and C*, Prentice Hall, New Jersey.

Eickmans, J. H., Hsieh, W. F. & Chang, R. K. 1987, 'Laser-induced explosion of water droplets: spatially resolved spectra', *Opt. Lett.*, vol. 12, no. 1, pp. 22-4.

Eisenthal, K. B. 1996a, 'Liquid interfaces probed by second-harmonic and sum-frequency spectroscopy', *Chemical Reviews*, vol. 96, no. 4, pp. 1343-1360.

Eisenthal, K. B. 1996b, 'Photochemistry and photophysics of liquid interfaces by second harmonic spectroscopy', *Journal of Physical Chemistry*, vol. 100, no. 31, pp. 12997-13006.

Finlayson-Pitts, B. J. & Pitts, J. N. 2000, *Chemistry of the upper and lower atmosphere : theory, experiments, and applications*, Academic Press, San Diego.

Fish, R. H. 1999, 'Fluorous biphasic catalysis: a new paradigm for the separation of homogeneous catalysts from their reaction substrates and products', *Chemistry--A European Journal*, vol. 5, no. 6, pp. 1677-1680.

Flatau, P. J. 2000, *'SCATTERLIB - Light Scattering Codes Library'*, Available at: http://atol.ucsd.edu/~pflatau/scatlib/scatterlib.htm

Flowers, B. H. 1995, *An introduction to numerical methods in C++*, Clarendon Press, Oxford ; New York.

Folan, L. M. & Arnold, S. 1992, 'Microparticle fluorescence and energy transfer', *Topic in Fluorescence Spectroscopy*, vol. 3, pp. 345-86.

Folan, L. M., Arnold, S. & Druger, S. D. 1985, 'Enhanced energy transfer within a microparticle', *Chemical Physics Letters*, vol. 118, no. 3, pp. 322-7.

Fotou, G. P., Kodas, T. T. & Anderson, B. 2000, 'Coating Titania Aerosol Particles with ZrO2, Al2O3/ZrO2, and SiO2/ZrO2 in a Gas-Phase Process', *Aerosol Science and Technology*, vol. 33, no. 6, pp. 557-71.

Fradin, C., Braslau, A., Luzet, D., Smilgies, D., Alba, M., Boudet, N., Mecke, K. & Daillant, J. 2000, 'Reduction in the surface energy of liquid interfaces at short length scales', *Nature*, vol. 403, no. 6772, pp. 871-874.

Froment, G. F. & Bischoff, K. B. 1990, *Chemical reactor analysis and design*, 2nd . edn, Wiley, New York.

Gilbert, A. & Baggott, J. E. 1991, *Essentials of molecular photochemistry*, Blackwell Scientific Publications, Oxford ; Boston.

Glikin, M., Kutakova, D. & Prin, E. 1999, 'Unsteady processes and aerosol catalysis', *Chemical Engineering Science*, vol. 54, no. 20, pp. 4337-4342.

Glikin, M. A. 1996, 'Aerosol catalysis', *Theoretical Foundations of Chemical Engineering*, vol. 30, no. 4, pp. 390-394.

Glikin, M. A., Kutakova, D. A., Glikina, I. M. & Volga, A. I. 2001, 'A new way to increase catalyst activity', *Adsorption Science & Technology*, vol. 19, no. 2, pp. 101-115.

Hanson, D. R. 1997, 'Surface-Specific Reactions on Liquids', *Journal of Physical Chemistry B*, vol. 101, no. 25, pp. 4998-5001.

Hatchard, C. G. & Parker, C. A. 1956, 'A new sensitive chemical actinometer. II. Potassium ferrioxalate as a standard chemical actinometer', *Proceedings of the Royal Society (London)*, vol. A235, pp. 518-36.

Hawkins, N. J., Mattraw, H. C., Sabol, W. W. & Carpenter, D. R. 1955, 'Spectroscopy of gaseous carbonyls. I. Infrared spectra and thermodynamic properties of chromium and molybdenum hexacarbonyls', *Journal of Chemical Physics*, vol. 23, pp. 2422-7.

Hennig, H., Billing, R. & Knoll, H. 1993, 'Photocatalysis: Definitions and Classifications', In *Photosensitization and photocatalysis using inorganic and organometallic compounds*, (eds) Kalyanasundaram, K. & Grätzel, M., Kluwer Academic Publishers, Dordrecht ; Boston, pp. xvi, 465.

Herrera, F., Lopez, A. & Kiwi, J. 2000, Photochemically activated degradation of reactive dyes. Statistical modeling of the reactor performance In *J. Photochem. Photobiol., A*, vol. 135, pp. 45-51.

Hinds, W. C. 1982, *Aerosol technology : properties, behavior, and measurement of airborne particles*, 1st edn, Wiley, New York.

Hsieh, W. F., Zheng, J. B., Wood, C. F., Chu, B. T. & Chang, R. K. 1987, 'Propagation velocity of laser-induced plasma inside and outside a transparent droplet', *Opt. Lett.*, vol. 12, no. 8, pp. 576-8.

http://Cens.Ioc.Ee/Projects/F2py2e/ F2PY

http://Pyfortran.Sourceforge.Net/ Pyfort

Hulst, H. C. V. D. 1957, *Light scattering by small particles*, Wiley, New York.

Ingebrethsen, B. J. & Matijevic, E. 1980, 'Preparation of uniform colloidal dispersions by chemical reactions in aerosols. 2. Spherical particles of aluminum hydrous oxide', *Journal of Aerosol Science*, vol. 11, no. 3, pp. 271-80.

Ingebrethsen, B. J., Matijevic, E. & Partch, R. E. 1983, 'Preparation of uniform colloidal dispersions by chemical reactions in aerosols. III. Mixed titania/alumina colloidal spheres', *Journal of Colloid and Interface Science*, vol. 95, no. 1, pp. 228-39.

Jayne, J. T., Davidovits, P., Worsnop, D. R., Zahniser, M. S. & Kolb, C. E. 1990, 'Uptake of sulfur dioxide(G) by aqueous surfaces as a function of pH: the effect of chemical reaction at the interface', *Journal of Physical Chemistry*, vol. 94, no. 15, pp. 6041-8.

Jayne, J. T., Duan, S. X., Davidovits, P., Worsnop, D. R., Zahniser, M. S. & Kolb, C. E. 1991, 'Uptake of gas-phase alcohol and organic acid molecules by water surfaces', *Journal of Physical Chemistry*, vol. 95, no. 16, pp. 6329-36.

Kerker, M. 1969, *The scattering of light, and other electromagnetic radiation*, Academic Press, New York.

Kiernan, V. 1999, 'The 'Open-Source Movement' Turns its Eye to Science', *The Chronicle of Higher Education*, November 5, p. A41.

Kim, S. M. & Vogelpohl, A. 1998, Degradation of organic pollutants by the Photo-Fenton-Process In *Chem. Eng. Technol.*, vol. 21, pp. 187-191.

Knipping, E. M., Lakin, M. J., Foster, K. L., Jungwirth, P., Tobias, D. J., Gerber, R. B., Dabdub, D. & Finlayson-Pitts, B. J. 2000, 'Experiments and simulations of ion-enhanced interfacial chemistry on aqueous NaCl aerosols', *Science*, vol. 288, no. 5464, pp. 301-306.

Knox, C. J. H. & Phillips, L. F. 1998, 'Capillary-wave model of gas-liquid exchange', *Journal of Physical Chemistry B*, vol. 102, no. 43, pp. 8469-8472.

Kodas, T. T. & Hampden-Smith, M. J. 1999, *Aerosol processing of materials*, Wiley-VCH, New York.

Kutal, C. 1985, 'Photochemistry of transition metal-organic systems', *Coordination Chemistry Reviews*, vol. 64, pp. 191-206.

Kutal, C. 1997, 'Transition Metal Complexes and Homogeneous Photocatalytic Transformation of Organic Substrates', In *Homogeneous Photocatalysis*, (ed.) Chanon, M., Wiley, Chichester ; New York, pp. 135-168.

Lage, P. L. C. & Rangel, R. H. 1991, 'Total Thermal Radiation Absorption Distribution inside a liquid Droplet Irradiated by a BlackBody', *HTD-Vol 166, Heat Transfer in Fire and Combustion Systems*, pp. 69 - 78.

Landron, C. 2000a, 'Recent Developments in the Structural Investigation by Synchrotron Radiation: Application to Ceramic Processing', In *Aerosol chemical processes in the environment*, (ed.) Spurný, K., Lewis Publishers, Boca Raton, Fla., p. 615fix.

Landron, C. 2000b, 'Syntheis and Online Characterisation of Zirconia Powder Produced by Atomisation', In *Aerosol chemical processes in the environment*, (ed.) Spurný, K., Lewis Publishers, Boca Raton, Fla., pp. 249-55.

Lawton, G. 2002, 'The Great Giveaway http://www.newscientist.com/hottopics/copyleft/copyleftart.jsp', *New Scientist*.

Mackowski, D. W. 1989, 'Photphoresis of aerosol particles in the free molecular and slip-flow regimes', *International Journal of Heat and Mass Transfer*, vol. 32, no. 5, pp. 843-854.

Malato, S., Caceres, J., Agueera, A., Mezcua, M., Hernando, D., Vial, J. & Fernandez-Alba, A. R. 2001, 'Degradation of Imidacloprid in Water by Photo-Fenton and TiO2

Photocatalysis at a Solar Pilot Plant: A Comparative Study', *Environmental Science and Technology*, vol. 35, no. 21, pp. 4359-4366.

Marczenko, Z. 1976, *Spectrophotometric determination of elements*, Ellis Horwood, Chichester.

Matejec, V., Kašík, I. & Chomát, M. 2000, 'Fundamentals and Perfomance of MCVD Aerosol Process', In *Aerosol chemical processes in the environment*, (ed.) Spurný, K., Lewis Publishers, Boca Raton, Fla., p. 615.

Matijevic, E., Zhong, Q. & Partch, R. E. 1995, 'Preparation of uniform colloidal dispersions by chemical reactions in aerosols. VI. Silica/titania composite particles', *Aerosol Science and Technology*, vol. 22, no. 2, pp. 162-71.

Mcginnis, B. D., Adams, V. D. & Middlebrooks, E. J. 2000, 'Degragation of Ethylene Glycol in Photo Fenton Systems', *Water Research*, vol. 34, no. 8, pp. 2346-2354.

Mcrae, D., Matijevic, E. & Davis, E. J. 1975, 'Chemical reactions in aerosols. I. Bromination of octadecene droplets', *Journal of Colloid and Interface Science*, vol. 53, no. 3, pp. 411-21.

Mcrae, D., Matijevic, E. & Davis, E. J. 1978, 'Chemical reactions in aerosols. II. The effects of various parameters on the bromination of 1-octadecene droplets', *Journal of Colloid and Interface Science*, vol. 67, no. 3, pp. 526-37.

Mészáros, E. 1999, *Fundamentals of atmospheric aerosol chemistry*, Akadémiai Kiadó, Budapest.

Nadtochenko, V. & Kiwi, J. 1998, Primary Photochemical Reactions in the Photo-Fenton System with Ferric Chloride. 1. A Case Study of Xylidine Oxidation as a Model Compound In *Environ. Sci. Technol.*, vol. 32, pp. 3273-3281.

Nakamoto, K. 1997, *Infrared and Raman spectra of inorganic and coordination compounds*, 5th edn, Wiley, New York.

Nakamura, K., Partch, R. E. & Matijevic, E. 1984, 'Preparation of polymer colloids by chemical reactions in aerosols. II. Large particles', *Journal of Colloid and Interface Science*, vol. 99, no. 1, pp. 118-27.

Nasielski, J., Kirsch, P. & Wilputte-Steinert, L. 1971, 'Photoinduced hydrogenation of conjugated dienes catalyzed by chromium hexacarbonyl', *Journal of Organometallic Chemistry*, vol. 27, no. 1, pp. C13-C14.

Nathanson, G. M., Davidovits, P., Worsnop, D. R. & Kolb, C. E. 1996, 'Dynamics and Kinetics at the Gas-Liquid Interface', *Journal of Physical Chemistry*, vol. 100, no. 31, pp. 13007-13020.

Nikitin, E. E. 1974 Theory of Elementary Atomic and Molecular Processes in Gases trans. Kearsley, M. J.,

Nussenzveig, H. M. 1977, 'The Theory of the Rainbow', *Scientific American*, vol. 236, pp. 116-127.

Ocana, M. & Matijevic, E. 1990, 'Preparation of uniform colloidal dispersions by chemical reactions in aerosols - V. Tin(IV) oxide', *Journal of Aerosol Science*, vol. 21, no. 6, pp. 811-20.

Parker, C. A. 1953, 'A new sensitive chemical actinometer. I. Potassium ferrioxalate as a standard chemical actinometer', *Proceedings of the Royal Society (London)*, vol. A220, p. 104.

Partch, R., Matijevic, E., Hodgson, A. W. & Aiken, B. E. 1983, 'Preparation of polymer colloids by chemical reactions in aerosols. I. Poly(p-tertiarybutylstyrene)', *Journal of Polymer Science, Polymers and Chemical Education*, vol. 21, no. 4, pp. 961-7.

Partch, R. E., Nakamura, K., Wolfe, K. J. & Matijevic, E. 1985, 'Preparation of polymer colloids by chemical reactions in aerosols. III. Polyurea and mixed polyurea-metal oxide particles', *Journal of Colloid and Interface Science*, vol. 105, no. 2, pp. 560-9.

Phillips, L. F. 1993, 'Effect of electrostatic interactions on effective cross-sections for collision of small particles with neutral molecules', *Australian Journal of Chemistry*, vol. 46, no. 1, pp. 13-20.

Phillips, L. F. 1997, 'Velocity and angular distributions of molecules emitted from a liquid surface', *Chemical Physics Letters*, vol. 266, no. 1,2, pp. 161-168.

Phillips, L. F. 2000a, 'Capillary waves, slope correlations, and evaporation at the surface of a drop', *Chemical Physics Letters*, vol. 320, no. 5,6, pp. 398-404.

Phillips, L. F. 2000b, 'Local-mode oscillations at a liquid interface', *Chemical Physics Letters*, vol. 330, no. 1,2, pp. 15-20.

Phillips, L. F. 2000c, 'Surface Correlations and Exchange at a Spherical Liquid Interface', *Journal of Physical Chemistry B*, vol. 104, no. 11, pp. 2534-2539.

Phillips, L. F. 2001a, 'Gaussian local modes of a liquid interface', *Journal of Physical Chemistry B*, vol. 105, no. 45, pp. 11283-11289.

Phillips, L. F. 2001b, 'Local Modes and the Surface-Bulk Exchange Rate at a Liquid Interface', *Journal of Physical Chemistry B*, vol. 105, no. 5, pp. 1041-1046.

Pouchert, C. J. 1985, *The Aldrich library of FT-IR spectra*, 1st edn, Aldrich Chemical Co., Milwaukee, Wis.

Purcell, E. M. 1946, 'Spontaneous Emission Probabilities at Radio Frequencies', *Physical Review*, vol. 69, no. 11-12, p. 681.

Ray, A. K. & Bhanti, D. D. 1997, 'Effect of optical resonances on photochemical reactions in microdroplets', *Appl. Opt.*, vol. 36, no. 12, pp. 2663-2674.

Rieger, P. H. 1994, *Electrochemistry*, 2nd . edn, Chapman & Hall, New York.

Roundhill, D. M. 1994, *Photochemistry and photophysics of metal complexes*, Plenum Press, New York.

Rowland, G. A. 2001, *The photochemistry of sulfuric acid aerosols : a thesis submitted in partial fulfillment of the requirements for the degree of Doctor of Philosophy in Chemistry in the University of Canterbury.*

Ruggaber, A., Dlugi, R., Bott, A., Forkel, R., Herrmann, H. & Jacobi, H.-W. 1997, 'Modelling of Radiation Quantities and Photolysis Frequencies in the Aqueous Phase in the Troposphere', *Atmospheric Environment*, vol. 31, no. 19, pp. 3137-3150.

Saecker, M. E. & Nathanson, G. M. 1993, 'Collisions of protic and aprotic gases with hydrogen bonding and hydrocarbon liquids', *Journal of Chemical Physics*, vol. 99, no. 9, pp. 7056-75.

Safarzadeh-Amiri, A., Bolton, J. R. & Cater, S. R. 1996, 'Ferrioxalate-Mediated Solar Degradation of Organic Contaminants in Water', *Solar Energy*, vol. 56, no. 5, pp. 439-443.

Salomon, R. G. 1983, 'Homogeneous metal catalysis in organic photochemistry', *Tetrahedron*, vol. 39, no. 4, pp. 485-575.

Sanfeld, A. 1998, 'Influence of capillarity on chemical stability and of electric field on surface tension near the critical point', *Philosophical Transactions of the Royal Society of London Series a-Mathematical Physical and Engineering Sciences*, vol. 356, no. 1739, pp. 819-828.

Sanfeld, A., Carlier, P. & Mouvier, G. 1995, 'Influence of Water Droplet Size on the Chemical Affinity - Applications to Supersaturated Moist Air', *Fluid Phase Equilibria*, vol. 107, no. 1, pp. 75-91.

Sanfeld, A., Sefiane, K., Benielli, D. & Steinchen, A. 2000, 'Does capillarity influence chemical reaction in drops and bubbles? A thermodynamic approach', *Advances in Colloid and Interface Science*, vol. 86, no. 3, pp. 153-193.

Sanfeld, A. & Steinchen, A. 1999, 'Chemical reactions in microdroplets and microbubbles. Thermodynamic approach', *Comptes Rendus De L Academie Des Sciences Serie Ii Fascicule C- Chimie*, vol. 2, no. 14, pp. 697-700.

Seipenbusch, M., Binnig, J., Heim, M., Weber, A. P. & Kasper, G. 2001, 'Aerosol catalysis: the influence of particle structure on the catalytic activity of platinum-nanoparticle agglomerates', *Helvetica Chimica Acta*, vol. 84, no. 12, pp. 3686-3701.

Sides, S. W., Grest, G. S. & Lacasse, M. D. 1999, 'Capillary waves at liquid-vapor interfaces: A molecular dynamics simulation', *Physical Review E*, vol. 60, no. 6, pp. 6708-6713.

Spurný, K. (ed.) 2000, *Aerosol chemical processes in the environment*, Lewis Publishers, Boca Raton, Fla.

Strauss, W. A. 1992, *Partial differential equations : an introduction*, Wiley, New York.

Strem192001-2003 *Chemicals for Research: metals, inorganics and organometallics*,

Stroustrup, B. 1997, *The C++ programming language*, 3rd edn, Addison-Wesley, Reading, Mass.

Szymanska-Buzar, T. 1997, 'Photochemical reactions of Group 6 metal carbonyls in catalytic transformation of alkenes and alkynes', *Coordination Chemistry Reviews*, vol. 159, pp. 205-220.

Taflin, D. C. & Davis, E. J. 1990, 'A study of aerosol chemical reactions by optical resonance spectroscopy', *Journal of Aerosol Science*, vol. 21, no. 1, pp. 73-86.

Taylor, R. S., Tay, D. & Garrett, B. C. 1997, 'Understanding the Mechanisim for the Mass Accommodation of Ethanol by a Water Droplet', *Journal of Physical Chemistry B*, vol. 101, no. 28, pp. 5473-5476.

Thurn, R. & Kiefer, W. 1984, 'Raman-microsampling technique applying optical levitation by radiation pressure', *Applied Spectroscocpy*, vol. 38, no. 1, pp. 78-83.

Tundo, P., Moraglio, G. & Trotta, F. 1989, 'Gas-Liquid Phase-Transfer Catalysis: A New Continuous-Flow Method in Organic Synthesis', *Industrial and Engineering Chemistry Research*, vol. 28, no. 7, pp. 881-890.

Tuntomo, A., Tien, C. L. & Park, S. H. 1991, 'Internal Distribution of Radiant Absorption in a Spherical Particle', *Journal of Mass Transfer*, vol. 113, pp. 407-412.

Tyndall, J. 1869, 'On the Blue Colour of the Shy, and on the Polarisation of Light', *The Philosophical Magazine, Series 4*, vol. 37, pp. 384-94.

Visca, M. & Matijevic, E. 1979, 'Preparation of uniform colloidal dispersions by chemical reactions in aerosols. I. Spherical particles of titanium dioxide', *Journal of Colloid and Interface Science*, vol. 68, no. 2, pp. 308-19.

Walling, C. 1975, 'Fenton's Reagent Revisited', *Accounts of Chemistry Research*, vol. 8, no. 4, pp. 125-131.

Weber, A. P., Seipenbusch, M. & Kasper, G. 2001, 'Application of aerosol techniques to study the catalytic formation of methane on gasborne nickel nanoparticles', *Journal of Physical Chemistry A*, vol. 105, no. 39, pp. 8958-8963.

Weissermel, K. & Arpe, H.-J. 1993, *Industrial organic chemistry*, 2nd rev. edn, Vch, Weinheim ; New York.

Willeke, K. & Baron, P. A. 1993, *Aerosol measurement : principles, techniques, and applications*, Van Nostrand Reinhold, New York.

Worsnop, D. R., Zahniser, M. S., Kolb, C. E., Gardner, J. A., Watson, L. R., Van Doren, J. M., Jayne, J. T. & Davidovits, P. 1989, 'The temperature dependence of mass accommodation of sulfur dioxide and hydrogen peroxide on aqueous surfaces', *Journal of Physical Chemistry*, vol. 93, no. 3, pp. 1159-72.

Wrenn, S. J., Butler, L. J., Rowland, G. A., Knox, C. J. H. & Phillips, L. F. 1999, 'The necessity for multiphoton processes in the 193-nm photochemistry of sulphuric acid aerosols', *Journal of Photochemistry and Photobiology A-Chemistry*, vol. 129, no. 3, pp. 101-104.

Wriedt, T. 2002, *'Electromagnetic Scattering Programs'*, Available at: http://www.t-matrix.de/

Wrighton, M. 1984, 'The Photochemistry of Metal Carbonyls', *Chemical Reviews*, vol. 74, no. 4, pp. 401-430.

Wrighton, M. & Schroeder, M. A. 1973, 'Structure and reactivity relations in chromium carbonyl photoassisted hydrogenation of 1,3-dienes', *J. Amer. Chem. Soc.*, vol. 95, no. 17, pp. 5764-5.

www.Netlib.org/Cephes Cephes Library

www.numpy.org The NumPy Website

www.openscience.org The Open Science Initiative Website

www.opensource.org The Open Source Initiative (OSI) Website

www.scintilla.org The Scintilla and SciTE Website

www.scipy.org The SciPy Website

www.wxwindows.org The wxWindows Website

Yang, H., Wright, N. J., Gagnon, A. M., Gerber, B. R. & Finlayson-Pitts, B. J. 2002, 'An upper limit to the concentration of an SO2 complex at the air-water interface at 298 K: infrared experiments and ab initio calculations', *Physical Chemistry Chemical Physics*, vol. 4, no. 10, pp. 1832-1838.

Zarzycki, R. & Chacuk, A. 1993, *Absorption : fundamentals & applications*, 1st . edn, Pergamon Press, Oxford ; New York.

Zuev, V. E. 1980 Nelineinye Opticheskie Effekty v Aerzolykah trans. as High-power laser radiation in atmospheric aerosols : nonlinear optics of aerodispersed media by D. Reidel Dordrecht 1985